Oxidation of Hydrocarbons Desorbed from the Lubricant Oil in Spark Ignition Engines

by

Michael G. Norris

B. S., Mechanical Engineering
Oregon State University, 1985

S.M., Mechanical Engineering
Massachusetts Institute of Technology, 1991

Submitted to the Department of Mechanical Engineering
in Partial Fulfillment of the Requirements for the Degrees of

Doctor of Philosophy

at the

Massachusetts Institute of Technology; September 1995

Signature of Author________________________________
Department of Mechanical Engineering
September 1995

Certified by________________________________
Simone Hochgreb
Assistant Professor, Department of Mechanical Engineering
Thesis Supervisor

Accepted by________________________________
A. A. Sonin, Chairman
Chairman, Department Committee on Graduate Studies
Department of Mechanical Engineering

(This page intentionally left blank)

Oxidation of Hydrocarbons Desorbed from the Lubricant Oil in Spark Ignition Engines

by

Michael G. Norris

Submitted to the Department of Mechanical Engineering on August 21, 1995 in Partial Fulfillment of the Requirements for the Degree of Doctor of Philosophy.

ABSTRACT

Direct measurements of the extent of oxidation of hydrocarbons desorbing from the oil layer have been made in a spark-ignition engine in which the lubricant oil was doped with a pure hydrocarbon fuel. By firing with diluted hydrogen-air mixtures, the hydrocarbon dopant desorbing from the lubricant oil was the only source of carbon-containing species in the exhaust gases. The extent of oxidation was determined by measuring the ratio of hydrocarbons to total carbon concentration in the exhaust gases. Experiments to characterize the hydrocarbon source found that the amount of hydrocarbon desorbed scales with the oil layer thickness indicating depletion of dopant from the oil layer during each revolution. The depletion hypothesis was supported by a one-dimensional analytical model.

The extent of oxidation was measured for several hydrocarbon dopants at a variety of operating conditions. At a mid-speed, mid-load condition, approximately three quarters of the post-flame desorbed fuel was oxidized in the engine. The fraction oxidized depended, as expected, on the hydrogen fuel-air ratio, load and chemical reactivity of the dopant hydrocarbon. Surprisingly, the fraction oxidized was only modestly dependent on spark timing, and dilution levels below 20%. Measurements of the hydrocarbon concentrations using a fast FID, sampling at the exhaust valve, showed that nearly all of the surviving dopant hydrocarbon emerges at the end of the exhaust stroke. The fraction oxidized in-cylinder was estimated from the measured levels of oxidation over the engine and estimates for the fractions oxidized in the port and retained in-cylinder. At the mid-speed mid-load condition, approximately half of the post-flame desorbed dopant was oxidized in-cylinder.

The estimated results for in-cylinder oxidation were in large part supported by a simplified one-dimensional numerical model of the oil layer and thermal boundary layer at the cylinder wall. The numerical model further showed that the rate of oxidation was strongly dependent on turbulence levels, chemical reactivity and the initial thickness of the thermal boundary layer. Dopant type and operating condition affect the level of oxidation primarily through the reactivity of the dopant and the cylinder temperature to which the desorbed dopant is exposed.

Thesis Supervisor:	Simone Hochgreb
Title:	Assistant Professor, Department of Mechanical Engineering

(This page intentionally left blank)

ACKNOWLEDGMENTS

I would like to thank the member of my committee for their guidance and support of this thesis. Professor Simone Hochgreb's guidance through the long process of defining a thesis topic and encouragement to get the details right and write clean papers were invaluable. Professor Wai Cheng was forever available to help with the engine experiments. Professor John Heywood provided a critical perspective on what was important in the work.

I especially want to thank my lab mates who were ceaselessly available to solve problems, provide information and just talk. One of the great strengths of the Sloan Lab is the easy sharing of resources and knowledge among the graduate students. In particular I would like to thank and acknowledge Wolf Bauer's help in the development of the one-dimensional code reported in Chapter 6. His shared interest in boundary layer heat transfer problems and implementation of the numerical scheme were invaluable. I want to thank the Goro Tamai, Tian Tian, Dr. Kyoung-Doug Min and Eric Deutsch for their help in developing the oil layer model. I also want to thank Pete Hinze, Kuo-Chaing Chen and Haissam Haiddar for graciously sharing the engine and testing equipment. I must thank Brian Corkrum for his patient help in building the experiment and keeping the lab organized and clean. I especially want to thank George Delagrammatikas, who put in long hours to assemble hardware and help run tests. The easy friendship of the other graduate students and staff made life at the Sloan Lab a real pleasure. I will especially miss my friends Gatis Basbauer, Vincient Frottier, Jon Fox, Dr. Jong-Hwa Lee, Dr. Andras Kovacs, Joan Kenny and Nancy Cook.

My wife Leslie has been my rock of support through my thesis work and is the best part of my life. I want to thank her for hanging in there during the all-work-and-no-play student life for the last couple of years. Leslie provided loving support through dark and bright days, while raising the most beautiful one-year old in the world, Rachel. Last and not least, I must thank my family for their endless support and encouragement that helped me bring this thesis to completion.

This work has been supported by the Engine-Fuels Interaction Consortium , whose members include Chevron Research Corporation, Exxon Research and Engineering Company, Nippon Oil Company Limited, and Shell Oil Company.

M.G. Norris
Septmeber, 1995

TABLE OF CONTENTS

LIST OF TABLES

ABBREVIATIONS

SYMBOL	DEFINITION	UNITS
A_0	pre-exponential term in Arrenhius form	(cm/mole s)^a
B	cylinder bore	m
Bi	Biot number	-
c_n	dopant carbon number	-
c_p	specific heat at constant pressure	j/mole K
CAD	crank angle degree	
d_v	diameter of roll-up vortex	m
D_i	effective diffusivity of species i in gas phase	m^2/s
D_o	molecular diffusivity of dopant in oil	m^2/s
E_a	activation energy term in Arrenhius from	j/mole
f_{cyl}	fraction of unburned hydrocarbons oxidized in-cylinder	-
f_{ex}	fraction of vortex retained in-cylinder at IVO	-
f_{HC}	fraction of unburned hydrocarbons exiting engine	-
f_{port}	fraction of unburned hydrocarbons oxidized in the exhaust port	-
f_{res}	fraction of unburned hydrocarbons retained in the residual mass	-
f_v	fraction of vortex retained in-cylinder at EVC	-
Fo	Fourier number	-
Δh_r	specific heat of reaction	j/mole
h_D	mass transfer coefficient	m/s
H_D	convective mass transfer including gas-oil interface	m/s
H^*	modified henry's constant: $H^* = H\ M_o/M_{HC}$	kPa
k	turbulent kinetic energy	m/s
k_o	initial turbulent kinetic energy	m/s
L_{EOC}	length of cylinder covered by piston at end of combustion	m
L_s	stroke length	m
m_{air}	measured mass of air inducted per cycle	kg/cycle
m_c	mass of dopant desorbed per cycle	kg/cycle
m_{co}	mass of dopant in oil layer per cycle	kg/cycle
m_{cr}	mass in crevice volume	kg
m_d	mass of dopant desorbed after the end of combustion	kg/cycle
m_{de}	dry mass exhausted per cycle	kg/cycle
m_e	mass exhausted per cycle	kg/cycle
m_{eb}	mass of exhaust reinducted into cylinder during valve overlap period	kg
m_{ed}	dry mass exhausted per cycle	kg/cycle
m_{HC}	mass of hydrocarbons in the exhaust	kg/cycle
m_q	mass of dopant surviving in quench layer	kg
m_r	residual mass	kg
M_{air}	molecular weight of air	kg/mole
M_e	molecular weight of exhaust	kg/mole
M_{ed}	molecular weight of dry exhaust	kg/mole
M_{HC}	molecular weight of dopant	kg/mole
M_{H2}	molecular weight of hydrogen	kg/mole
M_{O2}	molecular weight of oxygen	kg/mole
M_{N2}	molecular weight of nitrogen	kg/mole
Mr	molecular weight of residual gas	kg/mole

ABBREVIATIONS

SYMBOL	DEFINITION	UNITS
MBT	maximum brake torque spark timing	CAD
N	engine speed	rpm
OF	valve overlap factor	mm CAD
P	cylinder pressure	bar
P_e	exhaust manifold pressure	bar
P_i	intake manifold pressure	bar
P_m	indicated mean effective pressure	bar
r_c	compression ratio	-
r_f	ratio of dopant concentration in oil on cylinder wall over concentration in bulk oil.	-
R	gas constant	j/mole K
R_{HC}	ratio of hydrocarbon concentration of residual to exhaust	-
S_L	laminar flame speed	m/s
S_P	piston speed	m/s
S^*_P	average piston speed	m/s
t	time	s
T	temperature	°K
T_c	adiabatic core gas temperature	°K
T_{cr}	top land crevice gas temperature	°K
T_{cool}	coolant temperature	°K
T_h	temperature measured at top of cylinder wall	°K
T_w	cylinder wall temperature as a function of axial position	°K
u	radial velocity	m/s
u_i'	ith component of turbulent intensity	m/s
V_{cl}	clearance volume	m^3
V_{cr}	top land crevice volume	m^3
V_v	vortex volume	m^3
w	velocity in axial direction	m/s
x	radial distance from cylinder wall	m
x^*	radial distance from cylinder wall normalized by oil thickness	-
x_r	residual mass fraction	-
X_D	molar fraction of diluent nitrogen in the intake mixture	-
X_f	dopant mass fraction in bulk lubricant oil	-
X_i	mass fraction of species i in the gas phase	-
X_o	mass fraction of dopant in the oil	-
X_{oi}	initial mass fraction of dopant in the oil	-
X_{le}	equilibrium mass fraction of dopant in the oil relative to bulk dopant mass fraction in gas phase	-
Y_e	engine-out hydrocarbon mole fraction	-
Y_c	cylinder-out hydrocarbon mole fraction	-
Y_r	hydrocarbon mole fraction in residual gas	-
Y_v	hydrocarbon mole fraction of roll-up vortex	-
Y_e	engine-out hydrocarbon mole fraction	-
Y_{HC}	hydrocarbon mole	-
Y_{CO}	carbon monoxide mole fraction	-
Y_{CO2}	carbon dioxide mole fraction	-
z	axial distance	m

SYMBOL	DEFINITION	UNITS
α	molecular thermal diffusivity	m^2/s
α_e	effective thermal diffusivity	m^2/s
α_T	turbulent thermal diffusivity	m^2/s
δ_{avg}	oil thickness	m
δ_o	oil thickness	m
δ_t	thermal boundary layer thickness	m
δ_{1P}	one-plate quench distance	m
δ_{2P}	two-plate quench distance	m
γ	ratio of specific heats	-
μ	viscosity	kg/m s
ν	dynamic viscosity	m^2/s
π	3.1415	-
ϕ	fuel-air equivalence ratio	-
ρ_o	oil density	kg/m^3
θ	dopant concentration in oil	
θ^*	non-dimensionalized dopant concentration in oil	
θ_{rs}	spark timing relative to timing that produces a maximum pressure approximately 17° after top center (ATC).	CAD
ω	reaction rate	$mole/m^3\ s$
ψ	molar ratio of nitrogen to oxygen in intake gas	-
ζ_1	first positive root to eqn. 3.2	
ζ_n	positive roots to eqn. 3.2	

(This page intentionally left blank)

CHAPTER 1

INTRODUCTION

1.1 Background

The emission of volatile organic gases, commonly called hydrocarbon emissions, are an important precursor to smog in urban areas and include all the exhaust gas toxins[*]. Hydrocarbons in the exhaust of spark-ignition engines results from the incomplete combustion of the fuel. Current regulations in California require that a significant fraction of new cars starting in 1997 meet Ultra Low Emission Vehicles (ULEVs) standards emitting less than a tenth as much non-methane hydrocarbons as current models. These ULEVs are also being considered for the northeast and mid-Atlantic states comprising the Ozone Transport Council. In order to meet these technical challenges researchers have pursued numerous investigations into the mechanisms that produce hydrocarbon emissions [1, 2][†]. Most of the work in this area has focused on the various mechanisms that result in hydrocarbons escaping oxidation during the main combustion event [3, 4]. The current investigation examines the post-fame processes leading to oxidation of unburned hydrocarbons in the cylinder and in the exhaust port.

The current understanding of how hydrocarbons escape the primary combustion event and are then transported to the exhaust manifold has developed over the last 40 or more years. The first studies into the origin of hydrocarbon emissions were made by Wentworth and Daniel in the 1960s [5]. Originally, hydrocarbon emissions were assumed primarily to be the result of the flame quenching at cylinder surfaces. It was suggested that the thermal boundary layer visible in schlieren photographs of engines protected these wall-quench hydrocarbons from oxidation during the expansion and exhaust strokes. In the late 1970s, experiments with combustion bombs and numerical modeling showed that wall-quench hydrocarbons quickly diffuse into the hot cylinder gases and are oxidized [6, 7, 8]. These studies pointed out that other sources such as crevices, the oil layer and deposits, which had previously been considered secondary hydrocarbon sources, were in fact the dominant sources of unburned hydrocarbons.

The current conceptual model of the mechanisms leading to unburned hydrocarbons in a warmed-up engine was presented by Cheng *et al.* [1] and is described schematically in Fig 1.1. The flame converts about 90% of the inducted fuel to complete combustion products, while the rest escapes the main

---

[*] Benzene, 1,3 butadiene, formaldehyde and acetaldehyde are toxins as defined by the United States Environmental Protection Agency.

[†] Numbers in brackets indicate references at end of text section.

combustion event through various mechanisms. The sources of unburned hydrocarbons are divided into fuel-air and fuel only sources, which appear to have very different post-combustion oxidation rates. The fuel-air sources includes storage in crevices, the wall-quench layer and unburned mixture escaping past the closed exhaust valve. The fuel-only sources include absorption by the oil layer and deposits and liquid-phase fuel on cylinder surfaces. During expansion, these various sources emit unburned fuel into the hot burned gases, where two-thirds of the fuel stored in fuel-air sources and one third of the fuel in fuel-only sources are oxidized in-cylinder. Approximately two-thirds of the remaining fuel is then exhausted into the exhaust port. In the port, oxidation consumes approximately a third of the exiting hydrocarbons. The remaining hydrocarbons are referred to as engine-out hydrocarbons and represent approximately two percent of the inducted fuel. Provided the catalytic converter has already lit-off, over 90% of the remaining hydrocarbons will be oxidized in the converter.

The largest source of unburned hydrocarbons are crevices, which store approximately five percent of the intake charge of fuel and air. Crevices are small volumes connected to the cylinder, which have entrances smaller than the two-wall quench distance of hydrocarbon flames in engines (~1 mm). Crevices store a larger fraction of the total mass than their volume would indicate, as the density in the crevice is approximately six times higher than the burned gases at peak pressure due to the cooling of the cylinder walls. The largest crevice is between the piston and cylinder liner, which stores approximately three percent of the intake charge. Although crevices in the cylinder head including the spark plug threads, valves and head gasket are much smaller than the piston top land crevice, engine-out hydrocarbon levels are more sensitive to changes in the head crevices as most of the piston crevice hydrocarbons are oxidized in-cylinder [1].

Other fuel-air sources are the wall-quench layer, which contains about one half percent of the intake fuel-air charge and exhaust valve leakage which typically allows 0.1% of the intake mixture to escape the engine. The wall-quench hydrocarbons are believed to be quickly oxidized during the expansion stroke and not significantly contribute to engine-out hydrocarbons. Poor sealing and exhaust valve rotation results in some of the unburned mixture escaping from the cylinder into the exhaust port. These escaped hydrocarbons exit the engine without further oxidation, thus contributing approximately five percent of engine-out hydrocarbons. The amount of valve leakage will vary considerably from engine to engine and over time, depending on valve deposit build up and valve seat wear.

Approximately two percent of the inducted fuel is absorbed by the lubricant oil layer on the cylinder wall or deposits on the piston crown and cylinder head. Quantifying the contributions of the oil layer and deposits to hydrocarbon emissions has continued to be a challenge. Estimates of the oil layer absorption/desorption contribution have ranged from zero to thirty percent of engine-out emissions [9, 10, 11]. The effect of deposits is even harder to determine, due in part to the dependence of deposit thickness and morphology on recent engine operation. In a couple of studies where deposits were deliberately built up and then removed, it was concluded that deposits can increase hydrocarbon emissions fifty to one hundred percent [12, 13]. Researchers studying a taxi fleet found deposits raised hydrocarbon emissions from ten to twenty percent [14]. Liquid phase fuel is quite important at cold starting conditions, where liquid fuel coats the cylinder surfaces and can raise hydrocarbon emissions by forty percent [15]. However at warmed up conditions, the effect of liquid phase fuel is estimated to be less than ten percent [16].

Forty years of research have produced good physical descriptions of the unburned hydrocarbon sources in spark-ignition engines and usable models for the crevice and oil sources. The same can not be said of the post-flame processes, which have often been treated in a most cursory way.

1.2 Previous work on post-flame oxidation

Although about three-quarters of the unburned hydrocarbons are estimated to undergo oxidation before exiting the engine, little is known about the processes of diffusion and mixing of hydrocarbons with burned gases and the resulting oxidation that occurs in the cylinder and exhaust port. The current conceptual model holds that unburned fuel emerges from the various sources (crevices, oil layer and deposits) into the thermal boundary layer next to the cylinder surfaces. Oxidation occurs when the hydrocarbons diffuse into or mix with the hot burned gases during the expansion and exhaust strokes. The oxidation rate is much lower than during the main combustion event and occurs either within a couple millimeters of the cylinder walls or during the complicated gas flow of the exhaust process making the oxidation process difficult to observe, optically or otherwise. Modeling and indirect experiments have been carried out to investigate in-cylinder oxidation and found that in-cylinder oxidation process are sensitive to the details of crevice location and size [16, 17].

Experiments to quantify the level of oxidation in the exhaust port were carried out by Mendillo and Heywood [18] and Drobot *et al.*[19]. In these experiments, reactions in the exiting cylinder gases were quenched by the rapid addition of CO_2. The resulting hydrocarbon concentrations in the exhaust were then compared to hydrocarbon levels under normal operation without quenching to determine the extent of oxidation downstream of the cylinder exit. It was found that nearly all the oxidation occurred within the exhaust port, before the gases reached the exhaust manifold. Oxidation levels at a mid-speed mid-load condition ranged from one third to one half. The level of oxidation was only modestly sensitive to the fuel type, but strongly dependent on operating conditions especially speed, load, spark timing and fuel-air ratio.

Recent experiments with gaseous fuels, in order to eliminate other hydrocarbon sources, have quantified the extent of oxidation of hydrocarbons and air emerging from crevices [16]. It was found that exhaust hydrocarbon levels were significantly more sensitive to changes in crevice volume for crevices near the exhaust port than other crevices such as the piston top land crevice. Min's one-dimensional model of the in-cylinder oxidation of top land crevice hydrocarbons showed most these hydrocarbons are oxidized during the expansion stroke leaving a thin layer of hydrocarbons on the bottom half of the cylinder wall that is scraped into the corner vortex as the piston rises during the exhaust stroke [16].

Kuo and Reitz [17] used the CFD code, KIVA, to model the emergence of hydrocarbons from the top land piston crevice and their subsequent oxidation in-cylinder. The model predicted very high levels of in-cylinder oxidation and indicated that the level of oxidation was higher for thinner crevices of the same volume due to higher velocities leaving the crevice.

1.3 Objectives

All previous estimates of post-flame oxidation have relied on a model to quantify the amount of hydrocarbons surviving the main-combustion event. The level of oxidation was then determined by comparing the estimated amount of hydrocarbons emerging from sources and the amount measured in the exhaust. The goal of this study was to make a direct measurement of the extent of post-flame oxidation in a firing engine and to develop an understanding of the controlling processes through experimentation and modeling .

The objectives of this study were to:

1) design and develop an experiment to measure the level of oxidation for a realistic hydrocarbon source in a firing engine;
2) measure the sensitivity of post-flame oxidation to hydrocarbon species and engine operating conditions;
3) develop an estimate of the in-cylinder oxidation levels as a function of operating conditions; and
4) identify the controlling parameters of post-flame in-cylinder oxidation, through appropriate modeling of the in-cylinder oxidation process.

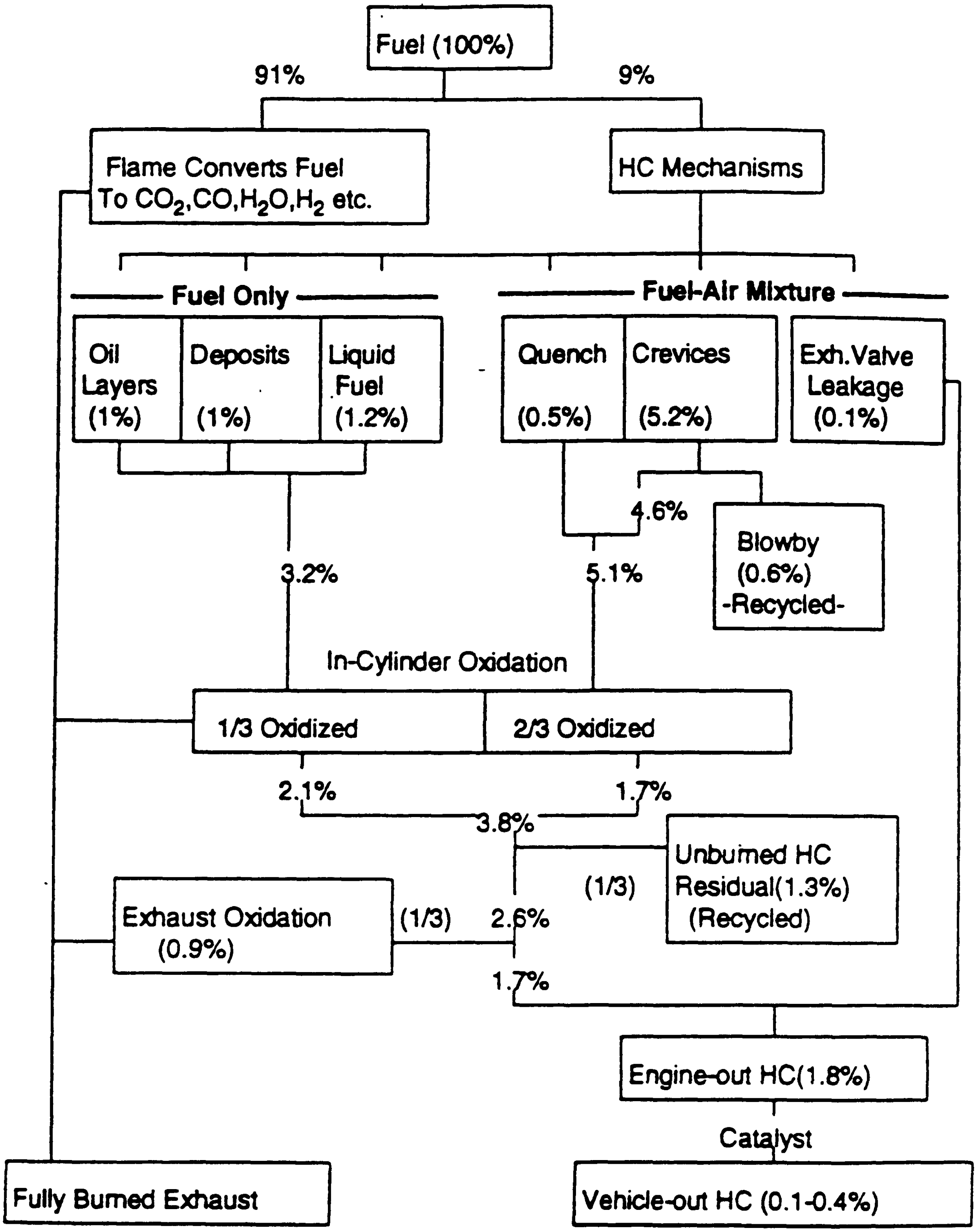

Fig. 1.1 Complete flow chart for the gasoline fuel, which enters each cylinder, through both the normal combustion process (left side) and the unburned hydrocarbon mechanisms (right side). Sources or processes by which some of the fuel escapes normal combustion are shown as boxes at the top of the diagram. In-cylinder oxidation, retention in the cylinder, and oxidation in the exhaust port and manifold, and catalyst are shown in sequence below. Numbers in parenthesis denote the HC emission index (% of gasoline entering the cylinder each cycle) for each step in the total process.

CHAPTER 2
EXPERIMENT

2.1 Concept

Previous investigations have been aimed to indirectly investigated post-flame oxidation of crevice-stored hydrocarbons by changing parameters affecting the storage of these hydrocarbons and observing the changes in hydrocarbon emissions [16]. This approach relies on reasonably accurate models to relate these parameters to changes in the hydrocarbon source. The approach in this work was therefore to develop a method to add a quantifiable amount of hydrocarbons into the post-flame cylinder gases in a manner representative of hydrocarbon sources in gasoline engines and observe the effects on hydrocarbon emissions. Initially, mechanical injection of hydrocarbons into the burned gases was considered, but rejected as difficult to implement and, moreover, to insure that the injection of hydrocarbons would produce mixing rates typical for normal hydrocarbons sources. The solution was found by realizing that by adding the hydrocarbon of interest as a dopant to the bulk oil, the oil layer itself could be used as a source of hydrocarbons. The dopant desorbs from the oil into the cylinder, when the lubricant layer is exposed to the cylinder gases. In the initial experiments, the engine was fired with methane, while the lubricant oil was doped with toluene, but the resultant changes in the overall emission levels were too small to determine accurately. A compromise was found by firing the engine with hydrogen, which isolated the hydrocarbons desorbing from the lubricant oil layer as the only source of carbon in the engine, and allowed the direct measurement of the oxidation levels by measurements of hydrocarbon concentrations, carbon monoxide and dioxide.

The experiment apparatus to measure the extent of post-flame oxidation is described in Fig. 2.1. The lubricant oil was doped by continuously adding a liquid hydrocarbon such as toluene or isooctane upstream of the oil pump. The hydrocarbon dopant was transported with the oil to the cylinder wall, where the dopant desorbed from the oil layer producing CO, CO_2 and HC emissions. The engine was fired with hydrogen, thus isolating the desorbed dopant as an identifiable source of hydrocarbons and oxidation products. However, in contrast with operation with hydrocarbon fuels, the dopant in the experiment desorbed from the oil layer not only during the expansion and exhaust strokes, but during all four strokes of the engine cycle and was oxidized both during flame passage and in the post-flame gases. The desorbed and partially oxidized dopant was transported out of the cylinder with the rest of the charge into the exhaust system, where the concentrations of HC, CO and CO_2 were measured.

A realistic post-flame environment was provided by firing the engine at typical speed and load on a hydrogen-air mixture and nitrogen dilution. Timing the spark so the quicker burning hydrogen mixture reached maximum pressure at the same time as a gasoline fired engine operated at MBT assured a similar pressure and temperature evolution during the expansion stroke. (Fig 2.2). During normal operation of a spark-ignition engine, hydrocarbons are absorbed into the oil layer as the unburned mixture is compressed in the combustion chamber, and desorbed as the partial pressure of hydrocarbons in the burned gases becomes negligible after flame passage. The experiment in Fig. 2.1 reproduced part of this process by allowing the desorption of typical hydrocarbon fuel species from the oil during the expansion and exhaust stroke.

2.2 Equipment

The experiments were carried out in a single cylinder of a modified 4-valve, 2-liter, 4-cylinder Nissan engine. The intake and exhaust of the number four cylinder were separated from the other three cylinders, allowing the number four cylinder to fire, while the others were motored. The engine was supplied with hydrogen, air and significant amounts of nitrogen dilution in order to vary the oxidizing environment and extend the operating range on hydrogen (Fig. 2.1). Pre-ignition of the fresh mixture by the hot residual gases during the intake process was minimized by timed injection of hydrogen through a tube at the intake valve seat during the intake stroke. The oil was doped continuously via a 1.6 mm OD stainless steel line connecting a pressurized bottle of liquid fuel to the intake of the engine oil pump. Oil samples were drawn from the pressurized lubricant circuit downstream of the pump.

The engine was instrumented to determine air, diluent and fuel flow rates, the exhaust gas concentrations and the engine operating state (Fig. 2.1). The air flow rate was measured with a Kurz flow meter (505-9A-02). The dilution mass fraction (X_D = mass diluent N_2/total mass) was determined from the molar oxygen concentration measured in the intake before the throttle with an NTK oxygen/lambda meter (NTK M0-1000)[1]. The fuel flow rate was determined with a second oxygen/lambda meter (Horiba Mexa-110λ) mounted in the exhaust. The exhaust hydrocarbon concentration was measured with a Rosemount Total Hydrocarbon Analyzer. Carbon monoxide was measured with a Beckman 864 analyzer, and carbon dioxide with a Rosemount 880A analyzer, after removing the water from the exhaust sample by passing the gas through a cold trap and a Dryerite® filter. Engine diagnostics included dynamic cylinder pressure measurements (Kistler model 6051A) and temperature measurements of the engine coolant out, oil

---

[1] The nitrogen dilution can be determined by from inlet oxygen molar concentration of the air-nitrogen mixture (Y_{O2I}) as

$$X_D = \left(\frac{0.21}{Y_{O2I}} - 1\right) M_{N2} \Bigg/ \left(M_{air} + \left(\frac{0.21}{Y_{O2I}} - 1\right) M_{N2} + 2 \cdot 0.21 \phi M_{H2}\right)$$

where M_i is the molecular weight of each species, and ϕ is the fuel-air equivalence ratio.

temperature in the pan, exhaust temperature and top of the cylinder liner temperature (type K thermocouples).

The motored experiments were all run with oil from a single drum of Penzoil 10W-30 multigrade lubricant oil. The fired experiments were run with oil from a single drum of Chevron 10W-30 oil. The dopant mass fraction (X_f) in the oil samples was determined with a HP5890 gas chromatograph using a 15 m HP-50+ column. Dopant mass fractions in the experiment ranged from two to eight percent, which were of the same order as those expected in firing gasoline engines. Murakami and Aihara reported in 1991, fuel concentrations in the oil sump of 2% and 6% for a gasoline engine running for 8 hours at coolant temperatures of 80 °C and 40 °C respectively [20].

2.3 Procedures

In fired experiments, the engine was fired with a mix of air, hydrogen and nitrogen until the cylinder liner, coolant and exhaust temperatures were stabilized. An oil sample was drawn for later analysis of the dopant mass fraction in the oil. The oil samples were stored in a closed container in a refrigerator between the time of collection and analysis. The exhaust gas concentrations of HC, CO and CO_2 were recorded along with the operating conditions. The mass of dopant desorbed from the oil layer and the fraction surviving per cycle were then calculated from the measured concentrations of HC, CO and CO_2, the total mass flow rate and the engine speed.

In addition to fired experiments, motored experiments were performed to measure the rate of desorption in a better characterized thermal environment. In the motored experiments the engine was heated to the desired coolant temperature by firing with methane. Once the coolant reached thermal steady state, an oil sample was drawn, the throttle was fully opened and the fuel supply shut off. Data were recorded after allowing the engine to motor for two minutes to achieve steady state during which time the wall temperature relaxed to approximately the coolant temperature. Finally the throttle was again partially closed and the fuel flow restarted, allowing the engine to fire. This procedure minimized the leakage of oil from the ring pack into the cylinder by motoring for a minimal amount of time (approximately three minutes) and at wide-open throttle.

In some of the fired experiments, the hydrocarbon concentration of the gas exiting the cylinder was sampled with a Fast Response FID to investigate the transport of hydrocarbons from the cylinder walls to the exhaust valve seat. The Fast Response FID (Cambustion Inc.) has a response time on the order of a millisecond and is known simply as a fast FID. The sampling tube was placed very close to the exhaust valve seat as noted in Fig. 2.1. The output signal was calibrated before starting the engine by flowing nitrogen into the cylinder from the spark plug hole with the exhaust valves open to provide a zero signal. Next the gain on the FID was set, while flowing 4500 ppmC1 span gas into the cylinder.

2.4 Experimental conditions

The operating conditions in the fired experiments were varied one parameter at a time about a baseline condition, which is a mid-speed, mid-load condition representative of the operating conditions during the Federal Testing Procedure (FTP). Five dopant species were selected: toluene, p-xylene, isooctane, hexane and methyl *tert.*-butyl ether (MTBE). The dopants cover an order of magnitude range in oil solubilities and a wide range in chemical reactivities. It was thought that the solubility of dopant in the oil, which affects the rate of emergence into the cylinder, and the chemical reactivity of the dopant would be the important fuel parameters. All the operating conditions were tested with the toluene dopant and most of these were repeated with the isooctane dopant (Table 2.1). The fuel-air ratio and dilution levels were varied for each of remaining dopants: p-xylene, hexane and MTBE. A total of 96 fired and 38 motored data points were recorded. The results are listed in Appendix A.

Table 2.1 Test conditions

test \ dopant	toluene C_7H_8	isooctane i-C_8H_{18}	p-xylene C_8H_9	hexane C_6H_{14}	MTBE $C_5H_{10}O$
$\phi = 0.75, 0.95, 1.2$	X	X	X	X	X
$X_D = 0.0, 0.2, 0.4$	X	X	X	X	X
$P_m = 2, 3, 3.6\ 4$ bar	X	X			
$\theta_{rs} = -10, 0, 10$	X	X			
N = 1000, 1500 rpm	X				
$T_{cool} = 40, 60, 90\ ^{\circ}C$	X				

Baseline: $\phi = 0.95$, $X_D = 0.2$, $\theta_{rs} = 0$, $P_m = 3.6$ bar, N = 1500 rpm and $T_{cool} = 90\ ^{\circ}C$.
ϕ : fuel-air equivalence ratio
X_D : molar fraction of added N_2 diluent
θ_{rs} : spark timing relative to timing that produces a maximum pressure 17 °ATC.
P_m: indicated gross mean effective pressure
T_{cool} : coolant temperature

2.5 Data analysis

The fraction of the dopant desorbed after the end of combustion that survives through the exhaust as hydrocarbon (f_{HC}) was chosen as the metric of post-combustion oxidation. The fraction of desorbed dopant surviving in these experiments is analogous to the fraction of stored hydrocarbons in a gasoline engine that survives to produce engine-out emissions. Therefore the trends in f_{HC} with operating conditions and dopant species can be compared to the trends in hydrocarbon emissions from gasoline engines in order to separate oxidation effects (as measured by f_{HC}) from source effects.

Changes in hydrocarbon emissions with operating conditions or type of dopant represent changes in both the amount of hydrocarbon escaping oxidation during flame passage and the level of post-flame oxidation. In order to estimate the level of oxidation strictly after flame passage, the mass of dopant desorbed after the end of combustion (m_d) is defined as

$$m_d = \frac{m_c}{2}\frac{L_{EOC}}{L_s}, \qquad (2.1)$$

where m_c is the total mass of hydrocarbon desorbed, L_s is the stroke length and L_{EOC} is the amount of cylinder covered at the end of combustion (EOC). Equation 2.1 is based on two assumptions: a) all the dopant in the oil layer desorbs into the cylinder gases and b) the dopant in the oil layer is refreshed equally with each upstroke of the piston (i.e. no difference in oil replacement behavior during compression and displacement strokes). The result of these two assumptions is that half of the total dopant desorbed is desorbed with each revolution. The ratio of L_{EOC}/L_s is close to unity and accounts for the fact that some of the refreshed oil is exposed before the flame reaches the cylinder wall. It is assumed that this dopant desorbs and is consumed as the flame arrives at the wall. The timing of EOC is determined from an averaged trace of 100 cycles of pressure data, by noting where the pressure-volume plot becomes a flat line on a log-log plot. The fraction surviving then is simply the mass of hydrocarbons in the exhaust over the mass of dopant desorbed after EOC or post-flame

$$f_{HC} = \frac{m_{HC}}{(m_c/2)(L_{EOC}/L_s)}. \qquad (2.2)$$

The total amount of dopant desorbed is calculated by summing the total carbon contained in hydrocarbons, carbon dioxide and carbon monoxide and converting to the equivalent amount of dopant mass,

$$m_c = \frac{M_{HC}}{c_n}\left[Y_{HC}\frac{m_e}{M_e} + \frac{m_{de}}{M_{de}}\left(Y_{CO} + Y_{CO2} - Y_{CO2Ad}\right)\right] \qquad (2.3)$$

where Y_{HC}, Y_{CO} and Y_{CO2} are the molar concentrations of hydrocarbons (in ppmC1), carbon monoxide and carbon dioxide respectively, m_e and m_{de} are the mass flow rates of wet and dry exhaust gases, M_{HC}, M_e and M_{de} are the molecular masses and c_n is the carbon number of the hydrocarbon dopant. The ambient CO_2 concentration in the dry exhaust gas (Y_{CO2Ad}) is determined by motoring the engine and correcting for the water removed from the burned gas during fired experiments. The mass of hydrocarbon surviving is then

$$m_{HC} = Y_{HC}\left(\frac{m_e}{M_e}\right)\left(\frac{M_{HC}}{c_n}\right). \tag{2.4}$$

In the motored experiments, the mass fuel desorbed (m_c) is determined from the air mass flow rate (m_{air}) and the hydrocarbon concentration in the exhaust (Y_{HC})

$$m_{HC} = Y_{HC}\left(\frac{m_{air}}{M_{air}}\right)\left(\frac{M_{HC}}{c_n}\right). \tag{2.5}$$

These calculations are described in greater detail in Appendix B.

2.6 Uncertainty analysis

The data interpretation is based on two important assumptions that will be examined in this section. The first is that the desorbed dopant is the only source of carbon species in the exhaust. The second is that when the flame passes through the cylinder all the desorbed dopant is oxidized to complete oxidation products.

The only other possible source of carbon in the cylinder is vaporized or partially oxidized oil. The oil contribution to carbon species in the exhaust was evaluated by firing the engine with hydrogen and using fresh undoped oil. At warmed up conditions, ($T_{cool} > 88$ °C), 6.4 to 14.4 μg of oil were consumed per cycle, of which approximately 0.25 to 1.0 μg /cycle was in the form of hydrocarbons. These values represent approximately ten percent of the typical values seen in fired experiments with doped oil. However, even if the effect of oil is neglected, the resulting errors in m_{HC} and m_c tend to cancel each other out in the calculation of f_{HC} (eqn. 2.1). Including both corrections to m_{HC} and m_c would change the value of f_{HC} by less than three percent for 80% of the cases and less than 6% for the rest, except for three cases, in which the amount of dopant desorbed was quite low. As the level of oil oxidation could not be measured during the actual doped oil experiments, but only estimated from previous clean oil experiments, the effect of oil oxidation was simply included in the uncertainty analysis. Incidentally, the oil consumption rate measured for the Nissan engine of 0.08 to 0.18 mg/s per cylinder is quite low compared to typical values of 0.6 to 0.8 mg/s [21]. It was found in similar motored experiments with undoped oil that the contribution of oil to exhaust hydrocarbons is negligible due perhaps to the lack of hot reactive combustion gases near the oil layer.

In order to estimate the fraction of desorbed hydrocarbon remaining in the cylinder after flame passage, an estimate for the quench distance can be made from scaling suggested by Kuo [22] and published quench distance for hydrocarbon flames. The two-plate quench distance (δ_{2P}) scales with the flame speed (S_L) and thermal diffusivity (α) as

$$\delta_{2P} \propto \frac{\alpha}{S_L} . \tag{2.6}$$

Therefore an estimate of the quenching distance for hydrogen can be made from the quench distance for hydrocarbons in internal combustion engines as

$$\delta_{2P}\big|_{H_2} = \delta_{2P}\big|_{HC}\left(\frac{S_L}{\alpha}\bigg|_{HC} \cdot \frac{\alpha}{S_L}\bigg|_{H_2}\right) \tag{2.7}$$

Table 2.2 lists the flame speeds, thermal diffusivity and quench distance of propane and hydrogen. The flame speed and thermal diffusivity were evaluated at a typical wall temperature (90 °C) and cylinder pressure at the end of combustion (20 bar). The flame speeds were evaluated from Milton and Keck [23] and the two-plate quench distance for propane in engines from Heywood [21] and Sterlepper *et al* [24].

Table 2.2 Two-plate quench distance

Fuel	δ_{2P} (m)	S_L (m/s)	α (m^2/s)
Propane	$1.0 \cdot 10^{-3}$	0.30	$1.06 \cdot 10^{-6}$
Hydrogen	$4.4 \cdot 10^{-5}$	6.27	$0.98 \cdot 10^{-6}$

The resulting two-plate quench distance of 0.044 mm is less than the typical 0.1 mm thickness of the piston crevice volume. Thus any dopant desorbed into the piston crevice and other crevices should be consumed by the flame as it penetrates these crevices. The single plate quench distance (δ_{1P}) is approximately one-fifth of the two-plate quench distance [25] so the wall quench thickness is 0.009 mm, a value approaching the roughness of the piston crown and cylinder head. The mass of unburned hydrocarbons can then be estimated by assuming the dopant is uniformly distributed in the combustion chamber except for the oil covered cylinder wall where the dopant concentration is assumed to be in equilibrium with initial dopant concentration in the oil. The mass of dopant in the quench layers (m_q) on the cylinder head, piston crown and cylinder wall can then be calculated as

$$m_q = \left[2\left(\frac{m_c/2}{m_e} \right) \rho_{max} \frac{\pi B^2}{4} + \frac{X_f H^* M_{HC}}{P_{max} M_e} \rho_{max} \pi B (L_s - L_{EOC}) \right] \delta_{1P} \tag{2.8}$$

where m_c and m_e are the mass desorbed and exhaust mass, ρ_{max} is the density evaluated at maximum cylinder pressure (P_{max}) and the wall temperature ($T_w = T_{cool}$), X_f is the dopant mass fraction in the oil, H^* is a modified Henry's constant and B is the cylinder bore. At warmed up conditions, the dopant mass is a linear function of the dopant mass fraction in the oil as will be shown in Chapter 3. Evaluation of m_q/m_c from eqn. 2.8 at warmed up conditions results in a value of less than 2% for the fraction of desorbed mass that survives flame passage in the wall-quench layer.

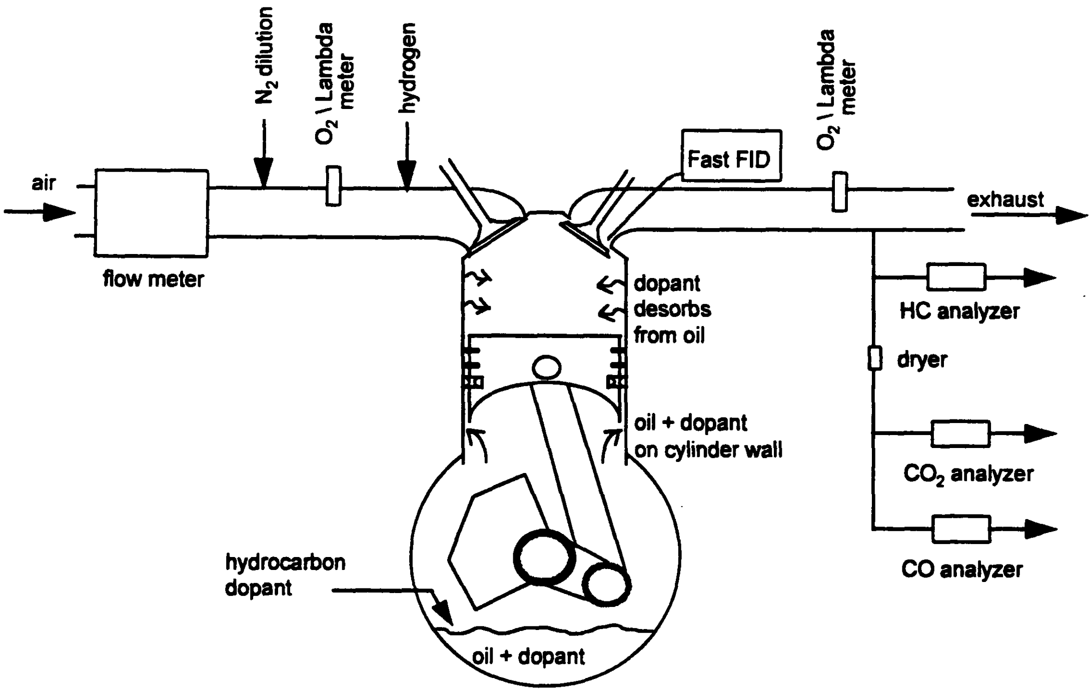

Fig. 2.1 Schematic of experiment.

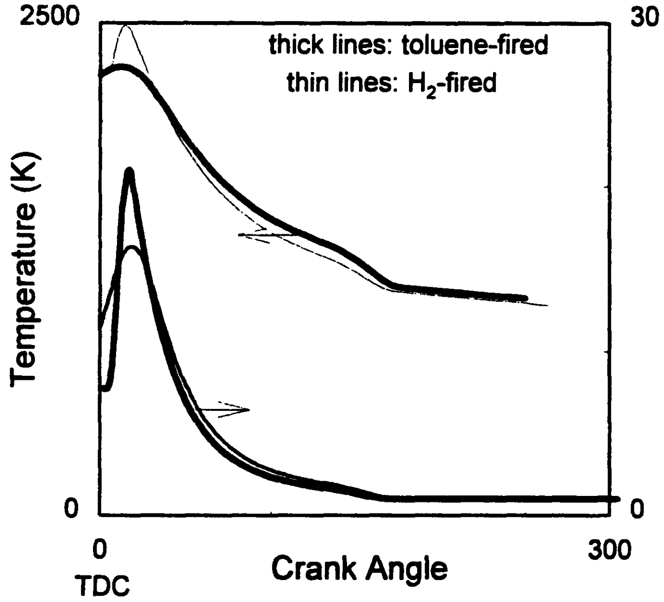

Fig. 2.2 Predicted cylinder pressure and gas temperatures for toluene-fired and H$_2$-fired engine with desorption at 1500 rpm, IMEP = 3.7 bar, T_{wall} = 100 °C and T_{cool} = 85 °C.

CHAPTER 3

DESORPTION EXPERIMENTS

In order to understand the characteristics of the hydrocarbon emergence process in the fired experiments, the rate of desorption of dopant from the oil layer was measured as a function of cylinder liner temperature and engine speed for three dopants: toluene, m-xylene and hexane. These hydrocarbons were chosen for their wide range of solubilities in oil. Toluene is 2.5 times and hexane is 10 times less soluble than m-xylene in oil at a coolant temperature of 90 ^{o}C. In this chapter, desorption test data for the three dopant species are presented as a function of cylinder wall temperature and engine speed. Data was collected primarily for motored experiments and a few fired experiments that demonstrated no observable differences between the two cases. Next, a scaling analysis is presented that offers a possible explanation of the most of the desorption data that are not consistent with a diffusion limited process. Finally, an analytical model based on the infinite plate solution of the diffusion equation is presented and compared to the measured values.

3.1 Desorption data

Effect of cylinder liner temperature

The experimental results in this chapter are normalized by the measured dopant mass fraction in the bulk oil. Experiments showed the amount of dopant desorbed from the oil is proportional to the concentration of the dopant in the bulk oil (X_f) for a range of operating conditions and dopant mass fractions (Fig. 3.1). The dopant mass fraction in the bulk oil varied from 1 to 8 percent in the tests, which is typical of gasoline concentrations expected in the oil of standard S.I. engines[20].

The results in Fig. 3.2 show the measured mass of total hydrocarbon desorbed from the oil layer as a function of the cylinder liner temperature and engine speed for the three dopant species tested. The wall temperature was taken as the average of the liner temperature at the top of the cylinder and the coolant temperature. The uncertainty in the scaled mass of dopant desorbed (m_c/X_f) is ±14% for the motored experiments and ±17% for the fired experiments. The largest sources of error are the repeatability of the chromatography results (±10%) and the air mass flow measurement (±8%).

The desorption characteristics were observed to be different for each dopant (Fig. 3.2a). For toluene, the scaled mass of dopant desorbed per cycle increases slightly with wall temperature at low temperatures up to a maximum, then decreases. For m-xylene, the mass desorbed changes little with temperature, and for hexane it decreases steadily with liner temperature. If the desorption process were controlled only by diffusion, one would expect that an increase in liner temperature would lead to increased desorption, since the diffusivity of dopant in the oil and gas and the solubility are increasing functions of temperature. However, as will be shown later, above a certain temperature for each dopant, desorption is not limited by the diffusion rate but solely by availability of dissolved dopant in the exposed oil layer.

The desorption characteristics in fired and motored experiments were equivalent, despite different pressure traces and cylinder gas temperatures (Fig. 3.2a). This good agreement indicates that the amount desorbed is not diffusion-rate limited and the transport of doped oil from the oil control ring to the cylinder liner is not strongly affected by the cylinder pressure.

Effect of engine speed

The effect of engine speed on the desorption of hydrocarbon dopants from the lubricant oil depends on the cylinder liner temperature and the dopant species, as shown in Fig. 3.2b. The amount of toluene desorbed remained constant or declined slightly with engine speed when the wall temperature was 32 ^{o}C. At a wall temperature of 72 ^{o}C, however, the desorption of toluene increased with engine speed. Tests with m-xylene showed a similar trend, where higher speed decreased desorption at 37 ^{o}C, but increased desorption at 75 ^{o}C. Hexane showed a consistent increase in desorption with engine speed at temperatures 37 ^{o}C and 48 ^{o}C. Again, an increase in desorption with engine speed is not consistent with a diffusion limited process, but is consistent with the expected increase in oil layer thickness at higher speeds, as discussed below.

3.2 Scaling of desorption with oil thickness

Since the dependence on speed and temperature do not scale with diffusion rate limits, an alternative explanation must be sought. One possible explanation is that at sufficiently high temperatures the time required for all of the dopant to desorb from the oil layer is significantly less than the available time during one revolution. At such temperatures all the dopant desorbs out of the oil layer and the amount desorbed is limited by the amount of dopant in the oil layer. Depletion of dopant from the oil layer occurs because the dopant diffusivity in the oil becomes higher, the solubility lower and the oil layer thinner at higher temperatures [26, 27, 28]. Under these conditions the mass of dopant desorbed per cycle (m_c) is equal to two times the mass of dopant initially in the oil layer per revolution (m_{CO}) ,

$$m_c = 2\, m_{co} = 2\, (\pi\, BL_s\, \delta_{avg}\, \rho_o\, X_f\, r_f), \qquad (3.1)$$

where B is the cylinder bore, ρ_o the oil density, and δ_{avg} is the oil layer thickness. The oil layer thickness is in general a function of axial position due to variations in the liner temperature and instantaneous piston speed along the cylinder liner. The factor r_f, which is the ratio of fuel concentration in the exposed oil layer to that in the bulk oil, is introduced to account for the fact that only part of the oil layer is replaced with each stroke. The mass of fuel desorbed (m_c) should then scale with the average oil layer thickness (δ_{avg}), if r_f is constant.

In order to explore whether the dominant parameter in dopant desorption was indeed the thickness of the oil layer, the scaling of the former with viscosity and speed was considered. The Reynolds equation predicts that the oil layer thickness should scale with the square root of the oil viscosity (μ) and engine speed (N) [26]. The standard Walther equation for viscosity was fit to data (Appendix C). Figure 3.3 shows the correlation between the scaled mass of dopant desorbed (m_c/X_f) and $(\mu N)^{0.5}$, for temperatures beyond the peak desorption rate shown in Fig. 3.2a and data points in Fig. 3.2b for which desorption increased with engine speed. The relative mass desorbed per cycle shows a strong linear dependence on $(\mu N)^{0.5}$ over a wide range of temperatures, engine speeds and dopant species.

The experimental values for the scaled mass of dopant desorbed (m_c/X_f) can be used to estimate r_f by substituting an expression for the oil thickness, (eqn. C.4) into eqn. 3.1 and solving for r_f. The ratio of dopant concentration in the wall film to that in the bulk oil (r_f) estimated by this method is 0.12±0.02 for toluene and m-xylene and 0.10±0.01 for hexane. The difference in values may be explained by recognizing the much more volatile hexane desorbs out of the oil and into the crankcase below the piston, thus reducing the amount of hexane transported to the cylinder oil layer. Supporting this assumption are measurements of the crankcase system from the positive crankcase ventilation line, which revealed that the concentration of hydrocarbons in the crankcase was 20 to 60% higher for hexane than for toluene.

Our measurements showed that viscosity was reduced by 10 percent for every percent of dopant added to the oil for toluene and xylene and by 13 percent for hexane. Although the bulk oil dopant concentrations ranged from two to eight percent by mass, the dopant concentration in the oil layer is less than one percent as the ratio of dopant concentration in the cylinder wall oil layer to the bulk oil (r_f) is approximately 0.1. The resulting five to ten percent decrease in the oil layer thickness was taken into account in the results shown in Fig. 3.3.

3.3 Analytical model of desorption

In order to understand the oxidation of the emerging hydrocarbons a model was developed to predict the rate of desorption of the dopant desorbing from the oil layer. The desorption process can be modeled as one-dimensional diffusion of dopant through the oil layer, with an impermeable wall on one boundary and a convective boundary condition at the gas-oil interface. The solution for the non-dimensional dopant concentration field θ^* can be found in standard texts as [29]:

$$\theta^* = \sum_{n=1}^{\infty} C_n e^{(-\zeta_n^2 Fo)} \cos(\zeta_n x^*) \qquad (3.2)$$

where

$$C_n = \frac{4\sin\zeta_n}{\zeta_n + \sin(2\zeta_n)}, \qquad \zeta_n \text{ are the positive roots to } \zeta_n \tan(\zeta_n) = Bi,$$

$$\theta^* = \frac{\theta}{\theta_i} = \frac{X_o - X_{le}}{X_{oi} - X_{le}}, \qquad x^* = \frac{x}{\delta_o(z)}, \qquad Fo = \frac{D_o t}{\delta_o{}^2},$$

$$Bi = \frac{H_D \delta_o(z)}{D_o} \qquad \text{and} \qquad H_D = h_D \frac{H^* M_{HC}}{RT\rho_o}.$$

The terms, x^*, Bi, Fo, H_D are respectively the non-dimensional distance from the gas-oil interface, Biot number, the Fourier number for the oil and the convective mass transfer including the gas-liquid interface resistance. The remaining terms are defined as follows: X_{oi} is the initial concentration of dopant in the oil, X_{le} the equilibrium concentration of dopant in oil relative to the bulk concentration in gas phase; t(z) the length of time each wall oil element at an axial distance z from the BDC position of the first compression ring is exposed to the cylinder environment, D_o the diffusion coefficient of the dopant hydrocarbon in oil, M_{HC} the molecular weight of the dopant, R the universal gas constant, T the absolute wall temperature, ρ_o the density of the oil and H^* a modified Henry's constant. The mass transfer coefficient h_D is the cycle averaged value obtained using the Colburn analogy and Woschni's engine heat transfer correlation [21]. An expression for the dopant diffusivity in the oil (D_o), the modified Henry's constant (H^*) and the oil layer thickness $\delta_o(z)$ can be found in Appendix C.

Higher order terms in eqn. (3.2) are negligible, so that the cumulative mass fraction desorbed per axial unit length can be obtained by integrating across the oil layer from $x^* = 0.0$ to 1.0 to yield the fraction of the initial mass desorbed at any position z and time t,

$$\frac{dm_c}{dm_{co}} = 1 - \frac{\sin(\zeta_1)}{\zeta_1} C_1 e^{(-\zeta_1^2 Fo)} \qquad (3.3)$$

where the terms ζ_1 and Fo are functions of δ and thus of z, dm_{co} is the mass of dopant available in a region dz of the oil layer ($dm_{co}=\pi$ B $\rho_o X_f \delta_o(z)$ dz) and dm_c is the mass of dopant desorbed per axial unit length during one revolution. The scaled mass of dopant desorbed per cycle (m_c/X_f) is calculated by integrating eqn. (3.3) over the stroke length and multiplying by two,

$$m_c/X_f = 2B\pi\rho r_f \int_0^{L_s}\left[1-\frac{\sin(\zeta_1)}{\zeta_1}C_1 e^{(-\zeta_1^2 Fo)}\right]\delta_o(z)dz\,. \qquad (3.4)$$

Comparison with data

The scaled mass of dopant desorbed (m_c/X_f) is compared to the results of the model in Fig. 3.4a. The model correctly predicts the existence of a peak in m_c/X_f as a function of temperature and the location of that peak. The measured slope of the mass of hexane desorbed as a function of temperature is steeper than predictions indicate. However, given the uncertainties and the simplicity of the model, the comparison is quite favorable.

The predicted and measured effects of engine speed on desorption are shown in Fig. 3.4b. The model under-predicts the desorption of xylene at the high speed, high temperature point for xylene, but otherwise captures the physics of the desorption problem and can therefore be used to predict the rate of desorption of dopant from the oil with some confidence.

Dopant desorption profiles

The oxidation of unburned hydrocarbons emerging from the various sources is very dependent on the temperature history experienced by the reactant. The evolution of the reaction of unburned hydrocarbons from the lubricant oil layer therefore depends heavily on the rate at which hydrocarbons emerge from the oil. The calculated time evolution of the axial distribution of the desorbed dopant is shown in Fig. 3.5 for toluene in the H_2-fired experiment. Each line represents the mass of dopant desorbed at a relative location along the cylinder liner from the time of initial exposure to burned gases to a given time. These desorption profiles start at zero for the most recently uncovered oil segment and increase until all the dopant is desorbed as shown by the 198 CAD line. The shape of the dopant fraction profile mirrors the axial profile of the oil layer thickness predicted by eqn. C.4. No dopant is assumed to desorb from the oil above the TDC position of the first compression ring as it is assumed that the oil in this region is not refreshed with dopant laden oil.

3.4 Conclusions

Experiments have characterized the desorption of dopant from the lubricant oil layer on the cylinder wall. At most of the wall temperatures tested (T_w>60 °C for m-xylene and >50 °C for m-xylene and >35 °C for hexane), the amount of dopant desorbed decreases with higher temperatures and lower engine speeds. This trend is consistent with the hypothesis that all the dopant present in the oil layer desorbs into the cylinder with each revolution, so that the mass desorbed scales with oil thickness. This hypothesis is supported by fact that both the amount of dopant desorbed and oil layer thickness in hydrodynamic lubrication scales with the square root of oil viscosity and engine speed. A simple analytical model including diffusion in the oil layer and the gas phase shows good agreement with the desorbed mass for all three dopants over a range of temperatures and engine speeds. This analytical model predicts that at warmer temperatures all of the dopant in the oil layer desorbs and that the desorbed dopant is evenly distributed along the length of the cylinder wall.

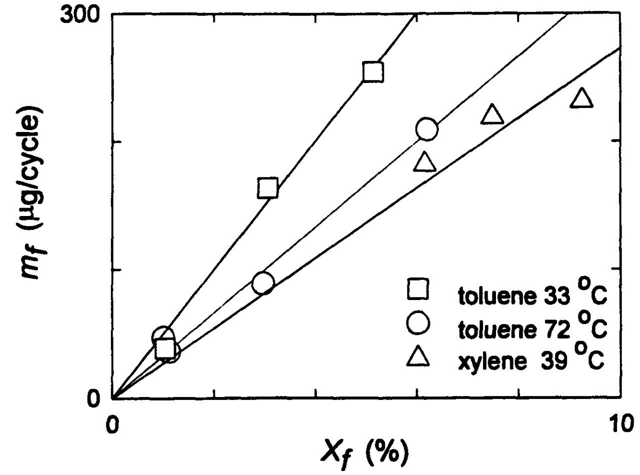

Fig. 3.1 Mass of dopant desorbed vs. dopant concentration in oil for 3 cases at 1500 rpm.

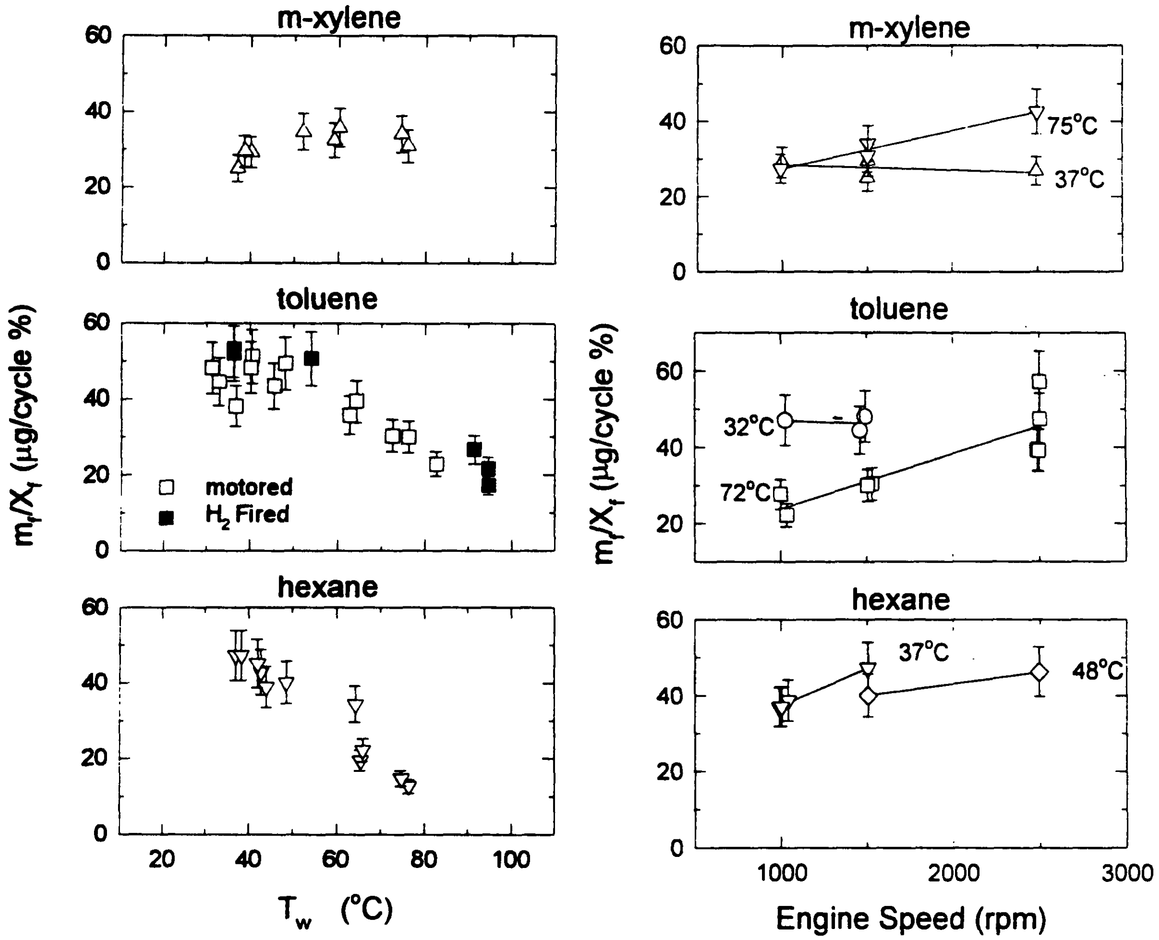

(a) (b)

Fig. 3.2 Mass of dopant fuel desorbed scaled by the dopant concentration in the bulk oil for motored and fired experiments. (a) motored data at 1500 rpm, WOT and fired data at 1500 rpm, IMEP = 3.7 bar. (b) motored data at WOT, cylinder liner temperatures as noted.

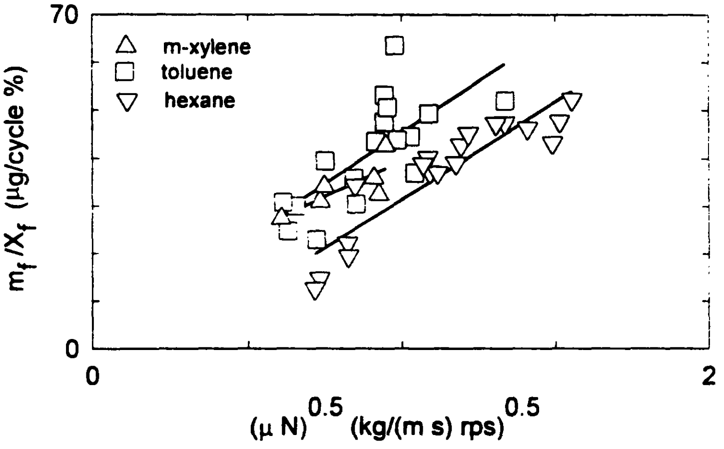

Fig. 3.3 Mass of dopant desorbed vs. square root of oil viscosity times engine speed in in motored experiments at WOT, N = 1000-2500 rpm and T_w = 50 to 80 °C for toluene, T_w = 56 to 80 °C for m-xylene, T_w = 35 to 80 °C for hexane, (lines are fits to data for each dopant).

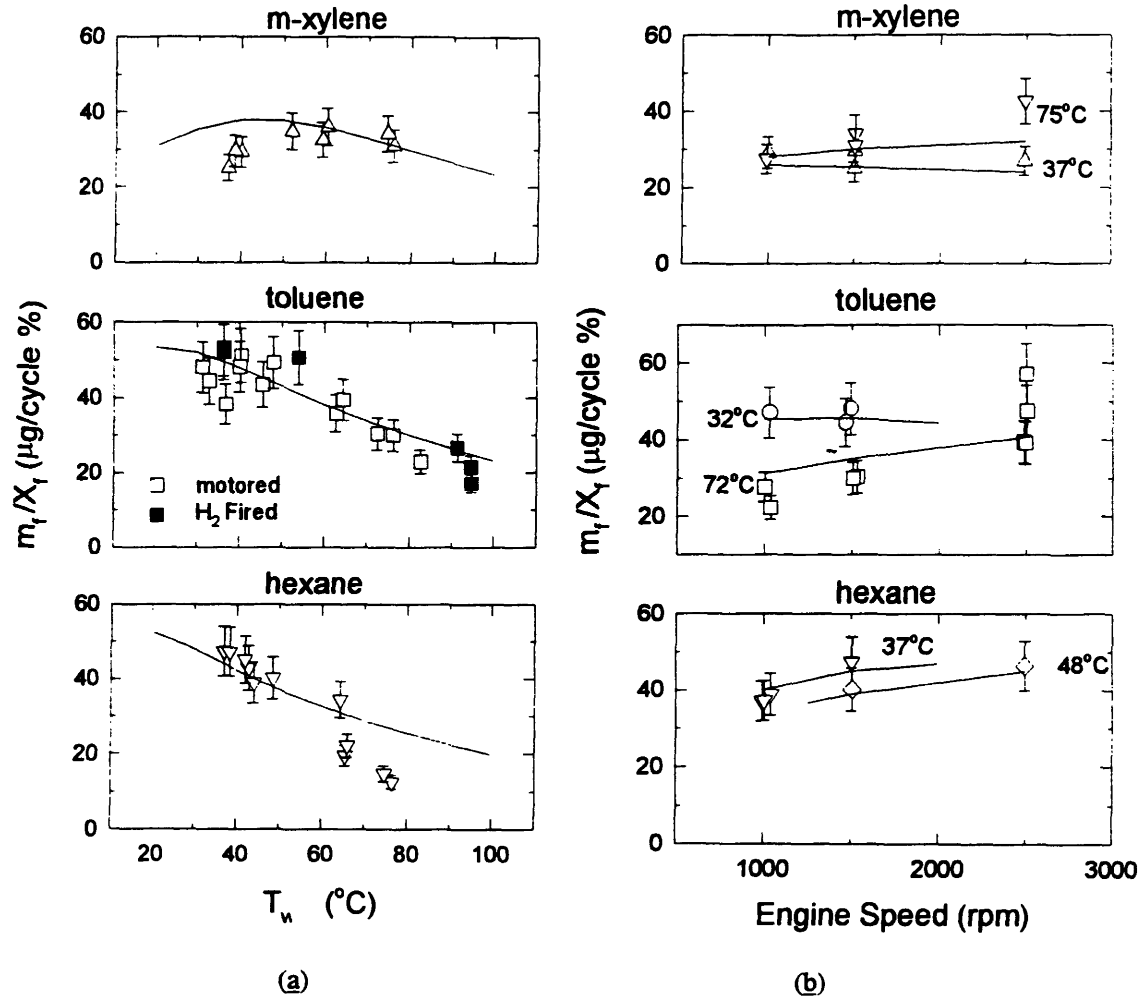

Fig. 3.4. Mass of dopant fuel desorbed scaled by the dopant concentration in the bulk oil for motored and fired experiments (symbols) and model (solid line). (a) motored data at 1500 rpm, WOT and fired data at 1500 rpm, IMEP = 3.7 bar. (b) motored data at WOT, cylinder liner temperatures as noted.

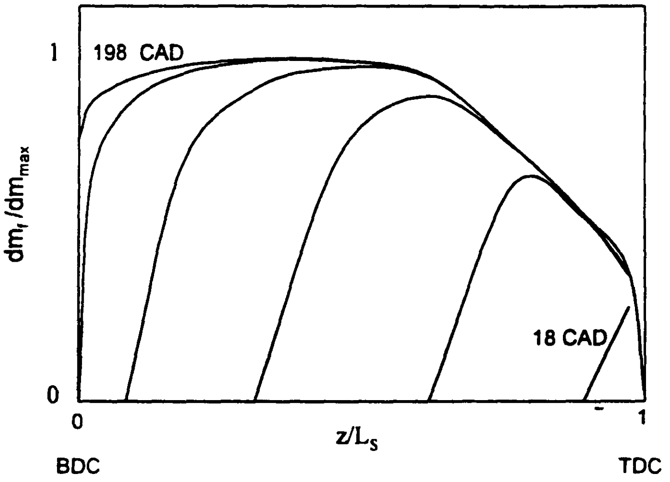

Fig. 3.5 Predicted dopant desorption vs. time and axial location for toluene in H_2 fired experiment at 1500 rpm, IMEP = 3.7 bar, T_w = 100 °C and T_{cool} = 85 °C. Lines represent the cumulative fuel desorbed normalized by the maximum available per unit axial length. The desorbed mass lines are plotted at intervals of 36 crank angles for the H_2 fired experiment. The interval between lines in the toluene fired engine is 20 crank angles. The labels TDC and BDC refer to the position of the first compression ring at top and bottom dead center.

CHAPTER 4

RESULTS FOR FIRED EXPERIMENTS

Experimental results for the fraction of post-flame desorbed dopant exiting the engine as hydrocarbons (f_{HC}) are presented in this Chapter as a function of operating conditions and dopant species. In addition, hydrocarbon concentration profiles were measured with a fast FID at the exhaust valve to gain insight into in-cylinder oxidation and flow conditions.

4.1 Oxidation results

Results are grouped by dopant species and reported in terms of the fraction of dopant desorbed from the oil after the end of combustion that exits the engine as hydrocarbons. The fraction of post-flame desorbed dopant surviving to the engine exit is plotted in Figs. 4.1 through 4.3 for different operating conditions (fuel-air ratios, dilution levels, load, engine speed, coolant temperature and spark timing) and different dopants (toluene, isooctane, p-xylene, hexane and MTBE) as listed in Table 2.1. The error bars were estimated from the estimated uncertainty in the O_2, HC, CO_2 and CO measurements. The fraction of desorbed dopant surviving varied between a low of 0.11 for the zero dilution MTBE case to a high of 0.52 for the 0.5 dilution, 4.1 bar IMEP toluene case. The range for f_{HC} at the baseline condition was from 0.13 for MTBE to 0.23 for toluene. The range is consistent with levels of post-combustion oxidation previously estimated for fuel-air sources ($f_{HC} = 0.14$) and for fuel-only sources ($f_{HC} = 0.29$) [1] (see Fig. 1.1).

Effect of operating conditions

The effect of changing the operating conditions is shown in Fig. 4.1 for the toluene dopant. The fraction surviving increases away from the stoichiometric point, due to colder temperatures on the lean and rich side and lack of oxygen on the rich side. Increased dilution also leads to lower temperatures and increased hydrocarbon survival, with the exception of the zero dilution case at 3.5 bar IMEP, for which an additional reduction in dilution produced no additional oxidation relative to the baseline case. One interesting result is for the baseline load case (IMEP = 3.6 bar), increasing dilution up to 0.20 had no effect on the fraction surviving.. However, the higher load case (IMEP = 4.1 bar) produced a constant rise in the fraction of dopant surviving for dilution levels from 0.05 to 0.40 (Fig. 4.1). In the case of toluene, engine load has a non-monatomic effect. The fraction surviving increases with IMEP from 3 to 4 bar, however the 2 bar value is approximately equal to the 3 bar value. Lower coolant temperatures (T_{cool}) results in less oxidation and a larger fractions of hydrocarbons surviving. The effects of increased speed and retarded spark timing, both of which lead to pronounced decreases in hydrocarbons emissions for gasoline engines, had little effect on the extent of oxidation in this experiment.

The results for isooctane dopant are similar to those for toluene (Fig. 4.2) except overall a lower fraction of isooctane dopant survives. Isooctane appears less sensitive to a lean fuel-air ratio than toluene, but has a similar response to a rich fuel-air ratio. Increasing the load produces an increase in the fraction surviving from an IMEP of 2 to 4 bar. The fraction of desorbed dopant surviving varied between a low of 0.14 for the 2 bar IMEP case to a high of 0.31 for the 1.15 fuel-air equivalence ratio case.

Similar behavior is observed for the other dopants tested, p-xylene, hexane and MTBE (Fig. 4.3). The fraction of dopant surviving increases as the burned gas mixture becomes leaner or richer. The fraction surviving shows little effect of dilution levels up to 0.2, beyond which the surviving fraction increases significantly.

The effect of operating conditions for all the dopant species is shown in Fig. 4.4. The results for different dopants were normalized by the average f_{HC} value at the baseline condition. In general the dopant species react similarly to changes in operating conditions.

Dopant effects

The effects of different dopants is shown in Fig. 4.5, where the fraction of dopant surviving is plotted for each dopant at a variety of operating conditions. Some of the data points are missing for the rich cases as not all dopants were tested at the same rich conditions. Clearly, the fraction of dopant surviving is a very strong function of dopant type and the ranking remains consistent: toluene has the lowest level of oxidation (highest fraction surviving), followed by p-xylene, isooctane, hexane and finally MTBE.

From the evidence above, the critical dopant parameter determining the fraction surviving appears to be the chemical reactivity of the dopant. In order to verify that hypothesis, calculated reaction times for three of the dopants were extracted from previous work [30]. The calculated times were obtained for oxidation of 1% dopant in an equilibrium mixture of burned gases at 1200 K and 1 bar, using a plug flow reactor model and full chemical kinetic mechanisms. The correlation between the calculated oxidation times and the fraction of hydrocarbons surviving (Fig. 4.6) clearly shows the impact of chemical reactivity.

Dopant solubility in the lubricant oil, appeared not to be critical at warmed-up wall temperatures (T_{cool}>88 °C). In principle, higher solubility results in delayed desorption of the dopant into colder burned gas, and might therefore lead to lower oxidation rates. However, there is little correlation between the solubility and the remaining fraction of hydrocarbons (Fig. 4.7). P-xylene is more than twice as soluble as toluene, yet survives at the same rate. Similarly, isooctane and hexane have the same survival rate despite the fact that isooctane is much more soluble than hexane. Finally, isooctane and toluene, which have similar solubilites, have very different survival rates.

4.2 Fast FID measurements

Fast FID measurements of the hydrocarbon levels at the exit of the cylinder were undertaken with two objectives in mind. The first was to gain insight into the physical process of oxidation and transport of hydrocarbons desorbing from the oil layer hydrocarbons. The second objective was to estimate the fraction of dopant that was retained in the residual gases by measuring the hydrocarbon concentration of the exhaust gases. The model for the residual gas retention of hydrocarbons based on these experiments is presented in Chapter 5. The present measurements were conducted using toluene dopant at nearly all operating conditions and three azimuthal locations near the valve seat.

A typical FID trace is plotted in Fig 4.8, which includes all the key features of the hydrocarbon traces seen in these experiments. The signal of 100 cycles was averaged and converted into a hydrocarbon concentration. The upper and lower thin lines are the average values $\pm\sigma$. The FID signal is plotted without correction for the transit time in the transfer tube, so the CAD values of the graph do not correspond to the actual cycle times. The signal was constant during the valve closed period before 350 CAD and after 625 CAD, as the mixture is too cold to oxidize in the exhaust port. Once the valve opens, the signal rises very briefly, then drops to nearly zero for the rest of the exhaust process until the end of the exhaust stroke, when the signal spikes up to a peak before dropping to the closed-valve value.

These hydrocarbon profiles are markedly different from hydrocarbon profiles recorded by other researchers in hydrocarbon fired engine [16, 32, 33]. Fast FID and sampling valve measurements in the exhaust port of hydrocarbon fired engines have shown two distinct peaks of hydrocarbons at the beginning and end of the exhaust with a non-zero hydrocarbon level through-out. In contrast, these experiments appear to generate a single hydrocarbon peak at the very end of the exhaust stroke (Figs. 4.8 through 4.10). Therefore, the evidence supports a physical mechanism where hydrocarbons emerging from the oil layer are oxidized close to the cylinder wall, and are not entrained in the bulk flow until the boundary layer is scarped by the piston.

A possible physical picture to describe the hydrocarbon trace at the valve seat is as follows. The rapid drop of the signal indicates that very little if any hydrocarbon material is near the cylinder head, when the exhaust valve opens. The nearly zero hydrocarbon level during the exhaust phase indicates no dopant is entrained during the blowdown and displacement exhaust. The peak at the end of the exhaust stroke is conventionally assumed to be the roll-up vortex that has formed as the piston scrapes off the hydrocarbon-rich boundary layer. At the end of the exhaust process, when the piston is near TDC (>560 CAD), part of the vortex is forced out of the cylinder producing a large signal. Next the intake valve opens, drawing back into the cylinder part of the hydrocarbon rich vortex mass (>590 CAD). The remaining hydrocarbons slowly mixes with the rest of the gases or perhaps oxidizes in the port to achieve the steady closed-valve value (600 to 630 CAD). The initial rise in the hydrocarbons signal at (350 CAD) is too small compared to the signal noise to be reliably interpreted.

The azimuthal variation in hydrocarbon levels at the valve seat is shown in Fig. 4.9 for three different positions. The signal was normalized by the average hydrocarbon levels in the engine-out exhaust (Y_e). Position (a) was the first position used and the data in Fig. 4.8 is also from this position. Next the sampling tube was moved to position (b) to get as close as possible to the cylinder wall. This position showed significantly higher peak hydrocarbon levels than position (a), but the same closed-valve value. Lastly, the sampling valve was placed in a position closest to the axial center line of the cylinder, position (c). Here the vortex peak was nearly absent and even the closed-valve value was considerable lower than for positions (a) and (b). It appears that the hydrocarbon rich vortex does not reach the far side of the valve. The fact that the closed-valve values for (c) are so much lower indicates that hydrocarbon stratification in the exhaust port survives into the next cycle. The difference between position (a) and (b) can be explained by the fact that (a) is somewhat further from the wall, so the measured concentrations reflect enhanced mixing and entrainment of core gases into the vortex.

Fast FID traces recorded at position (b) for motored operation are plotted in Fig. 4.10. The average of one hundred cycles is plotted, along with the highest and lowest values at each CAD. A trace for the baseline fired condition previously plotted in 4.9 is included for comparison. The hydrocarbon level in the motored experiment remains relatively high during the open valve period because dopant desorbed during the first revolution is not oxidized, mixes with the core gas and exits throughout the exhaust stroke. This is in contrast to the fired experiment, where the flame consumes the dopant desorbed during the first revolution and much of what desorbs after the flame passage is also oxidized. The highest peak hydrocarbon value for the 100 motored cycles is of the same order as the peak values seen in fired experiments. However, a hydrocarbon peak at the end of the exhaust stroke only occurred in 15 of the 100 motored cycles indicating that the vortex often broke down. The calculated Reynolds number for the vortex in the motored experiment is approximately 15,500, which is near the fully turbulent limit of 17,500 [31] as compared to the hotter fired experiment which had a Reynolds number approximately 5,000, well below the stable vortex upper limit of 12,500. The vortex in the motored experiments is turbulent and therefore more likely to breakdown than the laminar vortex in the fired experiments.

The general shape of the hydrocarbon traces at the valve seat was essentially constant for different operating conditions. The peak hydrocarbon concentration did show significant variation with operating conditions. The peak value is assumed to be the hydrocarbon concentration of the vortex, which will be used in the next chapter to estimate the fraction of hydrocarbon retained in the residual mass. Figure 4.11 shows the peak or vortex hydrocarbon levels (Y_v) normalized by the engine-out hydrocarbon level (Y_e) for 13 different operating conditions.

4.3 Conclusions

Experimental results for the fraction of post-flame desorbed dopant exiting the engine as hydrocarbons (f_{HC}) have been presented in this Chapter. At mid-speed, mid-load, warmed up conditions (baseline) the fraction of post-flame desorbed dopant exiting the engine as hydrocarbons (f_{HC}) varied from 15% for MTBE to 23% for toluene. Operating conditions had a significant effect on f_{HC} especially N_2 dilution, load, fuel-air equivalence ratios and coolant temperature. Engine speed and spark timing had little effect on f_{HC}. The fraction surviving was strongly dependent on dopant reactivity. A strong correlation was found between the extent of oxidation and the reactivity of the particular dopant, as expressed by current calculations of reaction rates. Therefore, reaction rates in the cylinder and exhaust port system are at least partially controlled by the chemical kinetic rates, rather than mixing rates.

Support for a physical picture of how hydrocarbons survive in these experiments was found in the measurements with a fast response FID mounted in the at the cylinder exhaust plane. All hydrocarbons desorbed before the passage of the flame are completely oxidized. A fraction of dopant desorbed after flame passage survives in the thin layer next to the cylinder wall and is scraped into a vortex at piston / cylinder corner and exits the cylinder at the end of the exhaust stroke.

In order to allow comparisons of this experimental data with a numerical model of in-cylinder oxidation, the fraction oxidized in-cylinder needs to be estimated, which is the subject of Chapter 5. The in-cylinder oxidized fraction will be estimated from the measured values for f_{HC} by developing models to estimate the fraction retained in the residual gas and fraction oxidized in the port.

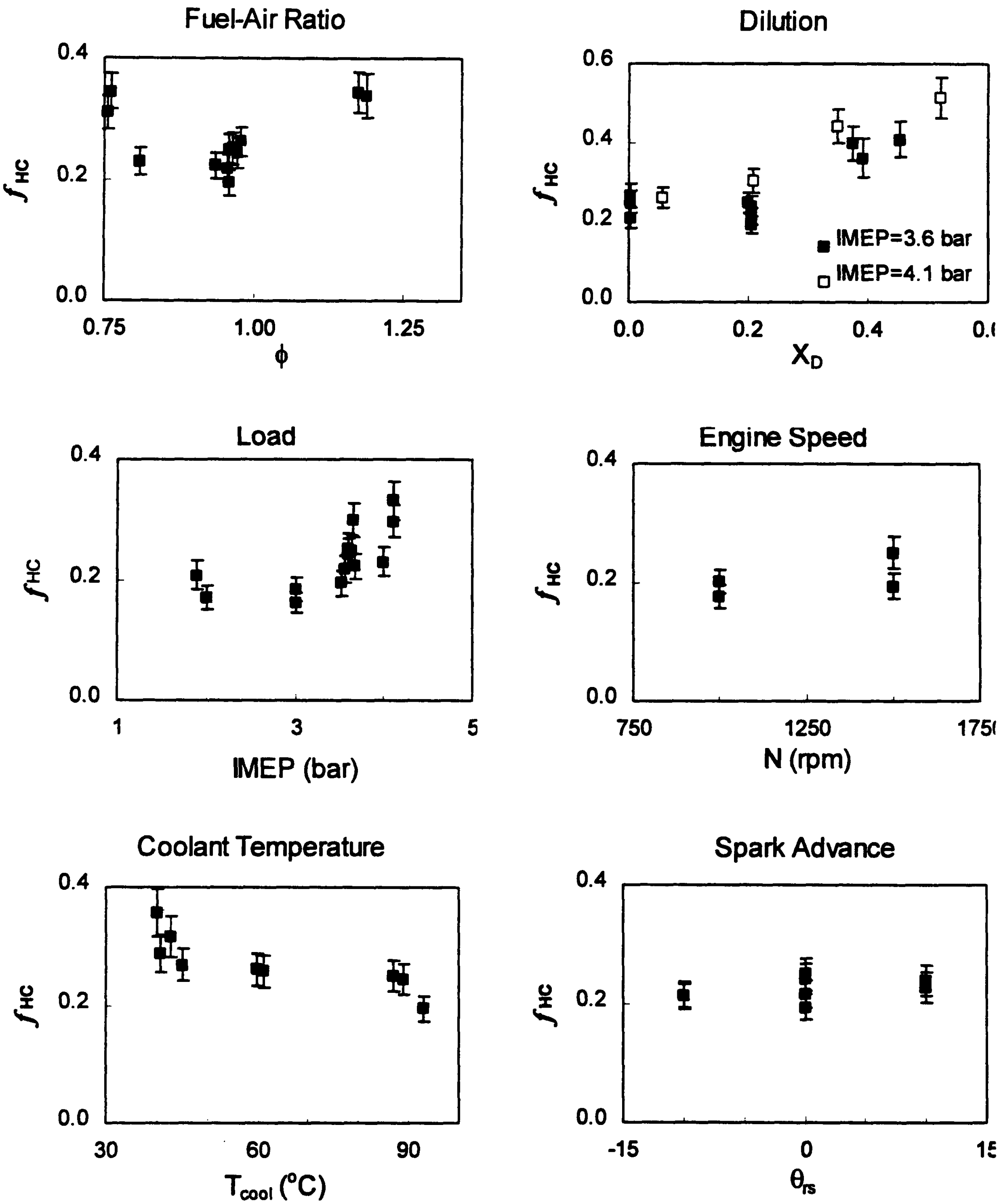

Fig. 4.1 Fraction of post-flame desorbed toluene surviving as hydrocarbon vs. operating conditions. The baseline condition is 1500 rpm, IMEP = 3.6 bar, MBT timing, $\phi = 0.95$, 20% dilution and $T_{cool} = 90$.

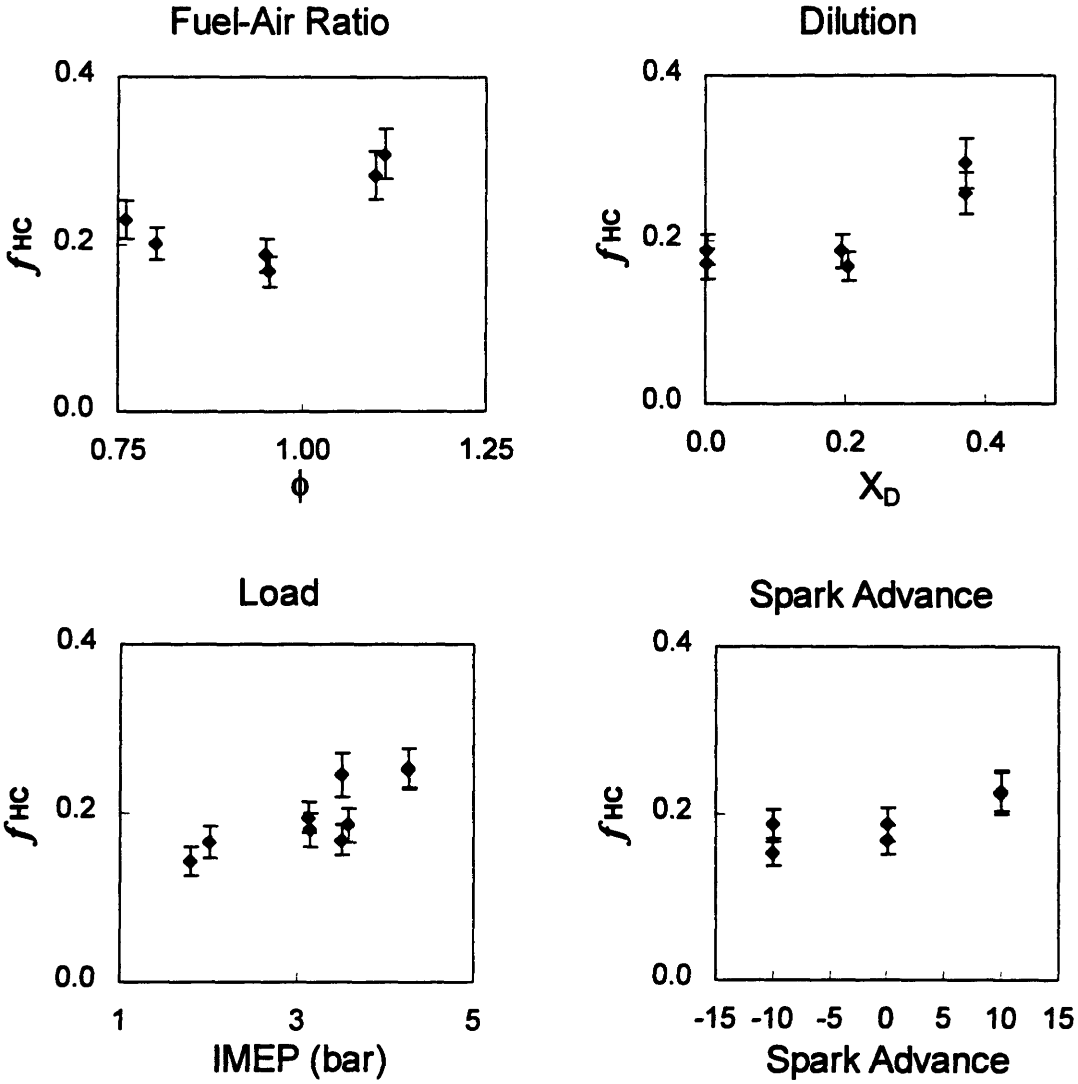

Fig. 4.2 Fraction of post-flame desorbed isooctane surviving as hydrocarbon vs. operating conditions. The baseline condition is 1500 rpm, IMEP = 3.6 bar, MBT timing, $\phi = 0.95$, 20% dilution and $T_{cool} = 90\ ^{\circ}C$.

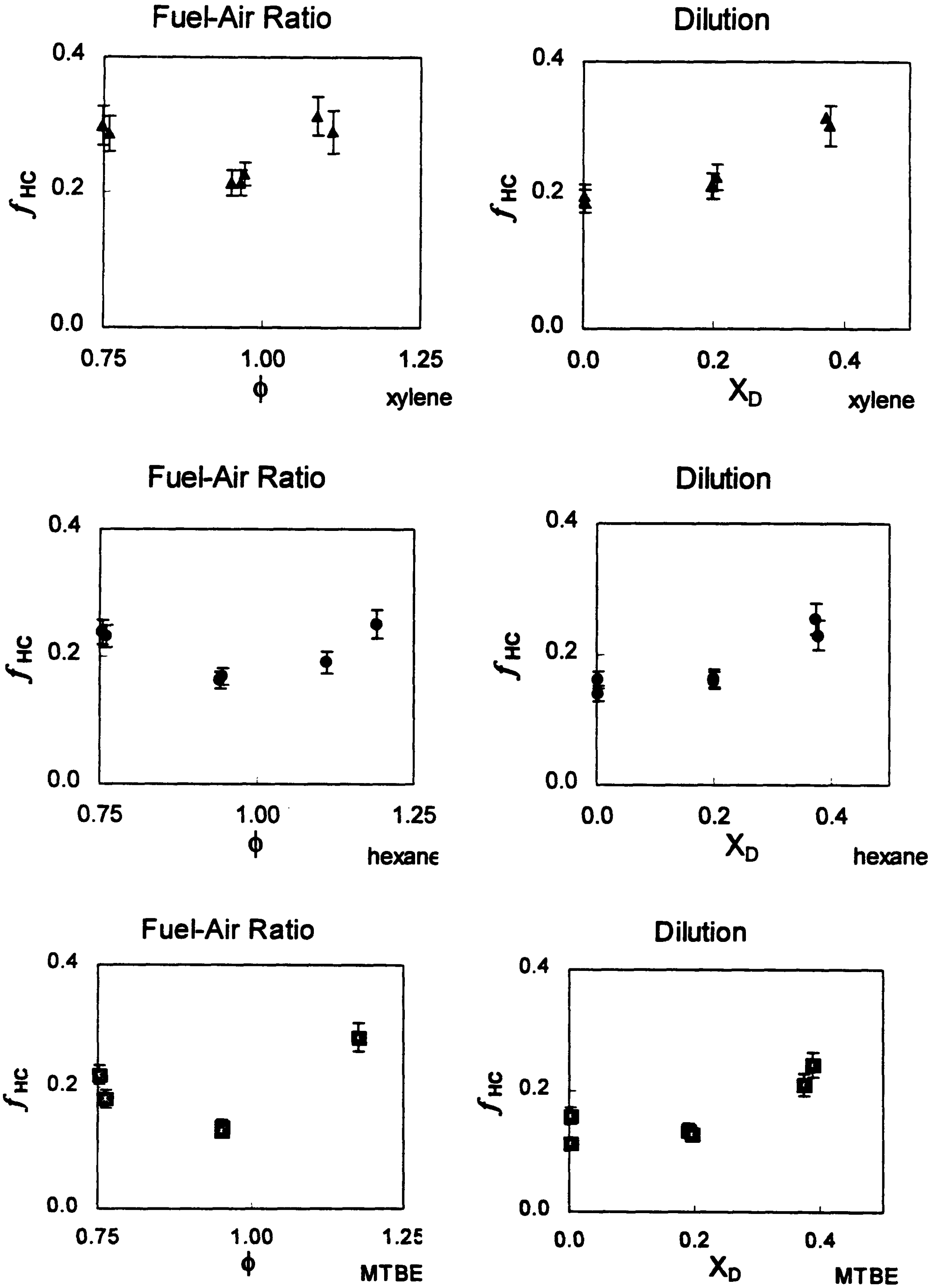

Fig. 4.3 Fraction of post-flame desorbed dopant (p-xylene, hexane and MTBE) surviving as hydrocarbon vs. operating conditions. The baseline condition is 1500 rpm, IMEP = 3.6 bar, MBT timing, ϕ = 0.95, 20% dilution and T_{cool} = 90 °C.

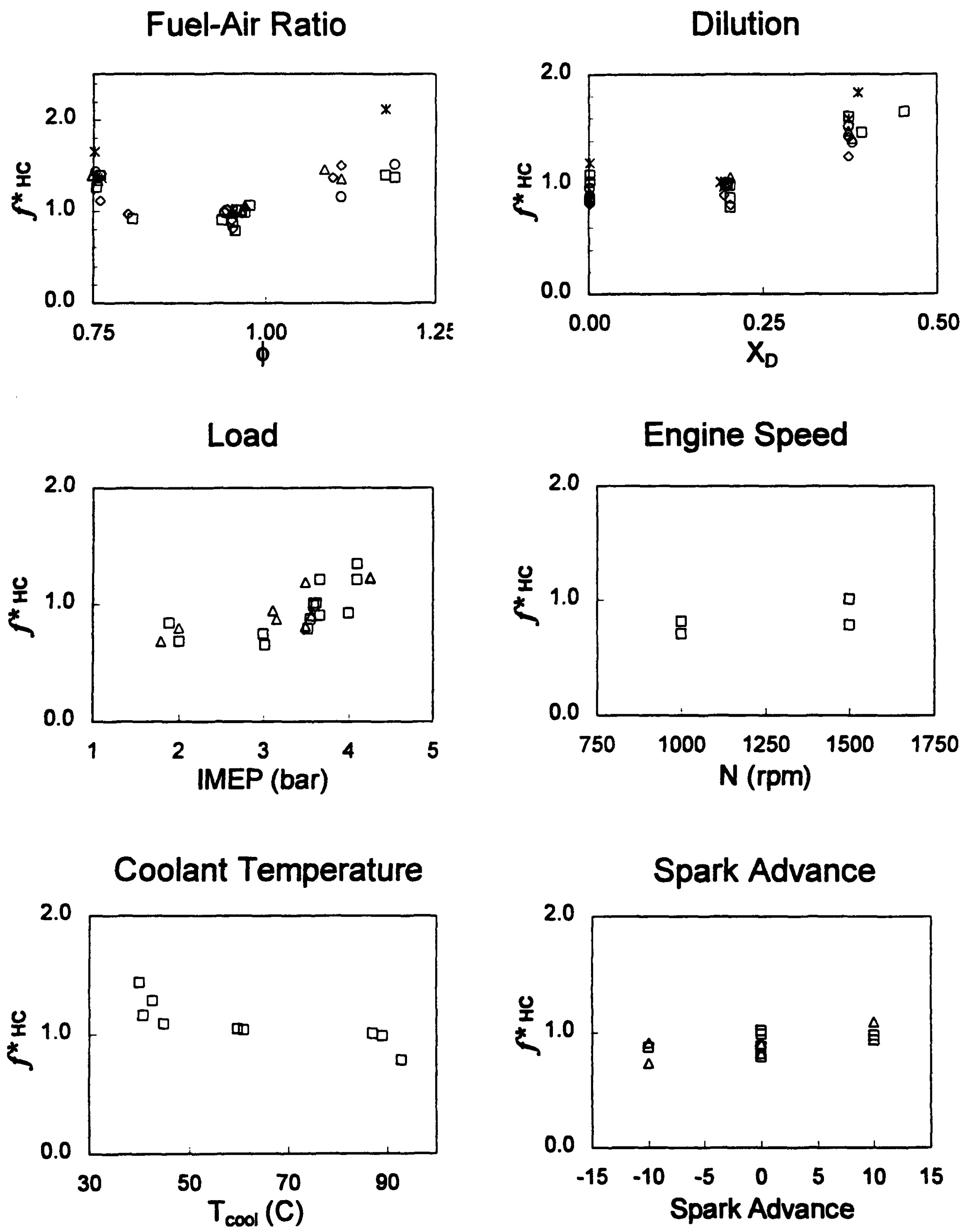

Fig. 4.4 Normalized fraction of post-flame desorbed dopant surviving as hydrocarbon vs. operating conditions for all dopants. Data for each dopant normalized by average baseline value of that dopant. The baseline condition is 1500 rpm, IMEP = 3.6 bar, MBT timing, $\phi = 0.95$, 20% dilution and $T_{cool} = 90\ ^{o}C$.

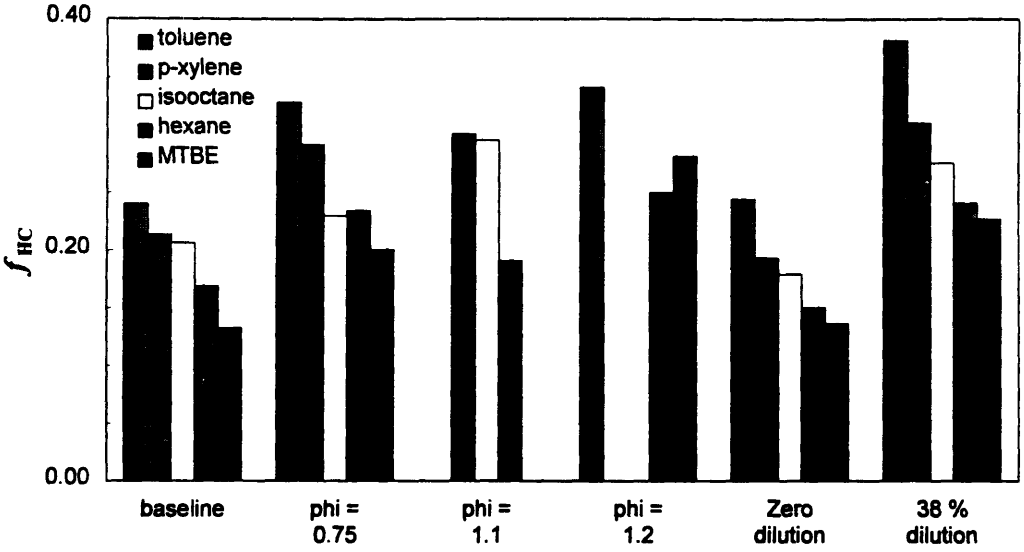

Fig. 4.5 Fraction of post-flame desorbed dopant surviving as hydrocarbon vs. dopant species for several operating conditions. The baseline condition is 1500 rpm, IMEP = 3.6 bar, MBT timing, $\phi = 0.95$, 20% dilution and $T_{cool} = 90$ °C.

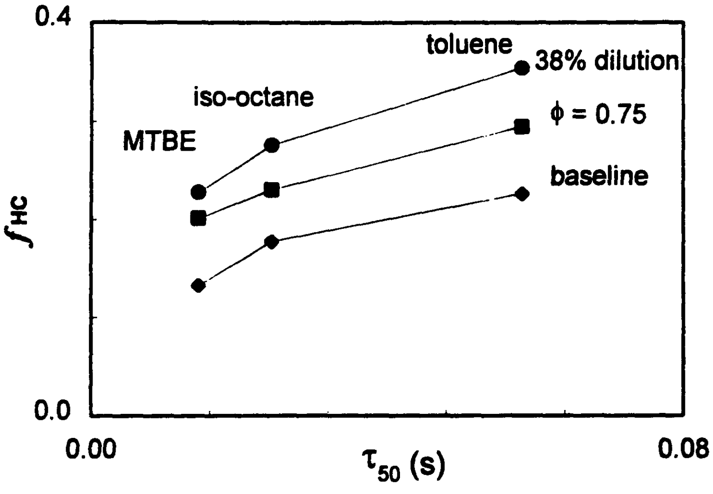

Fig. 4.6 Fraction of post-flame desorbed dopant surviving versus time τ_{50}, calculated half life of total hydrocarbons. Reaction times calculated with full kinetic models in a PFR at 1200 K, 1 atm and 1% unburned fuel-air mixture at typical exhaust gas composition. The baseline condition is 1500 rpm, IMEP = 3.6 bar, MBT timing, $\phi = 0.95$, 20% dilution and $T_{cool} = 90$ °C.

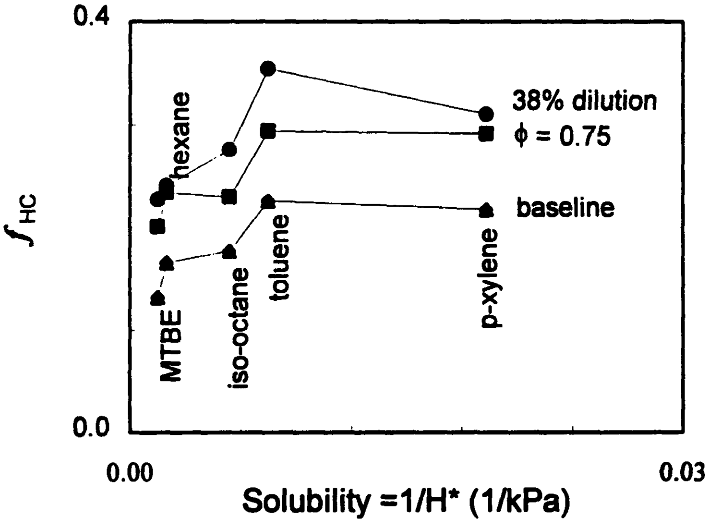

Fig. 4.7 Fraction of post-flame desorbed dopant surviving versus solubility defined as 1/H* evaluated at 90 °C in 10w-30 oil by Schramm and Sorenson [28]. The baseline condition is 1500 rpm, IMEP = 3.6 bar, MBT timing, $\phi = 0.95$, 20% dilution and $T_{cool} = 90$ °C.

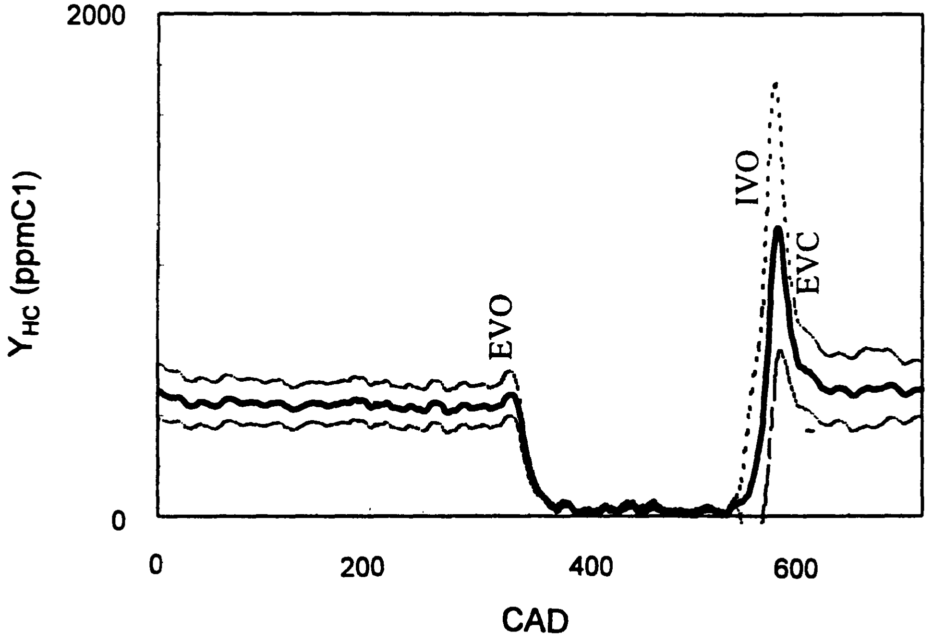

Fig. 4.8 Hydrocarbon profile at exhaust valve seat (position (a)) at baseline condition: 1500 rpm, IMEP = 3.6 bar, MBT timing, $\phi = 0.95$, 20% dilution and $T_{cool} = 90$ °C. Time axis has not be corrected for transit time in sampling tube.

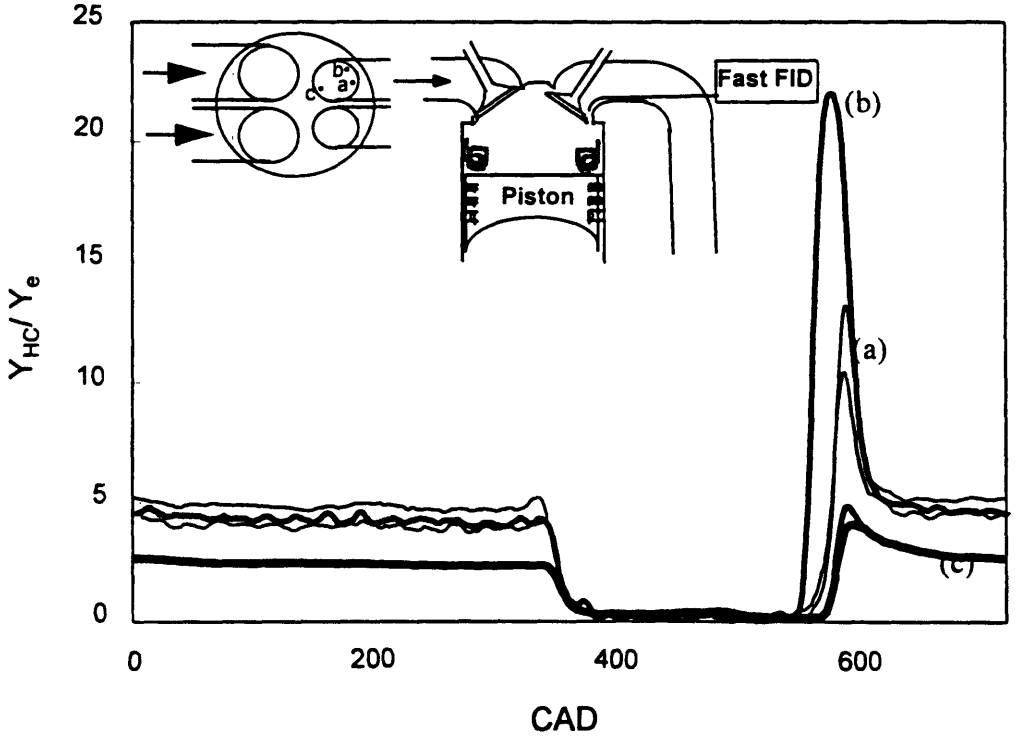

Fig. 4.9 Hydrocarbon profile at exhaust valve seat at baseline condition is 1500 rpm, IMEP = 3.6 bar, MBT timing, $\phi = 0.95$, 20% dilution and $T_{cool} = 90$ °C.. HC levels normalized by exhaust HC levels.

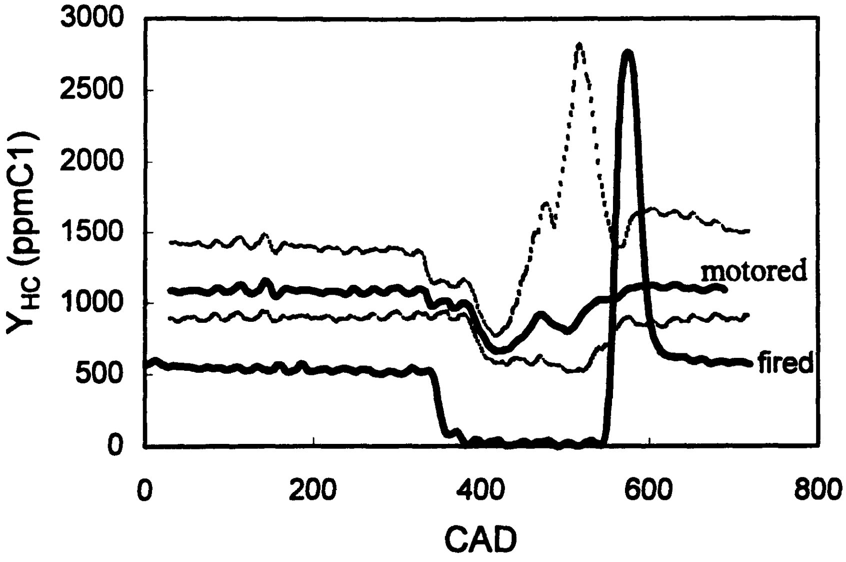

Fig. 4.10 Hydrocarbon profile at exhaust valve seat (position (b)) at baseline condition: 1500 rpm, IMEP = 3.6 bar, MBT timing, $\phi = 0.95$, 20% dilution and $T_{cool} = 90$ °C. Motored traces plotted for all 100 cycles and for 15 cycles with highest HC peak.

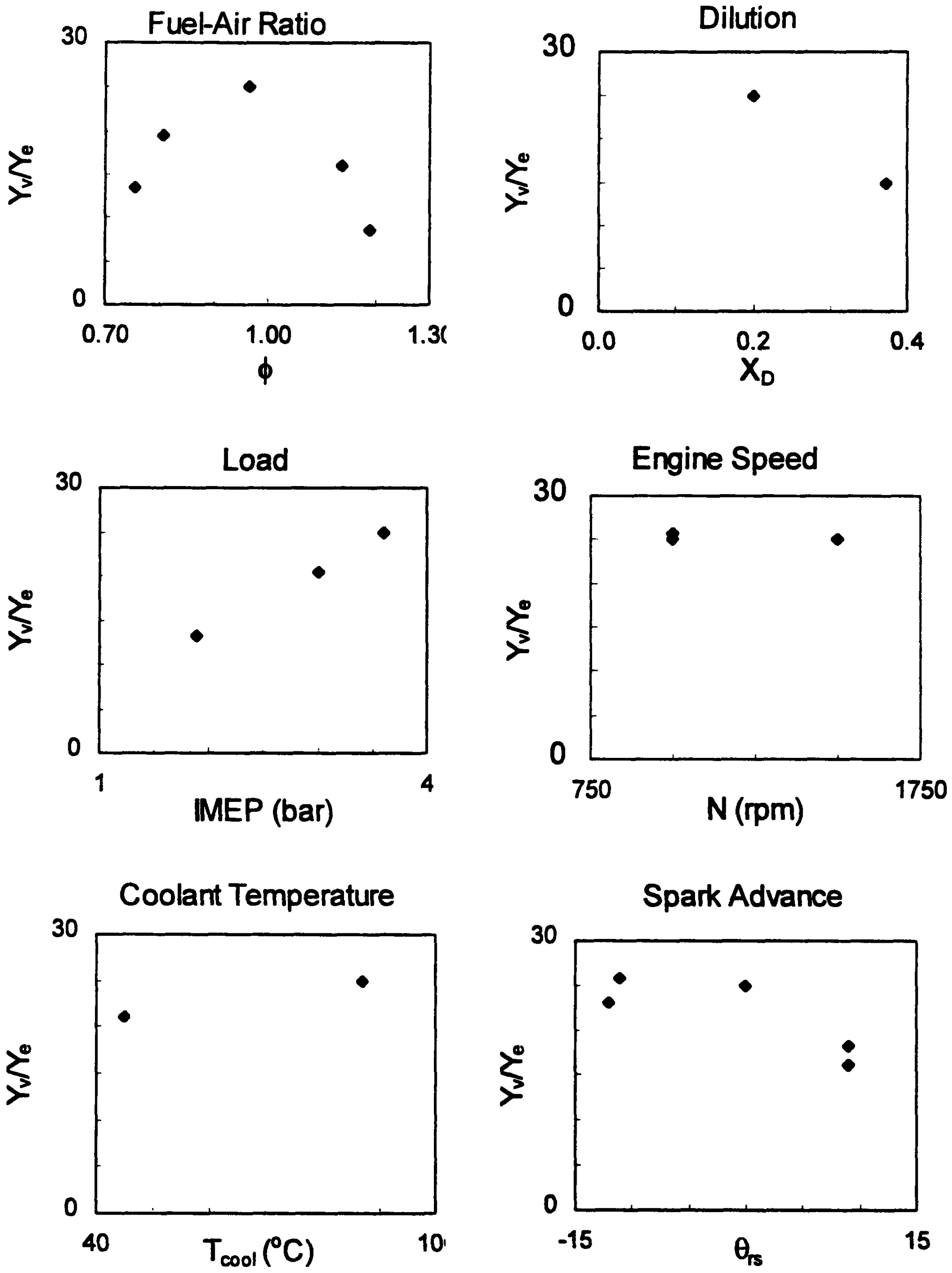

Fig. 4.13 Vortex hydrocarbon levels normalized by exhaust hydrocarbon levels (HC_V/HC_e). Data fitted parametricly to operating condtions in eqn. 5.5. Vortex hydrocarbon level is peak hydrocarbon level recorded by fast FID in position (b) as described in Fig. 4.9. Operating condtions are variations as noted on the baseline condtion: 1500 rpm, IMEP = 3.6 bar, MBT, $\phi = 0.95$, $X_D = 0.2$ and $T_{cool} = 90$ °C.

Chapter 5

IN-CYLINDER OXIDATION LEVELS

One of the objectives of this work is to isolate the fraction of unburned hydrocarbons oxidized in-cylinder. However, the experimental measurements shown in Chapter 4 are the result of hydrocarbon oxidation in-cylinder and in the exhaust port, as well as retention in the residual gas. Therefore, in order to estimate the fraction oxidized in-cylinder (f_{cyl}) from the total fraction oxidized ($1-f_{HC}$) estimates for the fraction retained in the residual (f_{res}) and fraction oxidized in the exhaust port (f_{port}) must be obtained. A another objective is to identify the controlling parameters for in-cylinder oxidation of unburned hydrocarbons through modeling. The oxidation levels predicted by a numerical model of in-cylinder oxidation can be compared to these estimates of in-cylinder oxidation levels for variations in operating condition and dopant species. The numerical model is the subject of the next Chapter.

The fraction oxidized in-cylinder (f_{cyl}) is related to fraction of post-flame desorbed dopant surviving as hydrocarbons (f_{HC}) by

$$f_{HC} = \frac{m_{HC}}{m_d} = (1-f_{cyl})(1-f_{res})(1-f_{port}) \qquad \text{or} \qquad f_{cyl} = 1 - \frac{f_{HC}}{(1-f_{res})(1-f_{port})} \tag{5.1}$$

where m_d is the mass of dopant desorbed post-flame (eqn. 2.1) and m_{HC} is the mass of hydrocarbons in the exhaust (eqn. 2.4). Thus, f_{cyl} can be estimated from the f_{HC} data if the contributions of port oxidation (f_{port}) and the fraction retained in the residual mass (f_{res}) are known.

In this Chapter, an algorithm is developed to estimate f_{cyl} from simple models for the fraction oxidized in the port and retained in the residual. The model for port oxidation is based on Hamrin's work [34] with additional data from Mendillo and Heywood [18] and Drobot *et al.*[19]. The model for the fraction retained in the residual mass is adapted from a method to predict the residual mass fraction by Fox *et al.*[35], and measurements of the hydrocarbon concentration in the roll-up vortex. Since the model for f_{port} is derived from experiments in hydrocarbon-fueled engines, there is some uncertainty about how well it represents the oxidation in the present experiments. Therefore, results for f_{cyl} and its sensitivity to the port oxidation model are considered. Finally, the relationship between the fraction of hydrocarbons retained (f_{res}) and the mass fraction retained (x_r) will be investigated.

5.1 Model for residual retained fraction (f_{res})

During normal engine operation, a fraction of the burned and unburned gas from the original charge remains trapped in the cylinder at exhaust valve close. This retained mass fraction, referred to as the residual mass fraction (x_r), is a function of operating conditions, engine geometry and valve timing. The retained mass has a significant hydrocarbon concentration, so that a fraction the unburned hydrocarbons are also retained in-cylinder. The fraction of hydrocarbons not oxidized in-cylinder that are retained in-cylinder (f_{res}) can be determined from models of the residual mass fraction and the hydrocarbon concentration of the residual gas as functions of operating condition. An expression will be developed to estimate the average hydrocarbon concentration of the residual gas, which will be combined with an available equation for the residual mass fraction. The dependence of the resulting expression for f_{res} on f_{port} will be discussed and evaluated at the operating conditions tested in Chapter 4.

The hydrocarbon residual fraction (f_{res}) is defined as the ratio of the mass of hydrocarbons in the residual gas over the sum of the hydrocarbon mass exiting the cylinder plus the hydrocarbon mass in the residual gas,

$$f_{res} = \frac{m_r Y_r (M_{HC}/M_r)}{m_r Y_r (M_{HC}/M_r) + m_e Y_c (M_{HC}/M_e)} \tag{5.2}$$

where m_r and m_e are the residual and exhaust masses per cycle, Y_r and Y_c are the average molar residual and cylinder-out hydrocarbon concentrations and M_r, M_{HC} and M_e are the molecular weights of the residual, dopant and exhaust gases respectively. The molecular weight of the residual and exhaust gases are essentially equal since Y_r and Y_c are much smaller than one.

Equation 5.2 can be simplified by making the following substitutions. The cylinder-out hydrocarbon concentration (Y_c) is difficult to measure. However Y_c is related to the measured engine-out hydrocarbon concentration (Y_e) by the fraction of desorbed hydrocarbons oxidized the port (f_{port})

$$\frac{Y_e}{Y_c} = 1 - f_{port} \tag{5.3}$$

The residual mass (m_r) and exhaust mass (m_e) terms can be replaced by the residual mass fraction (x_r), which is the ratio of the retained to charge mass ($m_e + m_r$),

$$x_r = \frac{m_r}{m_e + m_r} \quad (5.4)$$

Substituting equations 5.3 and 5.4 into 5.2 yields a relationship for f_{res} as a function of x_r, f_{port} and the ratio of residual to exhaust hydrocarbon concentration ($R_{HC} = Y_r/Y_e$),

$$f_{res} = \frac{x_r R_{HC}}{x_r R_{HC} - (1 - x_r)/(1 - f_{port})} \quad (5.5)$$

This section develops expressions for x_r, R_{HC} and f_{port} so that f_{res} can be estimated as a function of operation conditions for the experiments reported in Chapter 4.

Model for residual mass fraction (x_r)

The expression used to estimate the residual mass fraction is based on the model developed by Fox [35] from in-cylinder measurements of hydrocarbon concentration just before ignition at different operating conditions and valve timings. The equation used in this work has been modified slightly to incorporate the effect of nitrogen dilution, which was not included in the original model,

$$x_r = 1.266 \frac{OF}{N} \left(\frac{p_e}{p_i} \right)^{\gamma-1/\gamma} \sqrt{p_e - p_i} + 0.632 \frac{\phi^*}{r_c} \left(\frac{p_e}{p_i} \right)^{1/\gamma} \quad (5.6)$$

where OF is the valve overlap factor (mm•degree), N is the engine speed (rps), r_c is the compression ratio, p_e and p_i are the exhaust and intake pressures respectively (bar) and ϕ^* is a fuel-air equivalence ratio modified to include nitrogen dilution. The first term on the RHS of the equation is the fraction of mass that flows back past the exhaust valve seat during the valve overlap period and the second term is the fraction of mass in the cylinder when the intake valve opens.

The original model included a fuel-air equivalence term (ϕ), added empirically to match data sighted by Fox [35] that showed the residual mass fraction (x_r) increased with higher ϕ for $\phi < 1$. Higher ϕ values produce higher peak and blowdown pressures, which in turn result in lower cylinder temperatures and higher densities at intake valve opening due to a smaller adiabatic expansion during the blowdown process. It is speculated that the increase in x_r with ϕ is due to these higher densities at the end of the exhaust stroke. In the present doped oil experiments, the effect of nitrogen dilution (X_D) on x_r was included by assuming that adding nitrogen to the intake mixture is equivalent to lowering the fuel-air equivalence ratio by adding air. Temperature data from the experiments reported here support this hypothesis: dilution with 20% nitrogen ($X_D = 0.2$, ϕ=0.97, T_e =780 °K) produced the same exhaust temperatures and blow-down pressures as dilution with 20% additional air (ϕ = 0.9, X_D = 0.0, T_e =782 °K). Therefore an effective ϕ^* was defined for equation 5.5 that included the effect of nitrogen dilution

$$\phi^* \equiv \frac{\left(\frac{m_f}{m_a + m_n}\right)_{act}}{\left(\frac{m_f}{m_a}\right)_{stoic}} = \frac{\phi}{1 + \frac{X_D(1+\phi F/A_s)}{1-X_D}} \tag{5.7}$$

where m_f, m_a and m_n are the mass of fuel, air and nitrogen diluent and F/A_s is the stoichiometric fuel-air ratio.

Residual hydrocarbon ratio (R_{HC})

The ratio of hydrocarbon concentration in the residual gas relative to that in the exhaust gas (R_{HC}) was estimated using the assumptions that: (a) all hydrocarbons are contained in the cold boundary layer scraped up by the piston and rolled into a vortex (i.e. zero concentration in the core gas); (b) the hydrocarbon concentration in the vortex is uniform, so that the concentration of hydrocarbons in the residual gas is proportional to the ratio of the vortex volume retained in-cylinder and the clearance volume. Assumption (a) is based on the measurements of hydrocarbon concentration as a function of distance from the cylinder wall, reported in Chapter 4 and described in Fig. 4.9. With these assumptions, the ratio of hydrocarbon concentration in the residual over that in the exhaust is given by

$$R_{HC} = \left(\frac{Y_v}{Y_e}\right)\left(\frac{V_v}{V_{cl}}\right) f_v \tag{5.8}$$

where Y_v is the average hydrocarbon concentrations in the vortex, Y_e the hydrocarbon concentration in the engine-out exhaust, V_v the vortex volume, V_{cl} is the clearance volume and f_v is the mass fraction of the vortex retained in the cylinder. As the vortex is assumed to be at uniform temperature, the mass fraction of the vortex retained is equal to the volume fraction retained.

The average engine-out hydrocarbon concentration, Y_e, was measured as part of the standard diagnostics for each data point. The vortex hydrocarbon concentrations (Y_v) are based on a set of measurements taken with the fast FID as reported in Chapter 4. The vortex hydrocarbon concentration (Y_v) is assumed to be the average peak concentration level recorded near the end of the exhaust stroke at position (b) in Figure 4.10 for each of the 13 operating conditions listed in Table 2.1 except for the zero dilution case (Fig. 4.14). The vortex to engine-out hydrocarbon ratio (Y_v/Y_e) showed a dependence on N_2 dilution (X_D) , fuel-air equivalence ratio (ϕ), load (IMEP), engine speed (N) and spark timing relative to timing that produces a maximum pressure 17 °ATC (θ_{RS}). The experimental results were combined assuming a linear dependence of Y_v/Y_e to the operating parameters over the interval of interest,

$$\frac{Y_v}{Y_e} = a_1 + b_1 \cdot X_D + c_1 \cdot |\phi - 1| + d_1 \cdot \theta_{RS} + e_1 \cdot P_m + f_1 \cdot (1500 - N) \tag{5.9}$$

where $a_1 = 12.69$, $b_1 = -29.82$, $c_1 = 21.37$, $d_1 = 0.31$ (CAD^{-1}), $e_1 = 4.41$ (bar) and $f_1 = 0.0087$ (rpm^{-1}). The linear correlation was reasonably good in the range considered ($r^2 = 0.87$).

The vortex to clearance volume ratio (V_v/V_{cl}) is evaluated from a scaling law for the size of the roll-up vortex [31] and the engine geometry,

$$\frac{V_v}{V_{cl}} = \frac{(B - d_v)\pi A_v}{V_{cl}} \tag{5.10}$$

where B is the cylinder bore, d_v the cross-sectional diameter ($d_v = (A_v\, 4/\pi)^{0.5}$), A_v the area of the vortex and V_{cl} the clearance volume. The cross sectional-area of the vortex is estimated from [31] as

$$\frac{A_v}{L_s^2} = 1.015 \left(\frac{S_p^* \cdot L_S}{\nu} \right)^{-0.5} , \tag{5.11}$$

where L_s is the stroke length, S^*_p is the average piston speed and ν is the gas viscosity. The vortex diameter is simply . The viscosity is evaluated at the arithmetic mean of the core and wall temperatures and the exhaust pressure, which is typically 1 bar.

The fraction of the vortex retained in-cylinder (f_v) consists of two terms, as suggested by Lavoie [2]. The first is the fraction of the vortex in the cylinder at IVO ($1-f_{ex}$) and the second is the fraction of the vortex in the exhaust port that reenters the cylinder during the backflow period when both valves are open

$$f_v = 1 - f_{ex} + \frac{m_{eb}}{m_v + (1 + a_{ex})} \tag{5.12}$$

where m_{eb} is the mass inducted from the exhaust port back into the cylinder during the valve overlap period, m_v is the mass of the vortex and a_{ex} is the vortex fraction of inducted exhaust port mass. The vortex fraction of the inducted exhaust gas (a_{ex}) is taken as 5 based on the typical ratio of the peak hydrocarbon level to the closed-valve value (Fig. 4.9).

The fraction of the vortex that has left the cylinder at IVO (f_{ex}) is estimated from a simple geometric model, where the cylinder clearance volume is simplified to a constant cross section and the vortex is split into two halves (Fig. 5.1) [2]. The cross sectional area of each vortex half (A_v) is calculated using eqn. 5.11. The vortex half on the valve closed side conforms to the area of the clearance volume. The vortex on the open exhaust valve side has a square cross section. The fraction of the total vortex cross sectional area that is outside the clearance volume or overlapped by the valve face is f_{ex} (Fig. 5.1). The exhausted vortex fraction (f_{ex}) was found to be 0.42 through a graphical analysis. The mass re-inducted from the exhaust port is calculated from the overlap term in eqn. 5.6, the exhaust mass and residual mass fraction,

$$m_{eb} = \left(\frac{m_e}{1-x_r}\right) \cdot 1.266 \frac{OF}{N} \left(\frac{p_e}{p_i}\right)^{\gamma-1/\gamma} \sqrt{p_e - p_i} \quad . \qquad (5.13)$$

The only remaining unknown needed to calculate the hydrocarbon residual fraction (f_{res}) in equation 5.5 is the fraction oxidized in the exhaust port (f_{port}), which is the subject of the next section. Before discussing a model for f_{port}, it is worth looking at the sensitivity of f_{res} to f_{port}. Two cases will be considered in this section which should bracket the possibilities. Measurements of port oxidation by Mendillo [18] and Drobot [19] indicate that f_{port} range from zero for rich cases ($\phi = 1.2$) to 0.45 for retarded spark timing (MBT-12). The resulting f_{res} values versus operating conditions are found in Fig. 5.2 for these two extreme f_{port} values. The calculated f_{res} values, using eqn. 5.5, vary from a low of 0.15 at high levels of dilution and high intake pressure to a high of 0.65 at zero dilution. Increasing f_{port} from 0.0 to 0.45 decreases f_{res} by approximately 30%, but had almost no effect on the sensitivity of f_{res} to operating conditions.

The hydrocarbon residual fraction (f_{res}) is very sensitive to the dilution level, modestly sensitive to the fuel-air ratio and engine speed, and not sensitive to load, coolant temperature and spark advance. The hydrocarbon residual fraction is not very sensitive to load despite the strong decrease in the residual mass fraction with load because the residual over exhaust hydrocarbon concentrations (Y_r/Y_e) increases sharply with load (Fig. 4.13). The hydrocarbon residual fraction decreased dramatically with dilution, due to higher intake pressures required to maintain the load with higher levels of dilution.

5.2 Model for port oxidation (f_{port})

An empirical model for the fraction of dopant oxidized in the exhaust port was developed to complete the estimation of the fraction oxidized in the cylinder (eqn. 5.1) as a function of operating conditions and dopant species. Drobot [19] found that f_{port} is a strong function of operating conditions, particularly load and spark timing, but only weakly dependent on hydrocarbon species.

As part of a larger effort to develop a model to explore the effect of operating conditions and design changes on hydrocarbon emissions, Hamrin [34] developed an empirical relationship for port oxidation. Exhaust port oxidation data by Drobot [19] from a typical two-valve production engine was fit to engine load, engine speed, coolant temperature and spark advance using a least squares linear regression. The data was sufficiently sparse to limit the analysis to a linear fit. The resulting equation had the following form,

$$f_{port} = a_2 - b_2 \cdot P_m - c_2 \cdot \theta_{RS} - d_2 \cdot N - e_2 \cdot T_{cool} \tag{5.14}$$

where a_2 through e_2 are fitted constants, P_m is the IMEP in bar, θ_{RS} the spark timing relative to the spark timing that produces peak pressure at approximately 17 ^{o}ATC, N the engine speed in rpm, T_{cool} is the coolant temperature and ϕ is the fuel-air equivalence ratio.

The exhaust port oxidation data was obtained from experiments with a single-cylinder, two-valved engine in which the rapid addition of CO_2 quenches the reactions in the exiting gases at the cylinder exit (quench plane 1 in Fig. 5.3). The amount of oxidation in the port was obtained by comparing the engine-out hydrocarbon levels with and without quenching the exhaust. These experiments were carried out for a range of operating conditions and fuels most recently with a modern engine by Drobot [19] and previously in a low compression CFR engine by Mendillo [18].

Hamrin's model of port oxidation was modified to include nitrogen dilution and fuel-air equivalence ratio. The coefficients for engine load, spark timing and the constant are unchanged from Hamrin's work [34]. These modifications are discussed below. The resulting values for f_{port} and associated uncertainties are discussed further on.

Effect of fuel-air equivalence ratio (ϕ)

The experimentally observed dependence of f_{port} on ϕ is somewhat conflicting between different studies. Whereas Drobot found a linear dependence of f_{port} on a fuel-air ratio equivalence ratio from 0.9 to 1.1, Mendillo found the expected peak in port oxidation at stoichiometric conditions, when the exhaust temperatures are highest (Table 5.1). It is speculated that had Drobot extended the tests to leaner mixtures, a peak in port oxidation would have been observed. Therefore, $\partial f_{port}/\partial(\phi - 1)$ is assumed to be positive and equal to 0.16 for lean mixtures and negative (-0.6) for rich mixtures.

$$\frac{\partial f_{\text{port}}}{\partial(\phi-1)} = \begin{cases} 0.16 & \text{for } \phi < 1.0 \\ -0.60 & \text{for } \phi > 1.0 \end{cases}$$

Table 5.1 Dependence of f_{port} on fuel-air equivalence ratio (ϕ)

fuel	$\frac{\partial f_{\text{port}}}{\partial(\phi-1)}$		
	Mendillo and Heywood [18]		Drobot *et al.* [19]
	$0.85 < \phi < 1.0$	$1.0 < \phi < 1.2$	$0.9 < \phi < 1.1$
propane			-0.50
isooctane	0.16	-0.65	-0.56
gasoline	0.44	-1.33	-0.73

Effect of engine speed (N)

Once again, the experimental evidence on the effect of engine speed on the fraction of hydrocarbons oxidized in the port is not consistent between Mendillo's and Drobot's data (Table 5.2). Drobot showed decreased port oxidation for gasoline and isooctane, but increased port oxidation for propane with increased speed. Mendillo found increased port oxidation for gasoline with increased speed. Since the evidence is contradictory and the dependence found by Drobot [19] relatively small, the dependence on speed was neglected in this study.

Table 5.2 Dependence of f_{port} on engine speed (N)

fuel	$\frac{\partial f_{\text{port}}}{\partial N}$	
	Mendillo and Heywood [18]	Drobot et al. [19]
propane		$2.22 \cdot 10^{-5}$
isooctane		$-8.38 \cdot 10^{-5}$
gasoline	$4 \cdot 10^{-4}$	$-5.60 \cdot 10^{-5}$

Effect of N_2 dilution (X_D)

The effect of nitrogen dilution was accounted for by assessing that under lean conditions, the main effect of nitrogen dilution is to decrease the exhaust temperature at the same rate as adding additional air. A secondary effect is to decrease available oxygen concentrations: however under excess oxygen concentrations, this effect should be minor. Therefore the dependence of f_{port} on dilution was

$$\frac{\partial f_{\text{port}}}{\partial X_d} = \left.\frac{\partial f_{\text{port}}}{\partial(\phi-1)}\right|_{\text{lean}} = 0.16 \cdot (\phi - 1)$$

Port oxidation model used in this work

The coefficients in eqn 5.14 for f_{port} can therefore be determined as

$$f_{port} = a_2 - b_2 \cdot p_m - c_2 \cdot \theta_{RS} - d_2 \cdot X_D - e_2 \cdot T_{cool} + f_2 \cdot (\phi - 1) \tag{5.15}$$

where $a_2 = 0.646$, $b_2 = 0.070$ (1/bar), $c_2 = 0.079$, $d_2 = 0.16$, $e_2 = 0.255 \times 10^{-4}$ (1/K) and $f_2 = 0.16$ if $\phi < 1$ or $f_2 = -0.60$ if $\phi > 1$. This equation was used to estimate the fraction oxidized in the hydrogen-fired oxidation experiments reported in Chapter 4. The results for the toluene dopant cases are plotted in Fig. 5.4.

There are two large uncertainties in this parametric model of port oxidation. The first source of uncertainty is the effect of different engine types. Mendillo and Drobot performed their tests in two-valve engines, while the engine used in the present experiments is a four-valve engine. The exhaust port in a four-valve engine has significantly more heat transfer area than a two-valve engine, which leads to higher heat transfer rates, lower temperatures and thus lower reaction rates. Hamrin [34] found after initially calibrating the engine hydrocarbon model for two-valve engines, that the port oxidation fraction needed to be reduced by 50% to match the hydrocarbon emission levels of one four-valve engine, but no change was required for a second four-valve engine. The fraction oxidized in the port is plotted versus operating conditions in Fig. 5.4 without reduction (high case) and a 50% reduction (low case) to reflect the uncertainty in applying eqn. 5.15 to four-valve engines.

The second source of uncertainty in applying this parametric model to the present hydrogen fueled experiments is that the parametric model was developed with data from hydrocarbon-fueled engines. As noted in Chapter 4, hydrocarbons exit the cylinder throughout the exhaust stroke in hydrocarbon fueled engines while most hydrocarbons exit the cylinder at the end of the exhaust stroke in the present experiments. Calculations by Wu *et al.* [30] found that most of the port oxidation occurs during the first half of the exhaust stroke, when the temperatures are higher. Whereas only much lower levels of port oxidation are possible for hydrocarbons leaving at the end of the exhaust stroke. Therefore, while the port oxidation estimates in Fig. 5.4 are valuable bounds to estimate the in-cylinder fraction, they should be treated cautiously.

5.3 Fraction oxidized in-cylinder (f_{cyl})

Once estimates for f_{res} and f_{port} have been made for each conditions, (eqns. 5.5 and 5.14), the fraction oxidized in-cylinder can be estimated from eqn. 5.1. Figures 5.5 to 5.7 show the calculated valves for f_{cyl} for all experimental cases. Again, the low and high cases for f_{port} are a 50% and 0% reduction respectively to reflect the uncertainty associated with four-valve engine operation. Since the models for f_{port} and f_{res} do not include a dependence on the type of hydrocarbon dopant, the dependence of f_{cyl} on dopant species is similar to that of f_{HC} in Figs. 4.1 to 4.3. The sensitivity of f_{cyl} to load, coolant temperature and spark timing is also similar that reported in Chapter 4 for f_{HC}, while the sensitivity to fuel-air ratio, engine speed and dilution were different. In contrast to the f_{HC} results, f_{cyl} is more sensitive to rich equivalence ratios than lean ratios, due to larger hydrocarbon residual fractions (f_{res}) at rich conditions than lean conditions (Fig. 5.2). The lower intake pressures of rich conditions produce larger f_{res} through a higher residual mass fractions. Both f_{cyl} and f_{HC} are relatively insensitive to engine speed, however the fraction oxidized over the engine decreased slightly with engine speed, while the fraction oxidized in-cylinder increased with engine speed . Again a larger f_{res} due to lower intake pressures at low speeds produces a lower estimate of f_{cyl}.

An increased dilution ratio (X_D) is expected to reduce the post-flame oxidation as the additional diluent reduces cylinder temperatures during the expansion stroke. Yet the trend in f_{cyl} shows the opposite effect at dilution levels below 0.2 in Figs 5.5 through 5.14. However, above a dilution level of 0.2, f_{cyl} demonstrates the expected trend, increasing significantly with additional dilution. These results are similar to those reported in Chapter 4, where the measured fraction of hydrocarbons surviving (f_{HC}) showed nearly zero sensitivity to increased dilution levels below 0.2, but additional dilution resulted in significantly higher (f_{HC}). Clearly the operating conditions at zero dilution are somehow different than those at higher dilution levels, however it is not physically plausible that in-cylinder oxidation would decrease from $X_D =$ 0.2 to 0.0. Therefore an error must be present in the estimation of f_{cyl} from the measured f_{HC} values for the zero dilution case.

The most likely source of error is in the model for the hydrocarbon fraction retained in-cylinder (f_{res}, eqn. 5.4) is based in part on measurements of the vortex hydrocarbon concentration as shown in Fig. 4.14. The vortex hydrocarbon concentration (Y_v) was not measured for the zero dilution case and therefore the value of f_{res} is based on extrapolating the data at 0.2 and 0.4 dilution levels. It is quite possible that Y_v does not have a linear dependence on X_D, which would result in a very different f_{cyl} at zero dilution levels.

5.4 The fraction exiting the cylinder (1-f_{res}) versus the residual mass fraction (x_r)

A separate result of this work develops the relationship between the fraction of hydrocarbons in the cylinder at EVO that are exhausted (1-f_{res}) and the residual mass fraction described by Daniel [36]. Daniel pointed out that the fraction of hydrocarbons in the cylinder at EVO that are exhausted (1-f_{res}) is zero when the residual mass fraction is one and one when the residual mass fraction is zero. Daniel had a single data point at $1\text{-}f_{res} = 0.66$ and $x_r = 0.05$ and drew an asymmetrical curve connecting the three points. In the present work, an equation is developed for that curve and the fraction exhausted from the cylinder $(1\text{-}f_{res})$ is correlated to the predicted residual mass fraction (x_r) for the toluene data. Equations to predict f_{res} (eqn. 5.5) and x_r (eqn. 5.6) are presented in Section 5.1.

Equation 5.5 can be rearranged so that $1\text{-}f_{res}$ and x_r are related by a single variable (A),

$$1-f_{res} = 1-\frac{1}{1-\dfrac{(1-x_r)}{x_r}\dfrac{1}{R_{HC}(1-f_{port})}} = 1-\frac{1}{1-(1-x_r)/(x_r A)} \qquad (5.16)$$

where A is equal to $R_{HC} \cdot (1\text{-}f_{port})$. The fraction of hydrocarbon mass exiting the cylinder $(1\text{-}f_{res})$ is plotted, against the residual mass fraction (x_r) for all operating conditions in Fig. 5.8. The calculated points fit onto a single line for each of the low and high f_{port} cases, fit by A = 4.11 and A = 5.25 respectively.

Daniel's single data point obtained in the 1960's with a low compression gasoline engine, falls somewhat below the estimated values of $1\text{-}f_{res}$ for these hydrogen-fired experiments in a high compression 4-valve engine. The hydrogen-fired experiments were expected to have a lower fraction of hydrocarbon exiting the cylinder $(1\text{-}f_{res})$ as most of the hydrocarbons exit the cylinder at the end of the exhaust stroke, whereas hydrocarbons exit from a gasoline-fired engine throughout the exhaust process. One possible explanation is that Daniel's engine had much more unburned fuel in the residual gas due to large piston crevices that are typical of older engines.

Two conclusions can be drawn from the good fit of the data to eqn. 5.16 for a single value of A. The fraction of hydrocarbon retained in-cylinder is related to the fraction of mass retained by a relatively simple relationship (eqn. 5.16). The good fit of eqn. 5.16 also indicates that at least for this experiment, that port oxidation (f_{port}) and the ratio of residual hydrocarbons to exhaust hydrocarbons (R_{HC}) scale together. However it must be noted that $1\text{-}f_{res}$ and x_r are not measured directly, but estimated based on operating conditions. The fraction of hydrocarbons exiting the cylinder were calculated with eqn 5.5, which was based on the measured ratio of vortex to exhaust hydrocarbon concentrations (Y_v/Y_e in Fig. 4.13) and empirical models for f_{port} and x_r.

5.5 Conclusion

In this Chapter the fraction of post-flame desorbed hydrocarbons oxidized in the cylinder (f_{cyl}) was estimated by considering appropriate assumptions for the hydrocarbon residual fraction (f_{res}) and the fraction oxidized in the port (f_{port}). Calculated values for the hydrocarbon residual fraction (f_{res}) range from 0.2 to 0.65 and generally scale inversely with intake pressure. At typical operating conditions represented by the baseline condition the hydrocarbon residual fraction is about 45%. The estimated fraction oxidized in the port has a very large uncertainty associated with the fact that experiments reported here were in hydrogen-fired four-valve engines and the expression for f_{port} is based on experiments in two-valve hydrocarbon-fired engines. Nevertheless, the uncertainty in f_{port} has only a modest effect on the estimates for the residual hydrocarbon fraction and fraction oxidized in-cylinder and no effect on the sensitivity to operating conditions and dopant species.

The fraction of hydrocarbon oxidized in-cylinder in these experiments ranges from 0.47 to 0.71 at baseline conditions. The lowest value is 0.2 for toluene at rich conditions and the highest value is 0.7 for MTBE at the baseline conditions. The sensitivity to fuel type and ranking is unchanged from the f_{HC} results reported in Chapter 4: toluene was oxidized the least, then p-xylene, isooctane, hexane and MTBE. The sensitivity of f_{cyl} to load, coolant temperature and spark timing is also similar to the f_{HC} results: in-cylinder oxidation increased with loads above 3 bar IMEP and coolant temperatures and was insensitive to spark timing. The fraction oxidized in-cylinder decreased more for rich conditions than for lean conditions and increased with engine speed. The fraction oxidized decreased with dilution above $X_D=0.2$ as in Chapter 4 for f_{HC}. The zero dilution data continues to be unexplained except perhaps that extrapolating the vortex to exhaust hydrocarbon concentration data from $X_D = 0.2$ to 0.4 to zero dilution is not appropriate.

In a separate result, a simple equation was developed to relate the fraction of hydrocarbons exiting the cylinder ($1-f_{res}$) to the residual gas fraction (x_r) (eqn. 5.16). Estimated values of $1-f_{res}$ versus x_r fall on a single line described by eqn. 5.16.

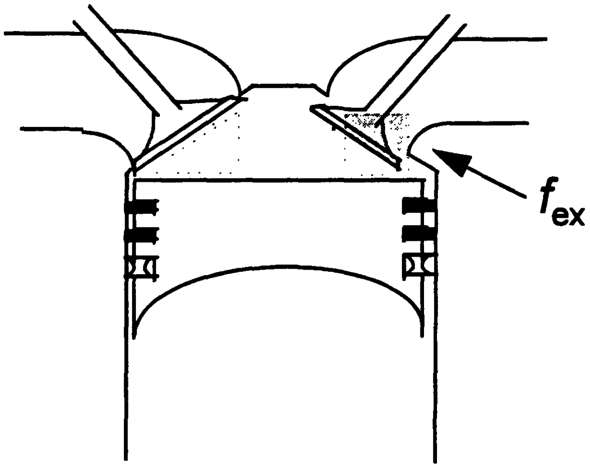

Fig. 5.1 Estimating fraction of the corner vortex gas that leaves the cylinder during exhaust, but before the backflow period. The resulting value was 0.42 for the cases considered in this research.

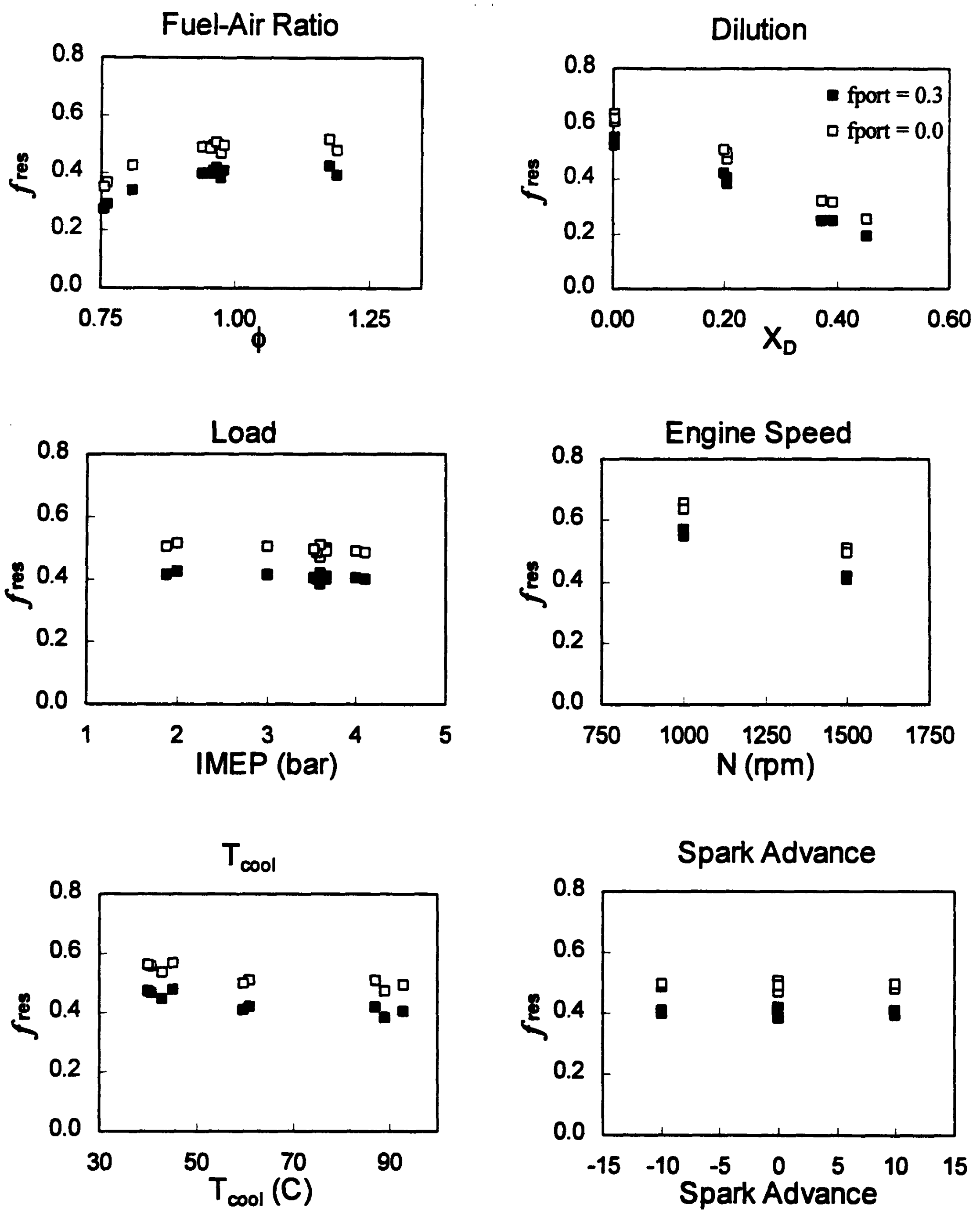

Fig. 5.2 Estimated fraction of post-flame desorbed hydrocarbons retained in residual mass with toluene dopant for two f_{port} cases.

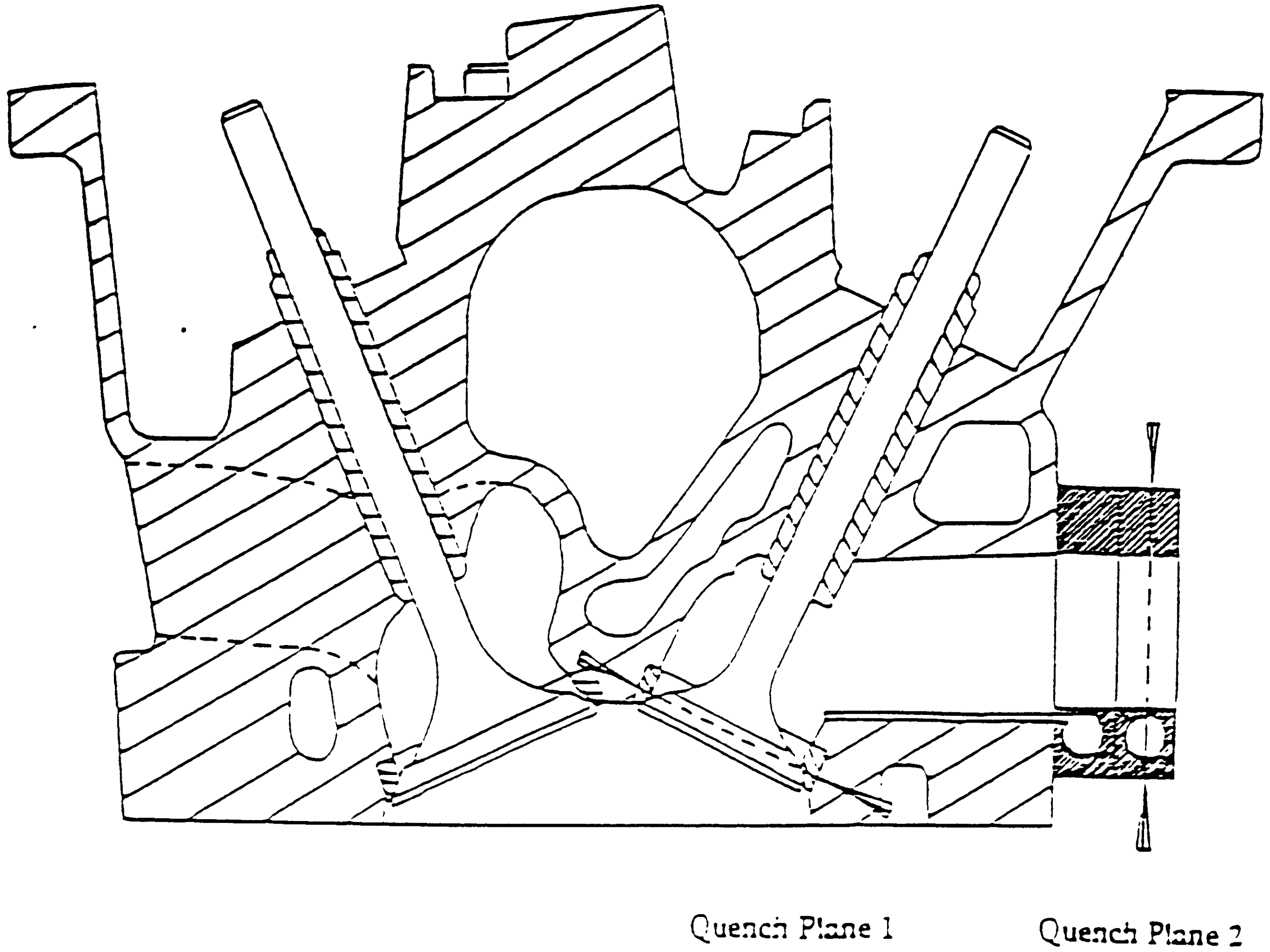

Fig. 5.3 Cross-sectional view of engine exhaust port with exhaust quenching apparatus.

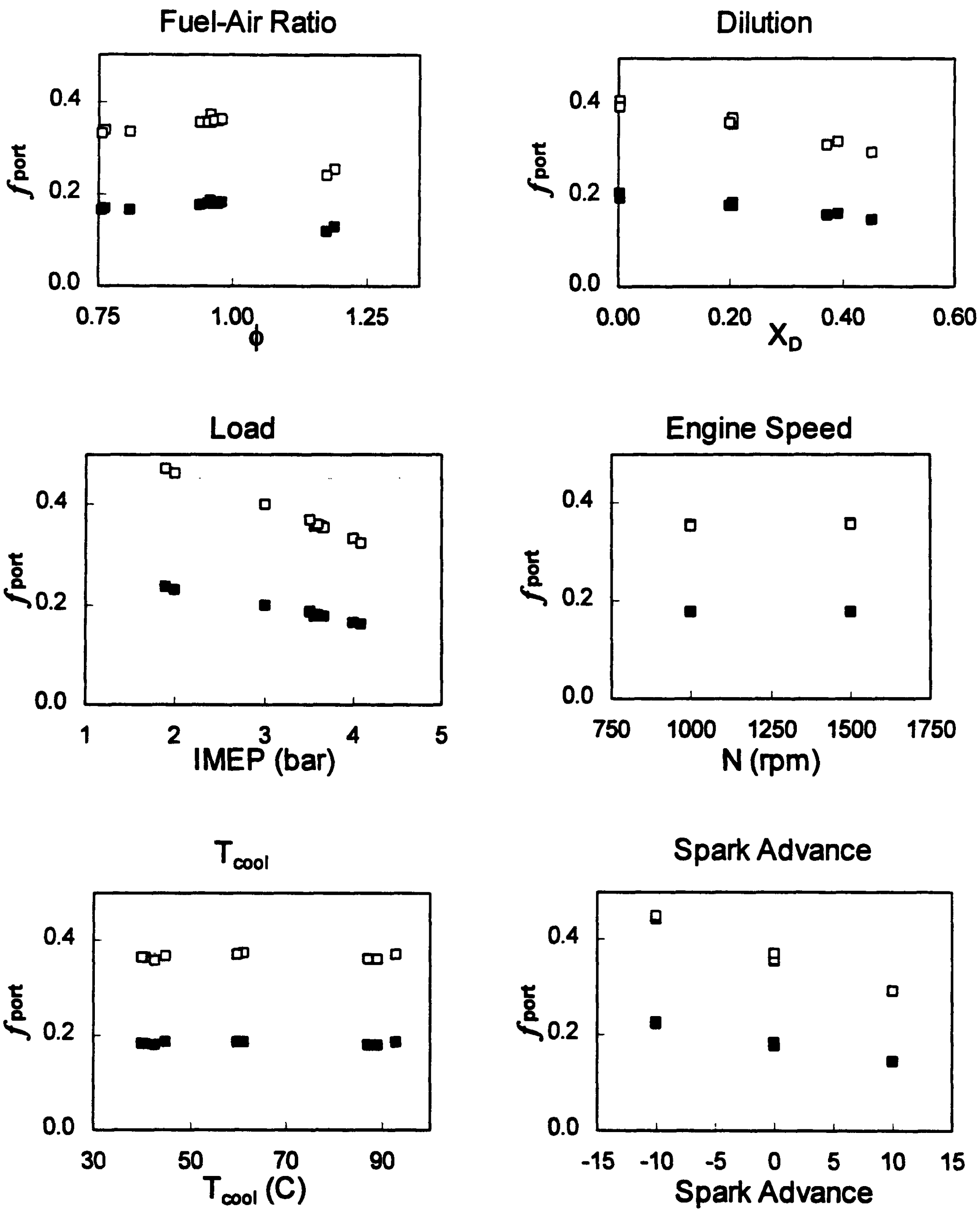

Fig. 5.4 Estimated fraction of post-flame desorbed hydrocarbons oxidized in the exhaust port for toluene cases for low and high cases. Operating condtions are variations as noted on the baseline condtion: 1500 rpm, IMEP = 3.6 bar, MBT, $\phi = 0.95$, $X_D = 0.2$ and $T_{cool} = 90$ °C.

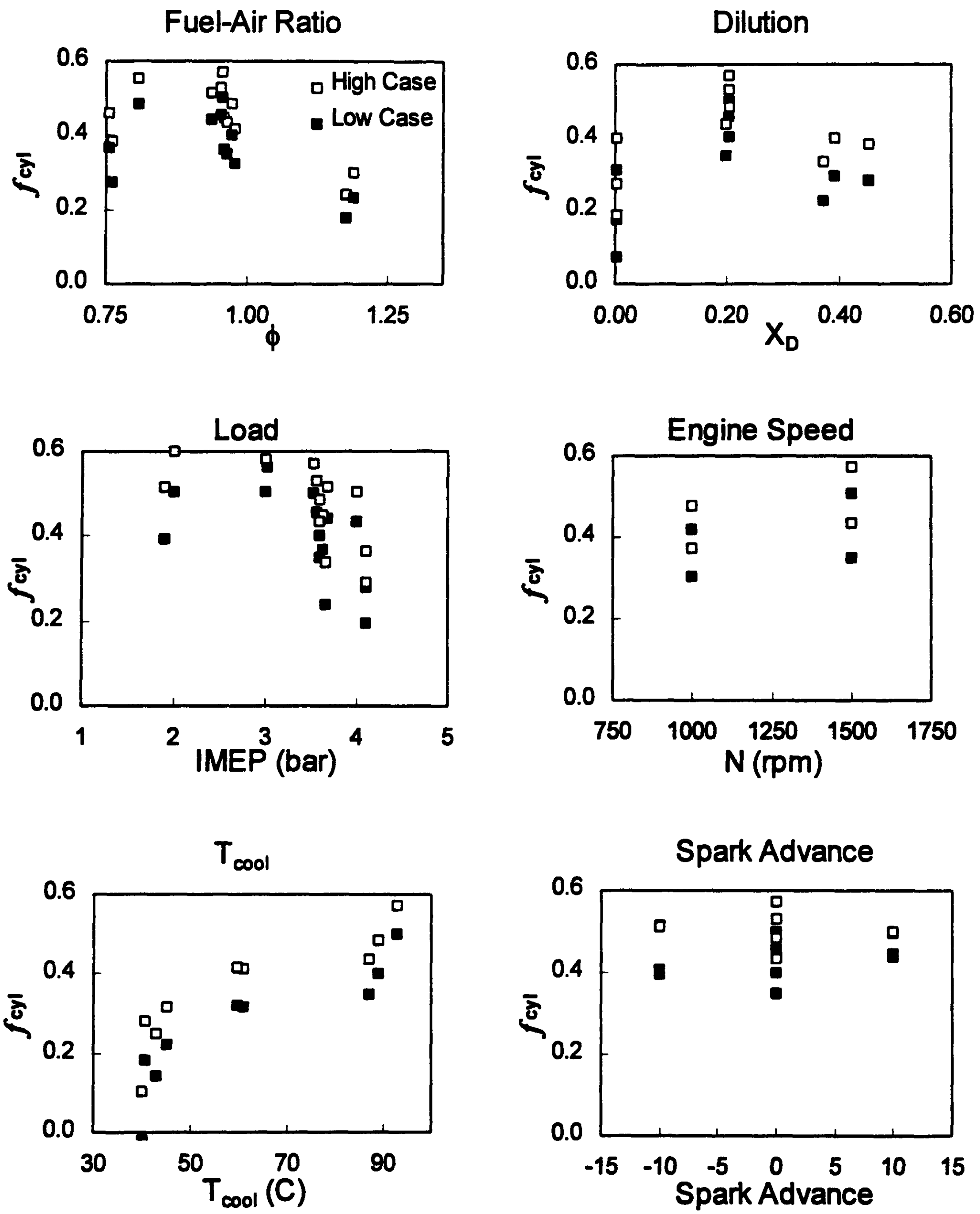

Fig. 5.5 Estimated fraction of post-flame desorbed hydrocarbons oxidized in-cylinder for toluene cases.

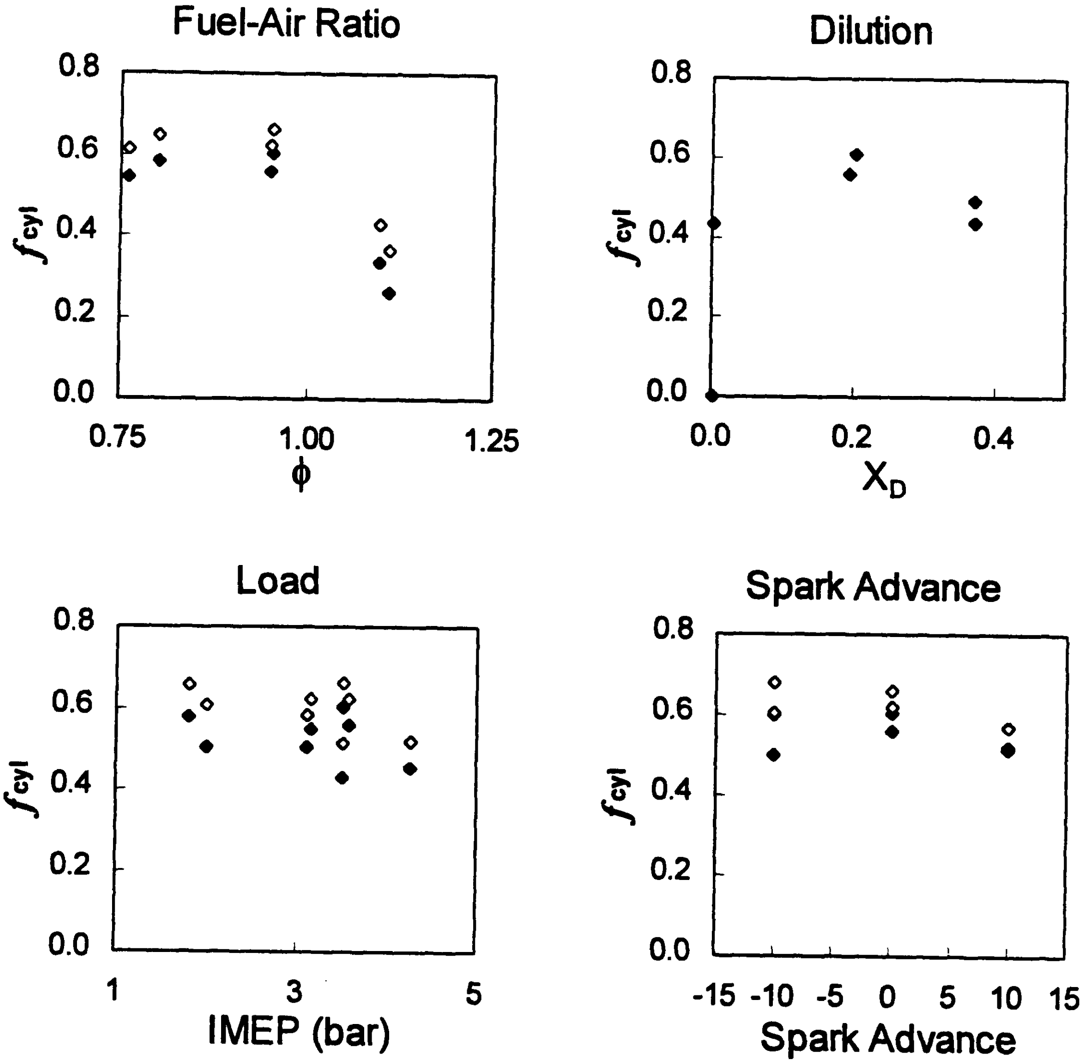

Fig. 5.6 Estimated fraction of post-flame desorbed hydrocarbons oxidized in-cylinder for isooctane cases.

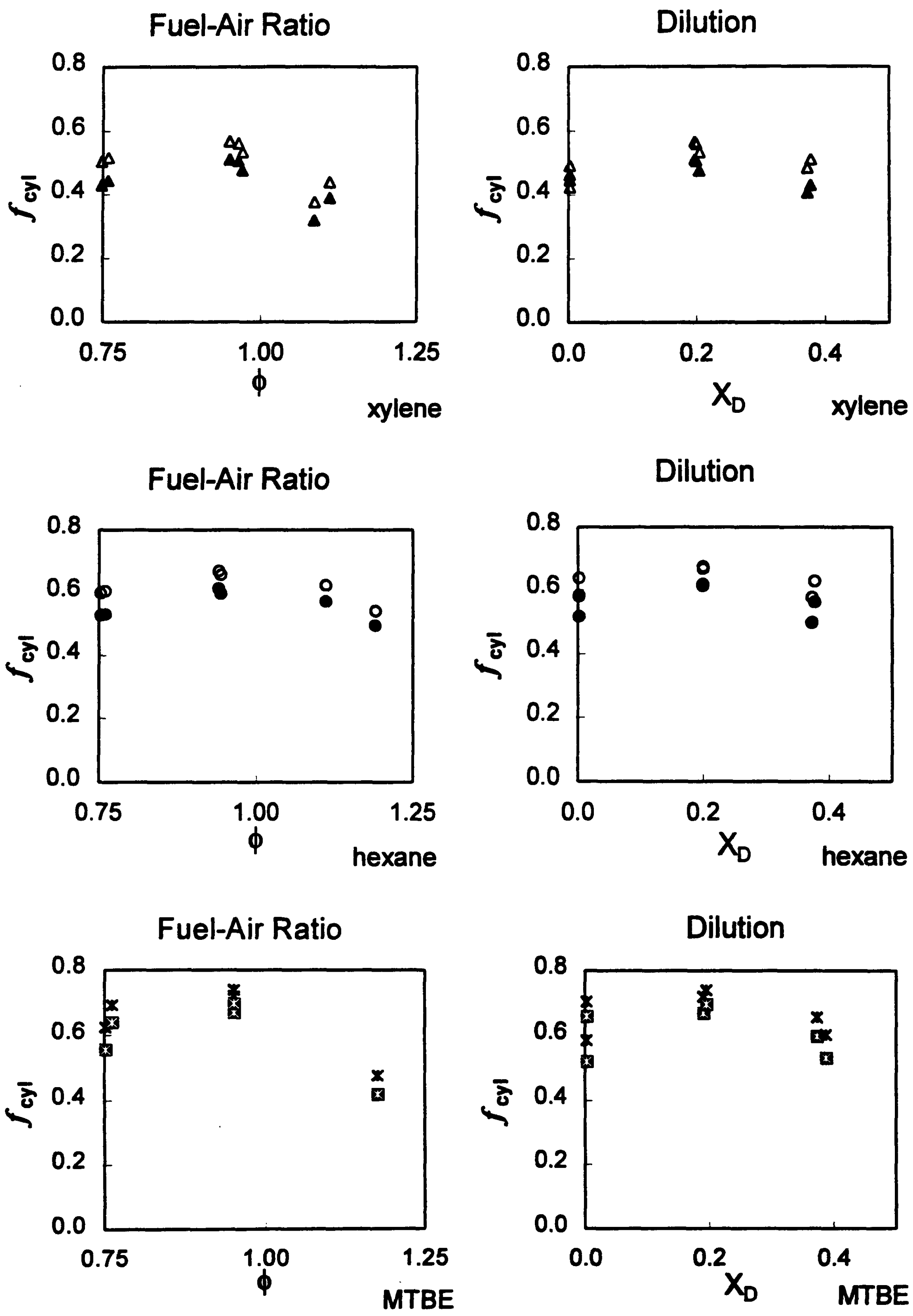

Fig. 5.7 Estimated fraction of post-flame desorbed hydrocarbons oxidized in-cylinder for p-xylene, hexane and MTBE cases.

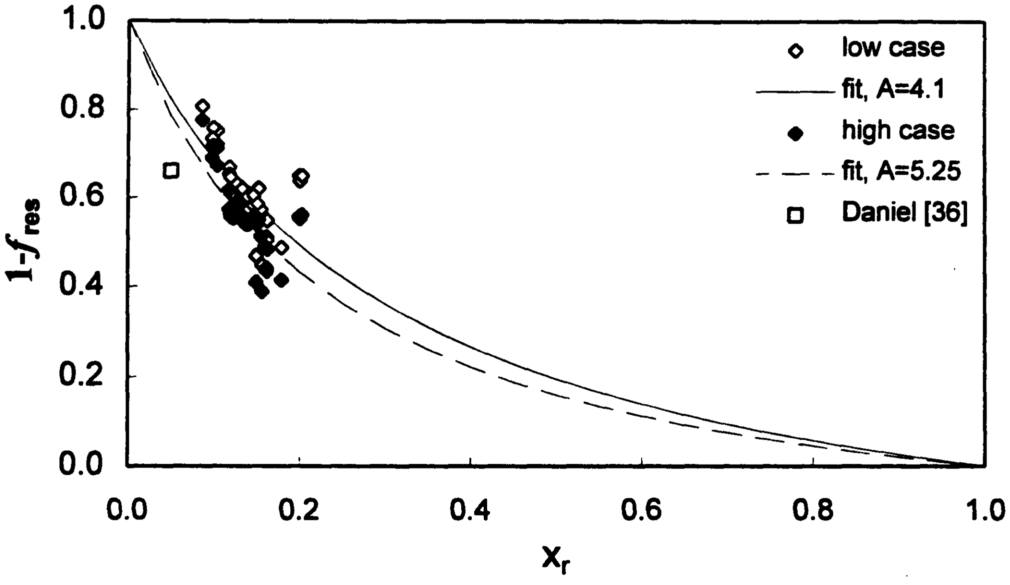

Fig. 5.8 Fraction of hydrocarbons exiting the cylinder (1-f_{res}) versus the residual mass fraction (x_r). Diamonds are estimates based on toluene dopant data using f_{port} as defined by eqn. 5.13 for the high case and a 50% reduction in f_{port} for the low case. Lines are fits to the data, where A = $R_{HC}(1-f_{port})$. The open square is Daniel's data point from a gasoline-fired engine experiment.

Chapter 6

DESORPTION - OXIDATION MODEL

Previous chapters have presented the experimental data on the nature of the hydrocarbon source and the oxidation of the hydrocarbons from this source for a variety of dopant species and operating conditions. This Chapter introduces a simplified one-dimensional model of the desorption and oxidation process near the cylinder walls during the expansion and exhaust stroke. Comparison of model and experimental results allows the systematic evaluation of the role of different physical processes occurring in-cylinder that can account for the observed variation in the oxidized fraction of hydrocarbons.

The current picture of the post-flame in-cylinder oxidation process assumes that the dopant hydrocarbons desorb out of the oil into the thermal and momentum boundary layer on the cylinder wall. After the passage of the flame, hydrocarbons desorb into the hot burned gases and can therefore be oxidized. The process is dynamic, as the core temperature drops due to expansion, and the thermal boundary layer grows due to heat transfer to the walls. During this period, hydrocarbons emerge into the thermal boundary layer and diffuse towards the hot burned adiabatic core gases. Hydrocarbons oxidize once a sufficient high temperature is reached. This diffusion, expansion and oxidation process continues at least until the exhaust valve opens and possibly until hydrocarbons are scraped up in the roll-up vortex. A numerical model of the unsteady dopant desorption and subsequent oxidation was developed in order to illuminate the controlling physical parameters in the oxidation process. The challenge is to include all the important physical processes, in order to obtain reasonable agreement with experimental values.

The one-dimensional model is described in the first section and comparison with the experimental results from Chapters 3 and 5 follow. The description of the model starts with the modeling assumptions, domain and governing equations presented along with the boundary and initial conditions. Next, a submodel of the diffusion of dopant through the oil layer is described, with the relevant initial and boundary conditions. Results from this oil layer submodel are evaluated against the desorption experiments reported in Chapter 3. Other submodels for the turbulent diffusivity, crevice flow and oxidation chemistry are then described. The predicted absolute values of the fraction of total hydrocarbons surviving as a function of operating conditions and dopant species can then be compared to the experimental data to evaluate the performance of the model.

6.1 Model description

The one-dimensional model is an extension of a model developed by Min [16] to investigate the oxidation of crevice-stored hydrocarbons. Several changes have been made to apply Min's model to the hydrogen-fired case. The first and most important was the addition of a model for the desorption of dopant from the oil layer. The second change was the introduction of a turbulent diffusion model, which proved to be critical to this work. Third, a simple crevice model was added to replace a more detailed model of crevice behavior contained in a separate code. Lastly, Arrhenius one-step constants for the oxidation of each dopant - toluene, isooctane and MTBE - were added.

Model assumptions

The model assumes that transport and oxidation of hydrocarbons during expansion takes place as one-dimensional radial transport of energy, mass, hydrocarbon and oxidizer through the thermal boundary layer gas adjacent to the gas-oil interface (Fig. 6.1). The flux of hydrocarbons into the gas phase is governed by the diffusion of dopant from the liquid oil phase. The gas-side domain extends three millimeters away from the oil layer, including the entire boundary layer. It is sufficient to limit the simulation to the boundary layer, as the simulation showed that the oxidation of the desorbed hydrocarbons is also limited to the thermal boundary layer. As will be shown in this Chapter, reaction rates become sufficiently fast as the gas temperature approaches the core temperature that all hydrocarbons are oxidized before reaching the core. The gas temperature outside the thermal boundary layer is the adiabatic core temperature predicted by a separate cycle simulation code [37]. The time varying cylinder pressure and temperature are predicted by this cycle simulation code. The initial thickness and subsequent growth of the thermal boundary layer are based on experiments performed in an optical engine [38].

The assumptions in the model are as follows:

1. The process is one-dimensional and planar, as the radial domain (3 mm) is much smaller than the engine bore (86 mm).
2. There is no transport of energy or mass in the axial direction (parallel to piston motion).
3. Oxidation of the hydrocarbons is expressed by one-step chemistry

The model solves the following differential equations for continuity, energy and species

$$\frac{\partial \rho}{\partial t}+\frac{\partial(\rho u)}{\partial x}=0$$

$$\frac{\partial X_i}{\partial t}+u\frac{\partial X_i}{\partial x}=\frac{1}{\rho}\frac{\partial}{\partial x}\left(D_i\frac{\partial X_i}{\partial x}\right)+\frac{\dot{\omega}_i}{\rho} \quad (i=1,2)$$

$$\frac{\partial T}{\partial t}+u\frac{\partial T}{\partial x}-\frac{1}{\rho c_p}\frac{dp}{dt}=\frac{1}{\rho c_p}\frac{\partial}{\partial x}\left(k_e\frac{\partial T}{\partial x}\right)-\frac{\Delta h_r}{\rho c_p}\frac{\dot{\omega}_1}{\rho}$$

(6.1)

where X_i is the mass fraction of species i, the hydrocarbon dopant (i=1) and oxygen (i=2), D_i is the effective diffusivity of species i in the gas phase, k_e is the effective thermal conductivity, $\dot{\omega}$ the reaction rate of species i, Δh_r is the specific enthalpy of the reaction, ρ is the gas density, T is the gas temperature, u is the velocity in the radial direction and x is the radial coordinate.

The one-dimensional implementation of the continuity equation does not capture the axial flow past the cylinder wall and thus can not correctly predict the convection term (u). During the expansion stroke, the gas expands primarily in the axial direction (z) as the piston moves away from the head. The one-dimensional continuity equation overstates $\partial u/\partial x$, as it neglects the $\partial w/\partial z$ term. This effect is most clearly shown by assuming isentropic expansion ($\rho \sim p^{\gamma}$), and considering the two dimensional continuity equation for spatially uniform pressure,

$$\frac{\partial u}{\partial x}=\frac{1}{\gamma p^{-\gamma}}\frac{\partial p^{-\gamma}}{\partial t}-\frac{\partial w}{\partial z}.$$

At the cylinder wall, the axial velocity (w) is zero so the gas only expands in the x direction. In the core gas the radial velocity (u) is zero, so the gas only expands axially. Therefore neglecting the term $\partial w/\partial z$ results in overstating the convective term (u) by greater and greater amounts as distance from the cylinder wall increases. The overstated convective term reduces the temperature gradient, resulting in the temperature at which oxidation can occur being further away from the oil layer. The model addresses these issues by specifying the boundary layer thickness at each time step and setting the temperature outside the boundary layer to the adiabatic core temperature predicted by the cycle simulation. In addition, the convective term outside the boundary layer is set to zero. Although this approach does not address the convection term and resulting temperature gradient within the thermal boundary layer, it fixes the end points of the radial temperature gradient to the correct values by holding the core temperature the appropriate distance from the cylinder wall. This approach also limits convection to the thermal boundary layer as is the case in an engine (assuming no large scale motion).

The assumed initial value and evolution of the thermal boundary layer thickness are based on schlieren measurements of the thermal boundary layer in an optical engine with a square piston [38]. Lyford-Pike and Heywood found that the growth of the measured boundary layer thickness obeys approximately the following expression:

$$\delta_t = 0.6\sqrt{\alpha t} \cdot \mathrm{Re}^{0.2} \tag{6.2}$$

where

$$\mathrm{Re} = \frac{\rho v(L_0 - L_S)}{\mu}, \qquad v = S_p \frac{L_0 - L_S}{L - L_S}$$

α is the molecular thermal diffusivity of the burned gases, t is time from when the location was uncovered by the piston crown, S_p is the instantaneous piston speed, L is the piston crown position relative to BDC as a function of time, L_S is the stroke length and L_0 is the axial location of the element being considered relative to the piston-crown BDC position.

Boundary conditions

The boundary conditions for the energy equations (6.1c) are a fixed temperatures at the wall and a specified temperature at the boundary layer-core gas interface. The wall temperature is fixed at each axial position and assumed to be given by

$$T_{w(z)} = T_h + (T_h - T_{cool})\, z/Ls$$

where z is the piston position measured from the BDC position, T_h is the temperature measured at the top of cylinder liner and T_{cool} is the coolant temperature. A cycle simulation model provides the core gas temperature as a function of time. Each operating condition was modeled using a cycle simulation code to generate pressure and temperature histories. The inputs and results of the cycle simulations are described in Appendix D. The predicted pressures are in reasonable agreement with the measured pressures, as shown in Fig. 6.2.

The boundary conditions for the species conservation equations on the core gas side of the domain are the fixed bulk values for hydrocarbon and oxygen concentration. The hydrocarbon mass fraction (X_1) in the core gas is assumed to be zero and the oxygen mass fraction (X_2) is specified by the nitrogen dilution and fuel-air equivalence ratio inputs as

$$X_2 = \frac{M_{O2} \cdot (1-\phi)}{M_{N2} \cdot \psi + M_{O2} \cdot (1-\phi) + M_{H2} \cdot (2\phi)} \tag{6.3}$$

where M_{O2}, M_{N2}, and M_{H2}, are the molecular weight of oxygen, nitrogen and hydrogen, ψ is the nitrogen to oxygen molar ratio and ϕ is the fuel air ratio. At the oil-gas interface, the boundary conditions are: an impermeable wall for oxygen and an imposed flux of hydrocarbons. The flux of hydrocarbons is obtained by solving the diffusion equation of dopant in the oil layer subject to the oil-gas interface conditions of mass conservation and dopant solubility in oil. The oil-dopant model is discussed in a later subsection.

Initial conditions

The initial radial temperature profile in the gas is based on experiments in optical engines where the boundary layer and temperatures were measured [38, 39] and assumptions about the flow of gas from the top-land crevice. The initial thermal conditions are set just as the axial position of interest is exposed to the cylinder gases at the top of the piston crown (Fig. 6.1b). It is assumed that the crevice gases exit the crevice at the wall temperature and form an isothermal layer between the oil layer and the burned gases (Fig. 6.3). Lyford-Pike and Heywood [38] found that the thermal boundary layer at any given axial position on the cylinder was 1 millimeter immediately after being uncovered by the piston crown and increased with time as described by eqn. 6.2. The initial radial variation in temperature is assumed to follow the behavior as measured by Lucht *et al.* [39] near the cylinder head using the CARS technique,

$$T(x) = T_c + \frac{T_c - T_w}{2.6} \log(x / \delta_t) \tag{6.4}$$

where T_c and T_w are the core and wall temperatures respectively.

The initial boundary layer thickness in these measurements should be used with some caution as the square-piston optical engine of Lyford-Pike and Heywood [38] is not representative of the hydrogen-fueled modern engine in the present experiments. It is quite possible that the initial thermal boundary layer thickness in these experiments is significantly smaller than the one millimeter measured in the square-piston engine. One would expect the initial thermal boundary layer thickness to scale with the quench distance for locations exposed to the flame and scale with the piston top-land crevice volume among other parameters for locations uncovered by the piston. The hydrogen flame quench distance is an order of magnitude shorter than that of a typical hydrocarbon flame as discussed in Chapter 2. The top-land crevice in these experiments is also an order of magnitude smaller than the top-land crevice in the square piston optical engine. A thinner initial boundary layer thickness is supported by Lutch's CARS result [39] that the thermal boundary layer thickness on the head was two to three times thinner than that measured in the square-piston engine.

Initially the dopant is limited to the oil layer is shown in Fig. 6.1a. The concentration is based on an typical dopant level of three percent by weight in the bulk oil. The mass fraction of dopant in the oil layer on the cylinder wall is approximately 0.4 % due to oil flow in the piston ring pack as explained in Chapter 3. The hydrocarbon concentration in the core gas and the crevice gas is initially zero as the hydrogen flame penetrates the crevice and burns all the hydrogen and hydrocarbons present. The initial oxidizer concentration is equal to the bulk concentration as defined by eqn. 6.3.

Crevice model

The piston crevice is modeled as a simple isothermal volume at the corner of the piston and cylinder. The pressure is assumed equal to the cylinder pressure and the exiting mass flow rate is determined from continuity and the ideal gas law. The mass flow rate out of the crevice ($\dot{m}_{cr}$) is equal to the change in mass in the crevice, which in turn is determined from the change in pressure,

$$\dot{m}_{cr} = \frac{dm_{cr}}{dt} = \frac{V_{cr}}{RT_{cr}}\frac{dp}{dt} \tag{6.5}$$

where T_{cr}, V_{cr} and m_{cr} are the temperature volume and mass in the top-land crevice. The resulting mass outflow rate as a function of distance is similar to results of the more complicated model used by Min [16] which also modeled the second and third lands as well as ring motion (Fig. 6.4).

Turbulence model

The transport rate of the desorbed dopant towards the hot gases and energy towards the wall and the chemical oxidation rate are the primary determinants of the hydrocarbon oxidation rate. Measurements have shown the presence of significant levels of turbulence during and just after flame passage, which then decays rapidly in time [40, 41]. The one-dimensional model includes the effect of turbulence by using effective mass (D_e) and thermal (α_e) diffusivities as the sum of turbulent and molecular contributions, with the turbulent Lewis number assumed to be unity, so that $D_T=\alpha_T$.

$$\begin{aligned} \alpha_e &= \alpha + \alpha_T \\ D_e &= D + \alpha_T \end{aligned} \tag{6.6}$$

The turbulent diffusivity (α_T) is derived from eddy diffusivity scaling arguments, based on the assumption that the turbulent kinetic energy is approximately uniform in the boundary layer and that the mixing length scales with distance to the wall,

$$\alpha_T = c_\mu \sqrt{k} \cdot x \quad , \qquad (6.7)$$

where k is the turbulent kinetic energy. The proportionality coefficient c_μ is assumed to be the same as in the case of the flat plate momentum boundary layer ($Pr_T = 1.0$), with the value 0.09 [42]. Equation 6.7 is appropriate for x smaller than the integral length scale in the core. The measured integral length scale is typical 2 to 6 mm in length at TDC, increasing as gas and the eddies expand with the dropping pressure [21, 43].

The turbulence decay model is based on the k-ε model of turbulence decay without production [44]

$$\frac{k}{k_0} = (1 + 0.9 \cdot t / \tau_0)^{-c_k} \qquad (6.8)$$

where

$$\tau_0 = \frac{\lambda_o}{\sqrt{k_o}}$$

k_0 is the initial turbulence kinetic energy, λ_o is the initial integral length scale, t is the time, and c_k is a constant equal to 1.11 based on measurements of decaying turbulence [45]. Hall *et al.* [40] found that the turbulence levels were constant for 15 CAD past the end of combustion and then decayed rapidly. Therefore, t in this model is taken as the time from 15 CAD past the end of combustion. The initial length scale (λ_o) was taken as 3 mm [43]. The resulting kinetic energy decay shows excellent agreement with the measured turbulent kinetic energy levels in a firing engine from Hall *et al.*[40], (Fig. 6.5). The turbulent kinetic energy (k) is the sum of the square of the three components of turbulent kinetic energy. It is assumed that after the end of combustion in the engine, the turbulence is isentropic and scales with the mean piston speed (S^*_p). The initial kinetic energy is then calculated as

$$k_0 = \frac{u_x'^2}{2} + \frac{u_y'^2}{2} + \frac{u_z'^2}{2} = 3\frac{u'^2}{2} = 3\frac{(\chi S_p^*)^2}{2} \qquad (6.9)$$

A review of the literature showed that measured levels of turbulence normalized by the mean piston speed ($\chi = u'/S^*_p$) in fired engines at TDC ranged from 0.6 to 0.84 [40, 41]. A value of 0.75 was selected for χ

as this modern pent-roof engine is expected to generate higher levels of turbulence during combustion than older designs and this value provided the best fit to the predicted heat transfer of the cycle simulation code.

The transport of hydrocarbons from the oil layer as well as transport of energy to the cylinder wall are turbulent in nature. Therefore, the adequacy of the turbulent transport model can be assessed by evaluating the heat transfer rate in the one-dimensional model from the predicted temperature gradient at the oil interface. The cycle simulation provides a reasonable prediction of the heat transfer rate as it uses the well established Woschni heat transfer correlation and provides good predictions of the pressure trace. The rate of heat transfer for several axial positions in the one-dimensional model is compared to the rate of heat transfer from the cycle simulation code for the baseline condition in Fig. 6.6. The heat transfer levels in the one-dimensional model show good agreement with the heat transfer rates predicted by the cycle simulation. The initial high heat transfer rates reflect the relaxation of the initial temperature profile defined by eqn. 6.4. An initial higher heat transfer rate, as a cylinder wall location is uncovered is seen experimentally in the decreasing rate of boundary layer growth observed in the square-piston optical engine [38].

Oxidation model

The oxidation chemistry submodel is a simple one-step global reaction with a rate obeying the Arrhenius form,

$$\dot{\omega}_1 = A_0 \rho_1^a \rho_2^b \exp\left(-E_a/RT\right) \tag{6.10}$$

where the ρ_{HC} and ρ_{O2} are the molar densities of hydrocarbon and oxygen. The constants A_O, a, b and E_a were taken from a study by Wu [30], in which full chemical kinetic mechanisms were used to investigate the rate of oxidation of hydrocarbons in the burned gas at temperatures and concentrations expected in the cylinder and port of a spark-ignition engines under uniform (plug flow) conditions. Wu investigated three of the five fuels used in the present experiments: toluene, isooctane and MTBE. For very low levels of unburned mixture concentration (0.1% unburned fuel-air mixture in burned gases) the oxidation rate was found to be much higher than for higher concentrations, since induction times were shortened by the availability of background radicals from the burned gases. Early results from the present one-dimensional model showed that oxidation was occurring at concentrations well below those of a 0.1% unburned mixture. Therefore, the pre-exponential constant (A_O) and the activation energy value (E_a) were refit to the lowest unburned gas concentration results (unburned mixture concentrations of 0.1%) for each of the three fuels, with the original fuel and oxygen exponentials recommended by Wu. The resulting A_O, E_a a and b are listed in Table 6.1.

Table 6.1 Global reaction rate constants

fuel	A_0 (cm^3/mole s)	E_a (cal/mole)	a	b
toluene	$7.78 \cdot 10^{14}$	40,900	0.583	1.515
isooctane	$2.49 \cdot 10^{16}$	49,840	0.836	1.08
MTBE	$3.56 \cdot 10^{12}$	50,596	0.843	0.489

Predictions using these global reaction rates should be considered approximate. Firstly, although detailed kinetics modeling of the oxidation of unburned mixture in burned gas is state of the art, it does not capture important details of the actual reaction environment, such as the diffusion of radicals into unburned gases. Secondly, the global reaction expression can only capture a limited range of conditions. Comparison of the times for 50% oxidation predicted by the global reaction rate fit and the full chemical kinetic results shows differences up to an order of magnitude (Fig. 6.7).

Oil desorption model

The oil layer desorption model solves the one-dimensional diffusion equation for dopant in the lubricant oil layer on the cylinder wall once it is uncovered by the piston ring-package. The diffusion equation is

$$\frac{\partial X_o}{\partial t} = D_o \frac{\partial^2 X_o}{\partial x^2} \qquad (6.4)$$

where X_o is the mass fraction of dopant in the oil and D_o is the diffusivity of dopant in the oil. The boundary conditions are

$$\begin{aligned} &\frac{\partial X_o(0,t)}{\partial x} = 0 \\ &X_o(\delta_o,t) = \frac{p}{H^*}\frac{M}{M_l} X_l(\delta_o,t) \\ &D_l \cdot \rho \frac{\partial X_l}{\partial x}(\delta_o,t) = D_o \cdot \rho_o \frac{\partial X_o}{\partial x}(\delta_o,t) \end{aligned} \qquad (6.5)$$

where H^* is the modified Henry's constant for the dopant in the oil, p is the gas pressure, M and M_l are the molecular weight for the burned gas at the wall and the dopant respectively, ρ_o is the oil density, ρ is the density of the gas mixture at the wall, X_l and X_o are the mass fraction of dopant in the gas phase and oil, D_l and D_o are the molecular diffusivity of dopant in the gas phase and oil and δ_o is the oil thickness. The calculated evolution of the dopant mass fraction in the oil is shown in Fig. 6.8. The level of dopant in the oil drops to a tenth of the original value in just 30 CAD. This rapid desorption supports the assertions made in Chapters 2 and 3 that all the dopant in the oil layer desorbs into the gas.

The model allows the dopant to begin desorbing into the crevice gas, as soon as the top compression ring uncovers the axial position (z) of interest. By the time this axial position is uncovered by the piston crown and exposed to the core gas, some of the dopant has already desorbed into the cylinder boundary layer as sketched in Fig. 6.1b. The distribution of dopant in the gas phase once out of the crevice is pictured in Fig. 6.9 for the toluene dopant at baseline condition.

The oil layer desorption model was evaluated by calculating the total amount of hydrocarbon desorbed and comparing these calculated results to the motored and fired data reported in Chapter 3. Initially, the results showed poor agreement with the data for the amount of toluene dopant desorbed at different wall temperatures (Fig. 6.10). The reason for the difference in the model results presented here and in Chapter 3 is that the analytical model in Chapter 3 assumes constant temperature and pressure, while the one-dimensional model includes the time varying pressures and temperatures in the gas phase. The cylinder pressures are an order of magnitude higher immediately after combustion than at the end of the expansion stroke. These higher pressures in the one-dimensional model lead to higher partial pressures for the same mass fraction and thus in a much lower hydrocarbon mass fraction on the gas side of the gas-oil interface due to the solubility boundary condition (eqn. 6.5). The lower gas concentration at the interface then results in a slower desorption rate.

In order to get good agreement with the desorption data, the oil layer thickness was reduced by 25%. This thinner oil layer gave good agreement with the measured amount of desorption for variations in wall temperature and dopant species (Fig. 6.10). Given the uncertainty in measurements of the oil layer thickness, a 25% change is not unreasonable, and in-fact yields results that are somewhat closer to the measured dependence on viscosity and engine speed by Tamai [47] (Fig. 6.11). However, it must be kept in mind that the oil thickness measurements were made in a single cylinder utility engine (Kohler CH14) and therefore their use should be limited to evaluating predicted oil thickness on an order of magnitude basis.

The dopant mass balance, expressed by eqn. 3.1, requires a higher concentration of dopant in the oil layer for a thinner oil layer to maintain the same level of desorption. The ratio of dopant mass fraction in the oil layer to that in the bulk oil (r_f) for the thinner oil layer can be obtained by substituting new value for the oil layer thickness into eqn. 3.1 and solving for r_f from the measured amounts of desorbed dopant.

The ratio r_f increases for the thinner oil layer from 0.1 for hexane and 0.12 for the aromatics to 0.13 and 0.16 respectively.

Solution method

Equations 6.1 through 6.10 are solved numerically by the Crank-Nicholson method [47]. The domain is 3 mm wide, with node sizes of 0.01 mm, small enough for a resolution of the crevice gas region. The time step is a minimum of $2.64 \cdot 10^{-6}$ seconds, which provides accuracy equivalent to a second order accurate system with a one crank angle time step at 1500 rpm. The energy and species equations are coupled, so although the energy and species equations are solved with the Crank-Nicholson method, which is second order accurate, the solution is only first order accurate as the energy and species are solved sequentially. The solution for each axial location (z) proceeds from the time it is uncovered by the piston top compression ring until it is covered again by the piston. At this point, the boundary layer is scraped by the piston into a fundamentally a two-dimensional structure, for which the one-dimensional formulation is not adequate. There was a concern that during blowdown the crevice mass would exit rapidly, stirring the boundary layer. Mass conservation calculations at the crevice exit during blowdown show that the exiting Reynolds number is in the stokes region (Re < 10) as the crevice volume is small and the pressure drop at these part load conditions is small.

The one-dimensional code steps through the calculations as follows. After setting up the initial conditions, the reaction rates and the radial velocity are calculated for each node. Next the energy equation is solved using the Crank-Nicholson algorithm. The oil side diffusion equation is solved with the simpler Euler method [47] using the same time step as the gas phase and a node size large enough insure numerical stability. If the node size required for stability results in less than four nodes across the oil layer, the time step is shortened for both the gas and oil phase to achieve numerical stability with four nodes across the oil layer. Next the species conservation equations for hydrocarbons and oxygen are solved using Crank-Nicholson. The temperatures and concentrations are then updated. Before starting the next time step, the cylinder pressure is updated using the input pressure history, the boundary layer thickness is updated using eqn. 6.2 and the temperatures in the nodes outside the boundary layer are updated with the input core temperature history.

Equations 6.1 through 6.10 are solved at axial positions corresponding to the piston crown position every 20 CAD. The first position considered is uncovered by the top compression ring and exposed to the crevice gases 1 CAD after top-center and exposed to the cylinder gases 28 CAD after top-center. The axial location of the piston crown 28 CAD after top-center 79.5 mm above the BDC position of the piston crown. The equations are then solved for axial locations corresponding to the piston crown position as listed in Table 6.2. The amount of dopant desorbed (dm_d/dz) and the amount of dopant surviving in the gas phase (dm_{HC}/dz) per unit axial length at each position are integrated over the stroke length using the trapezoidal rule to obtain the total amount of post-flame desorbed dopant (m_d) and surviving dopant (m_{HC}) as shown schematically in Fig. 6.12. The predicted in-cylinder oxidized fraction (f_{cyl}) is then $(m_d-m_{HC})/m_d$.

Table 6.2 Axial locations considered

CAD after top-center	axial position (z/L_s)	CAD after top-center	axial position (z/L_s)
28	0.92	108	0.27
48	0.75	128	0.14
68	0.62	148	0.06
88	0.44	168	0.01

6.2 Model results

The one-dimensional model results are presented in this section and compared to the estimated in-cylinder oxidation levels reported in Chapter 5. Detailed results for toluene dopant at the baseline case operating condition are reported and compared to the estimated f_{cyl}. The sensitivity of the predicted f_{cyl} to modeling assumptions is then evaluated in order to determine the controlling physical processes. In the last part, the sensitivity of the one-dimensional model to operating conditions and dopant species is evaluated and compared to the measured sensitivity.

Baseline condition

The baseline condition was modeled extensively with the one-dimensional model in order to understand the model, the critical assumptions and the controlling physical processes. The first step is to examine the evolution of temperature and the diffusion and oxidation of the desorbed hydrocarbons in the one-dimensional model. Next the predicted f_{cyl} is compared to the estimated value of f_{cyl} and the sensitivity of f_{cyl} to various modeling assumptions is explored. Finally the sensitivity of f_{cyl} to dopant type and operating conditions is compared to experimental results of Chapter 5.

The baseline condition is based on a mid-speed, mid-load condition typical of city driving. The inputs for the baseline condition are listed in Table 2.1. These inputs in the cycle simulation code produced the pressure and core temperature history found in Fig. 6.2.

The evolution of temperatures, hydrocarbon mass fractions in the gas phase and reaction rates will be considered for two axial locations, z/L_s = 0.75 and 0.44, which have significantly different oxidation results. The evolution of temperature and hydrocarbon mass fraction are shown in Fig. 6.13 for the 0.75 axial position. The initial temperature profile of constant temperature across the crevice gas layer relaxes within 2 CAD to a temperature profile with a steadily decreasing dT/dx. The boundary layer thickness is noticeable as the distance from the wall to the point where the temperature becomes constant. The initial high concentration of the hydrocarbon in crevice gas also quickly diffuses toward the burned gases. The initial high mass fraction of hydrocarbons in the crevice gas results from the assumption that the dopant desorbs from the oil into the crevice gas before being uncovered by the piston crown. The hydrocarbon concentrations are quite low beyond one millimeter from the cylinder wall oil layer due to oxidation.

The spatial and thermal evolution of the oxidation rate is shown in Fig. 6.14. It is clear from the spatial plot that the oxidation zone, initially near the wall, moves toward the center of the cylinder as the boundary layer grows. The rate of oxidation also decreases significantly with time and the width of the reaction zone widens. A plot of the reaction rate against the gas temperature shows that the maximum oxidation rate occurs at approximately the same temperature (~1600 °K) as the boundary layer expands. The reaction rate initially rises with temperature as expected and then drops off at higher temperatures due to the low hydrocarbon concentrations in the burned gas. Since the peak oxidation rate occurs at a constant temperature, the decrease in oxidation rates with time is due to lower concentrations of hydrocarbons in the high temperature region.

The temperature and hydrocarbon mass-fraction results at the mid-stroke position are similar to those discussed previously (Fig. 6.15). Obviously the core temperatures are significantly lower, as this axial position is uncovered 88 CAD after top-center. The lower pressures and temperatures at which peak oxidation occurs, produces significantly lower oxidation rates (Fig. 6.16). The timing of the maximum oxidation rate is delayed and the temperature at which it occurs is lower as the desorbed hydrocarbons must diffuse further to reach oxidizing temperatures.

Figures 6.13 through 6.16 support the assumptions that the oxidation of hydrocarbons is limited to the thermal boundary layer. The hydrocarbon mass fractions drop to nearly zero within 2 mm of the wall (Figs. 6.13 and 6.15). The oxidation rate also drops to zero inside the boundary layer as the hydrocarbons are exhausted (Figs. 6.14 and 6.16). Throughout the expansion stroke the peak oxidation levels occur at temperatures below the core temperatures (Fig. 6.2).

The resulting axial distribution of desorbed and surviving hydrocarbons is shown in Fig. 6.16 along with the fraction oxidized at each axial location. The amount of mass desorbed reflects the amount of dopant in the lubricant oil layer. Most of the in-cylinder oxidation takes place near the top of the cylinder wall, where desorbed hydrocarbons are exposed to the highest temperature.

Comparison to baseline data

The average measured oxidation rate for toluene at the baseline condition is 77% and the estimated in-cylinder oxidation rate is 46% based on averaging the high and low port oxidation cases. The one-dimensional simulation predicts 17.5% of the desorbed dopant oxidizes in-cylinder, which is about two and half times less than the estimated value based the experiments. The one-dimensional model is expected to produce lower than observed levels of oxidation as it does not attempt to model the three-dimensional flow and mixing processes that occur during exhaust. The adiabatic core gas, which is a constant 1530 °K during the exhaust process, is hot enough to quickly oxidize any entrained hydrocarbons. It is difficult to assess this effect as the in-cylinder exhaust flows are relatively complicated.

In addition to the limitation of the one-dimensional assumption, the model includes a number of assumptions which may have a significant impact on the predicted level of in-cylinder oxidation. The oxidation reaction rates are based on a zero-dimensional model that may not capture the diffusional nature of the oxidation process. The sub-model for turbulent transport near the walls is based on turbulence measurements in different engines and a simple scaling law for transport near the wall. The in-cylinder temperatures predicted by the cycle simulation are approximate values that could easily be 100 °K different with little effect on the predicted pressure. The sensitivity of the predicted oxidation levels to these and other assumptions is explored in the next subsection.

Sensitivity studies

The sensitivity of dopant oxidation in the toluene baseline case was investigated for assumptions about the turbulence model, chemical reactivity, desorption into the crevice, temperatures, axial distribution of dopant concentration the oil layer and crevice size. The sensitivity results are listed in Table 6.2. The values were generally chosen to capture the range of uncertainty in the input values. Some of the inputs such as turbulence and turbulence decay were selected to demonstrate the relative importance of quantity. The largest changes are due to changing the initial turbulence levels, turbulence decay and the chemical activation energy. Other important parameters are the initial boundary layer, the oil concentration axial distribution and core temperatures.

The turbulence sensitivity results indicate several important conclusions. Turbulent transport has a significant effect on the fraction oxidized and can not be neglected in the one-dimensional model. The one-dimensional model must also consider some kind of turbulence decay. Some uncertainty in the initial turbulence level is acceptable as the fraction oxidized is not particularly sensitivity to variations in the initial turbulence level around the value baseline value: ($u'=0.75\ S^*_p$).

Table 6.3 Sensitivity Studies

Parameter	Value	f_{cyl} at BDC	f_{cyl} at IVO	$\Delta\%$ in f_{cyl} at IVO
Turbulence	0.0	1.0	2.6	- 85
	$S^*_p \cdot 0.75$	13.6	17.6	0
	$S^*_p \cdot 1.5$	18.7	22.8	30
Turbulence decay	no	32.1	41.8	138
Chemical Reactivity	$0.5 \cdot A_0$	10.4	12.7	28
	A_0, E_a	13.6	17.6	0
	$2.0 \cdot A_0$	17.9	23.9	36
	$0.8 \cdot E_a$	35.7	51.4	192
	$1.2 \cdot E_a$	4.3	4.6	- 74
Initial Boundary Layer (mm)	2	11.8	20.3	15
	1	13.6	17.6	0
	0.5	17.9	22.8	30
	0.25	21.5	26.8	52
	0.12	23.8	29.5	68
Core Temperature (^{o}K)	-100	10.3	12.1	- 31
	nominal	13.6	17.6	0
	+100	17.8	24.7	40
Axial Dopant Distribution	uniform	13.6	17.6	0
	linear variation with more at bottom of cylinder	6.6	9.7	- 45
Desorbing into Crevice	yes	13.6	17.6	0
	no	12.2	15.4	- 13
Forced Boundary Layer	no	11.5	14.2	- 19
Crevice Size (cm^3)	0.255	16.0	20.6	17
	0.511	13.6	17.6	0
	1.022	10.9	14.4	-18
Average experimental value		46		

The sensitivity to the oxidation rate expression indicates the extent of oxidation is modestly dependent on the pre-exponential term and very dependent on the activation energy as expected. Changing the pre-exponential term by a factor of two changed the extent oxidized by about 30%.

Decreasing the activation energy by 20%, tripled the extent oxidized, while increasing the activation energy by 20% reduced the extent oxidized to a quarter of the nominal value. Changing the pre-exponential term by a factor of two is equivalent to changing the τ_{50} by a factor of two, while reducing the activation energy by 20% changes the characteristic time to oxidize hydrocarbons by one to two orders of magnitude.

The initial boundary layer thickness has a significant effect on the fraction of dopant oxidized that becomes very important at thicknesses less than 0.25 mm. As previously discussed, the initial boundary layer thickness is based on experiments in a low compression square-piston engine, which is quite different from the hydrogen-fueled pent-roof engine used in this study. It is possible that the boundary layer in the modern pent-roof engine is much thinner than the 1 mm measured in the square optical engine. If the initial boundary layer thickness scales with the crevice volume, then an initial thickness of 0.12 mm would be appropriate producing a 68 % increase in the fraction of dopant oxidized.

The extent oxidized is also sensitive to the core temperatures predicted by the cycle simulation code. A 100 °K increase in the core temperatures produces a 40% increase in the fraction burned and a similar but opposite effect for a 100 °K reduction.

The extent oxidized is somewhat sensitive the axial distribution of dopant within the lubricant oil layer. The nominal one-dimension model assumes the concentration of dopant in the oil layer is initially uniform. An alternative to the uniform distribution is that the dopant concentration is higher in the oil nearer the bottom of the piston stroke as this oil may be exposed longer to sump oil and thus absorb more dopant than oil layer near the top of the cylinder. The sensitivity study considered this effect by linearly varying the dopant concentration from zero at the top of the cylinder to twice the nominal dopant concentration at the bottom of the cylinder. The resulting extent of oxidation was approximately half the original value.

The effect of crevice size, dopant desorption into the crevice, and the assumption of a specified thermal boundary layer have small effects on the extent oxidized relative to the other parameters, and thus will not be considered further.

Good agreement of the predicted in-cylinder oxidation (f_{cyl}) levels with the experimental values can be obtained for a number of different, reasonable changes in the modeling assumptions. It is possible the initial thermal boundary layer thickness is much too large and a value on the order of 0.1 mm is more appropriate. This change alone would put the predicted f_{cyl} within 30% of the estimated value. Similarly raising the core temperature prediction would have a large effect and combining it with a thinner initial boundary layer would predict oxidation rates near or above the estimated values. Another obvious change is to decrease the chemical activation energy by 15%, which produces predicted oxidation levels (f_{cyl} = 0.42) equivalent to the estimated value of 0.45. The resulting axial distribution of desorbed and surviving hydrocarbons is shown in Fig. 6.17 along with the fraction oxidized at each axial location. This 15% decrease in activation energy is used in the next subsection to evaluate the predicted dependence on dopant type and operating condition.

Sensitivity of f_{cyl} to fuel type and operating conditions: model vs. experiment

The sensitivity of model results to fuel type was evaluated at the baseline condition for the three fuels for which one-step oxidation constants were available: toluene, isooctane and MTBE. The effect of operating conditions were evaluated for the toluene dopant as the majority of the data was taken with toluene. The comparisons are made with the nominal predicted values of the one dimensional model and those predicted for a 15% reduction in the chemical activity, which gave good agreement on the absolute oxidation level.

The sensitivity of the fraction oxidized in-cylinder to dopant type at baseline condition is shown in Fig. 6.18. The nominal values, though low, show the correct ranking of fuels. The results for the reduced activation energy case shows good agreement with the measured sensitivity of oxidation to dopant type. This good agreement on the dopant dependence indicates that the model has a reasonable balance between the reaction rates and transport in the gas phase. If the oxidation process were limited by transport then there would be little difference between the fuels.

The other effect of dopant type is the solubility of the dopant in the oil, which at warmed up conditions does not appear to be a dominant factor. This view is supported by the results of an attempt to model the desorption and oxidation of the xylene dopant. Solubility data for xylene in oil was used as it was available. The oxidation was modeled with the Arrenhius coefficients for toluene as it has a similar chemical structure to xylene. Relative to the toluene results, the one dimensional model predicted an oxidation rate 12% lower due to the five times higher solubility and thus slower desorption of xylene from the oil. However, the data showed a 20% increase in oxidation levels for xylene relative to the toluene data. Similarly hexane was modeled using Arrenhius coefficients for isooctane. In this case, the model predicted a 12% increase in oxidation for the faster desorption of hexane compared to toluene, while the data only showed a three percent increase. Solubility of the dopant in the oil is not the controlling parameter in these cases and in general is of secondary importance relative to the chemical reactivity.

The fraction oxidized in-cylinder as estimated from data and predicted by the one-dimensional model for all the operating conditions with a toluene dopant are shown in Fig. 6.19. The sensitivity of f_{cyl}

to operating conditions is similar for both the nominal inputs and for the reduced activation energy case. The model and data show good agreement for dilution levels above 0.2 and the effect of coolant temperature. These are the operating variables, which make the largest difference in f_{cyl}. Not surprisingly the model significantly over-predicts the level of in-cylinder oxidation for the zero dilution case. The zero dilution results for f_{cyl} appear to be incorrect possibly due to an incorrect estimate of the hydrocarbon residual fraction (f_{res}) as discussed in Chapter 5. Although the model and data show opposite trends with engine speed, spark timing and lean fuel-air ratios, the effect of these parameters is small in both the data and model. The chemical reaction submodel is not valid for fuel rich conditions, so the model was limited to lean cases. At lower loads, both the predicted and estimated oxidation levels showed weak dependence on load. The model shows poor agreement with the estimated f_{cyl} levels at loads above an IMEP of 3.5 bar, which decreased significantly with increased load, while the predicted f_{cyl} rose slightly. However, the f_{cyl} values for loads above an IMEP of 3.5 shows significant amounts of scatter. Reviewing the f_{cyl} values for isooctane (Fig 5.6) finds little dependence of f_{cyl} on load over the same range in IMEP, which is similar to the predicted sensitivity of f_{cyl} to load for toluene.

The relatively good agreement on the effects of fuels and operating conditions on the fraction oxidized allows the one-dimensional model to be used to identify the controlling physical processes. As previously noted, the critical variable between dopants at warmed-up conditions is the chemical reactivity. The effect of operating conditions can be understood by plotting the cylinder temperature as a function of the fraction of dopant desorbed after the end of combustion (Figs. 6.21 through 6.26). The adiabatic core temperature histories are shown in the upper plot for each group of operating conditions. These temperatures are predicted by the cycle simulation code and are an input to the one-dimensional simulation. The fraction of desorbed mass overtime is an output of the one-dimensional model using the reduced activation energy. The figures 6.21 through 6.26 plot the fraction of the desorbed hydrocarbon exposed to a given cylinder temperature. In general, the more dopant mass exposed to higher temperatures, the more will be oxidized in-cylinder. The predicted fraction oxidized in-cylinder (f_{cyl}) predicted by the one-dimensional model is marked for each case with a vertical line from the axes to the appropriate curve. The fraction oxidized for most operating conditions corresponds to a temperature of approximately 1700 °K on the temperature-fraction desorbed curves.

It is clear in Figs. 6.21-6.25 that a correlation exists between the fraction of dopant desorbed when the cylinder temperature is approximately 1700 °K and the fraction oxidized in-cylinder. This correlation holds for changes in the dilution level, engine load, spark timing and engine speed, which produced different temperature histories and changes in the coolant temperature which produced different desorption rates. Increasing the dilution level significantly lowers the gas temperatures as shown in Fig. 6.21a, which leads to decreasing amounts of dopant desorbed before the cylinder temperature reaches approximately

1700 °K. The result shown in Fig. 6.21b is consistent with the one-dimension simulation results and the experimental value for f_{cyl} except for the zero dilution case, which never reached 1700 K. Similarly, advancing the spark decreases temperatures during the expansion stroke leading to somewhat lower f_{cyl} results from the one-dimensional model (Fig. 6.22b). The load had little effect on the temperature or the desorption except for the low load point, which is consistent with the experimental values for f_{cyl} (Fig. 6.23b). The efffect of different engine speeds had little effect on the cylinder temperatures at these condtionns (Fig. 6.24a). The f_{cyl} values are nearly equal although the low speed case generates more oxidation due possibly to more time to transport to the hot core geases(Fig. 6.24b). The cylinder temperatures changed little with coolant temperature (Fig. 6.25a), while the fraction desorbed changed significantly. The resulting temperature versus fraction desorbed plot shows good agreement between the mass desorbed at 1700 °K and the fraction oxidized in-cylinder obtained in the experiments (Fig. 6.25b). The last result is interesting in that it indicates that increased solubility of the dopant in the oil is the primary mechanism leading to lower rates of oxidation at lower temperatures.

The effects of fuel-air ratio on the fraction oxidized in-cylinder can not be explained by the core temperature and the timing of dopant desorption alone. The one-dimensional model predicted that a larger fraction of dopant is oxidized despite lower cylinder temperatures at the lean operating condition (Fig. 6.26). Closer examination of the one-dimensional results found that the higher oxygen concentrations at the lean condition more than compensated for the lower cylinder temperatures: the oxygen concentration in burned gases is four times higher in the burned gas for $\phi=0.8$ than for $\phi=0.95$ and the reaction rate is proportional to the oxygen density to the 1.5 power for toluene (eqn. 6.10).

The good correlation between the fraction of dopant desorbed at a cylinder temperature of 1700 °K and the f_{cyl} values predicted by the one-dimensional model is shown in Fig. 6.27. The predicted f_{cyl} values show a one to one correspondance to the fraction of dopant desorbed for most of the conditions modeled. The exceptions are lean operation where the excess oxidation acounts for a higher oxidation rate, zero dilution and to a lesser extent the retarded timing case.

6.3 Conclusion

A one-dimensional model has been developed of the desorption, diffusion and oxidation of hydrocarbons stored in the oil layer. The model solves the one-dimensional equations for energy, mass and species during the expansion and exhaust strokes. The core temperatures and cylinder pressures are inputs calculated with a separate cycle simulation code. The oxidation process is modeled using a one-step Arrenhius form with the constants taken from the results of a full chemical kinetics study of post-flame oxidation of hydrocarbons. A turbulent transport model was including turbulence decay and the effect of the wall was also added to the one-dimensional model.

The nominal predicted oxidation levels are two and half times lower than those estimated from data for toluene dopant at baseline conditions. A sensitivity study found that turbulence, chemistry, the initial thermal boundary layer thickness and core temperatures were important variables in controlling the predicted oxidation level. Decreasing the oxidation activation energy by 15% produced oxidation level equivalent to the values estimated from the experimental data.

The model showed good agreement on the sensitivity of oxidation levels to dopant type and operating conditions that produces significant changes in oxidation levels: dilution and coolant temperatures. The oxidation level in the model and experiments showed weak dependence on engine speed, spark timing, loads below 3.5 and lean air-fuel ratios. These trends in the data and model were equivalent given the uncertainty in both the model and data.

Analysis of the one-dimensional modeling results showed that the dominant dopant effect at warmed up conditions is a change in chemical reactivity and that solubility effects are secondary. The primarily effect of different operating conditions is to change cylinder temperature to which the dopant is exposed. This is occurs either by changing cylinder temperature history (engine load, dilution levels and spark timing) or the rate at which dopant desorbs into the cylinder (coolant temperature). The coolant temperature results indicate that solubility effects are important at colder temperatures. The level of oxidation is also somewhat sensitive to the oxygen content of the burned gases.

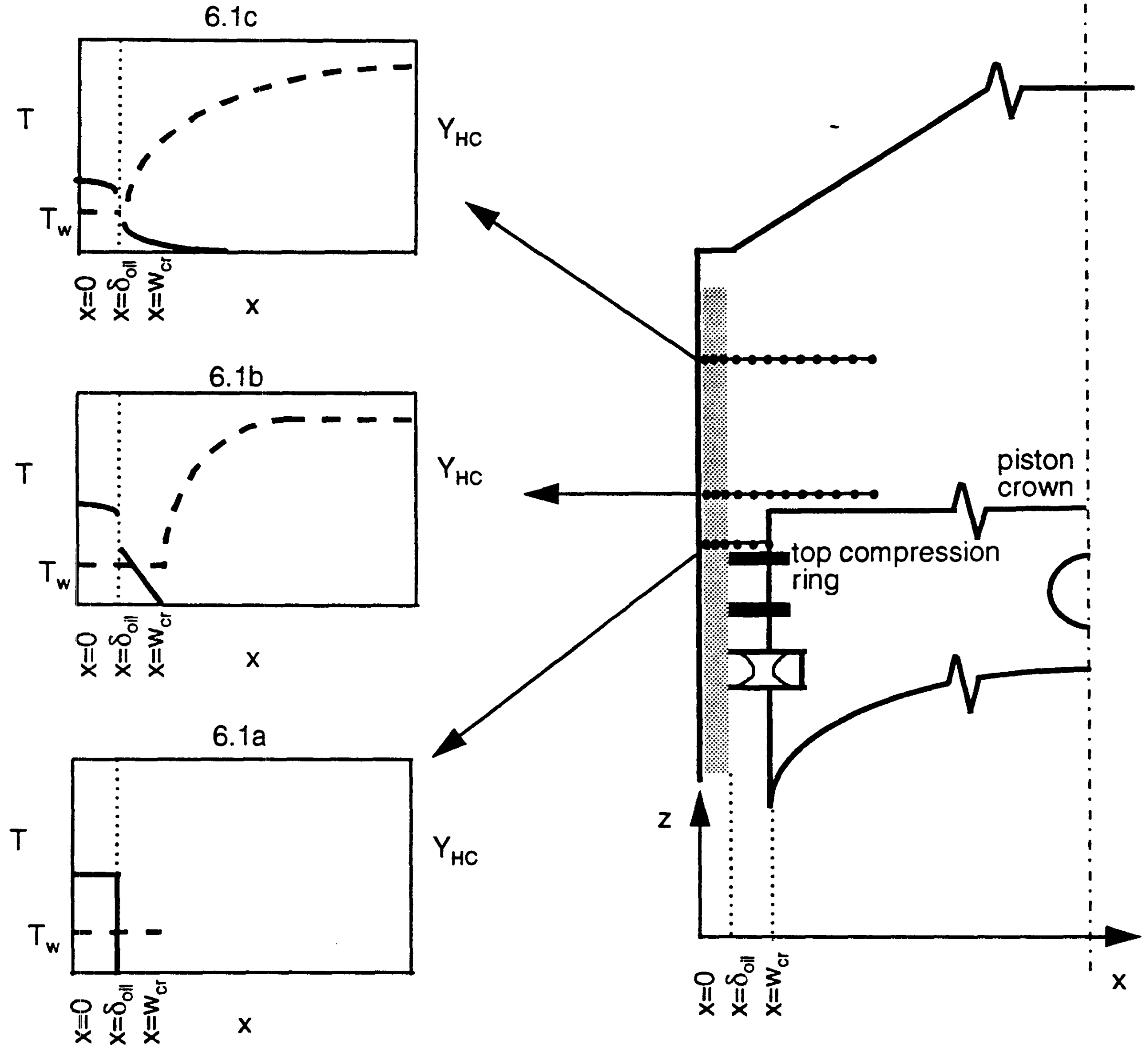

Fig. 6.1 Schematic of the one-dimensional model. The three charts sketch the temperature (dashed line) and hydrocarbon concentration (solid line) of three different oil and gas axial positions. Figure 6.1a describes the initial hydrocarbon level in the oil and crevice temperature, just as the oil layer is exposed to the burned gases in the crevice. Figure 6.1b shows the initial temperature profile once the segment is exposed to the cylinder gases and the dopant that has desorbed into the crevice gases. Figure 6.1c shows the continued desorption of dopant and relaxation of the temperature.

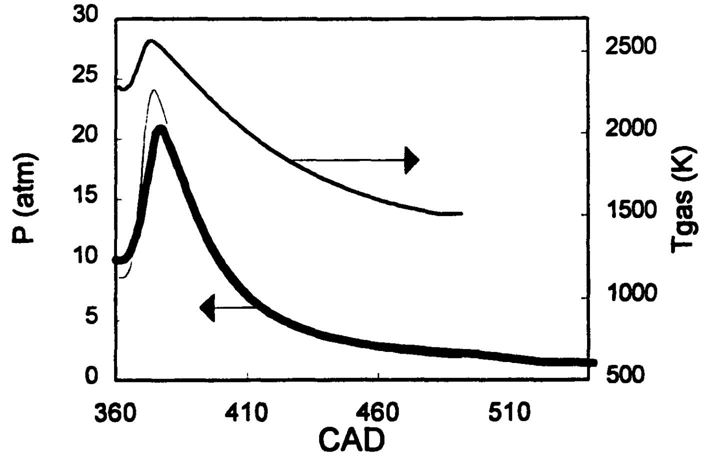

Fig. 6.2 Pressure and core temperature from cycle simulation (thin lines) for baseline case and measured pressure trace (thickline).

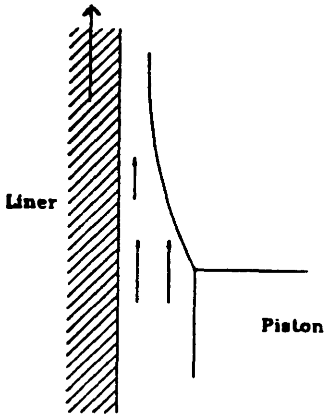

Fig. 6.3 Flow of crevice mass relative to piston motion.

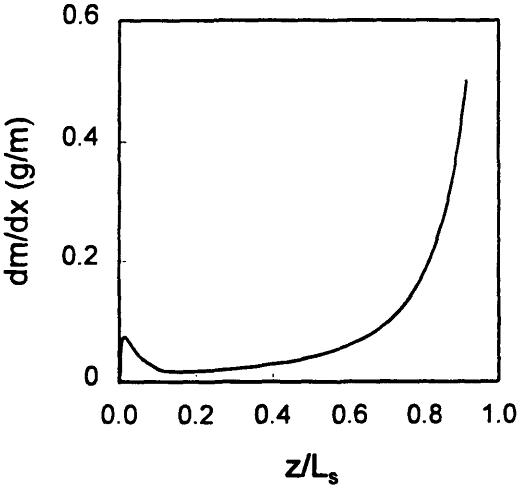

Fig. 6.4 Piston crevice distribution along the liner during the expansion stroke for baseline case.

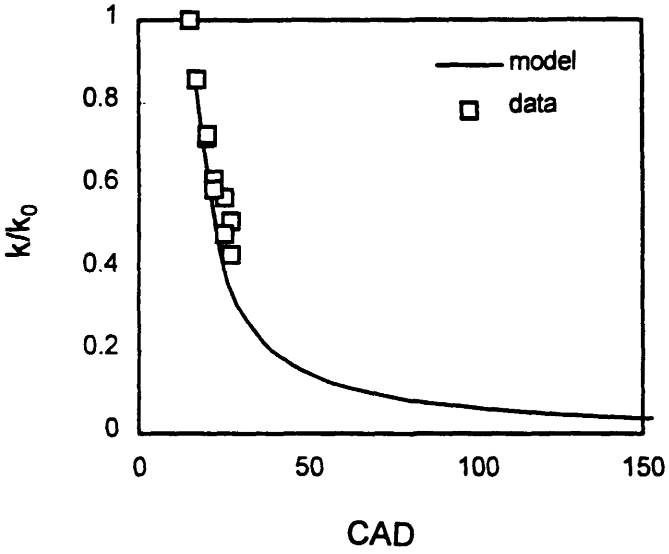

Fig. 6.5 Turbulent energy decay model and turbulent energy data from Hall et al. (1983). Zero CAD is end of combustion and initial turbulent energy in model (k_0) is equal to 1.5 $(0.75 \cdot S^*_p)^2$.

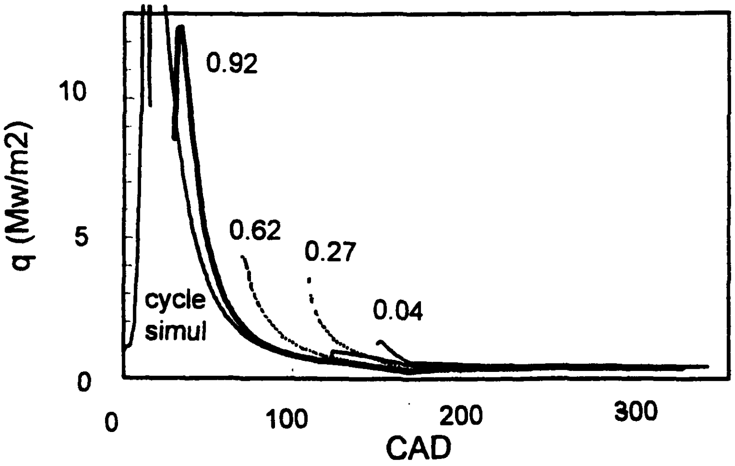

Fig. 6.6 Calculated heat transfer rate at several axial postions using the one-dimensional model versus the cylinder wall heat transfer rate predicted by the cycle simulation for the baseline case.

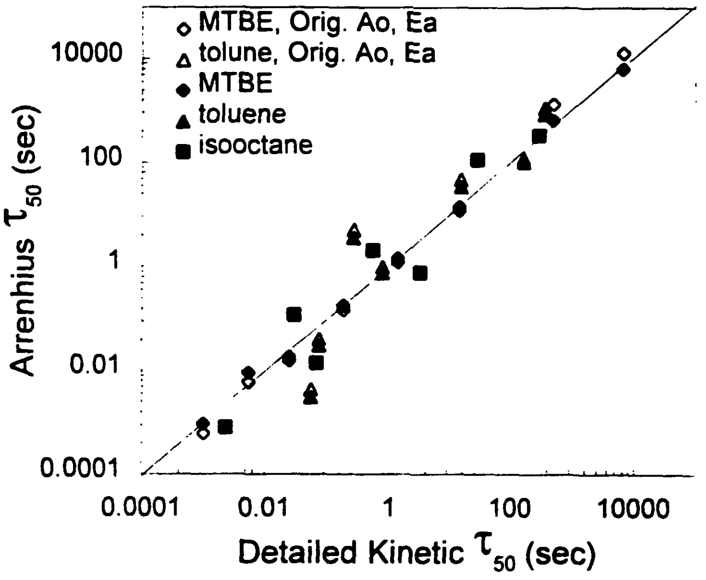

Fig. 6.7 Comparison of predicted hydrocarbon half lives (τ_{50}) using the Arrenhius equation to results using the full chemical kinetic mechanisms for lean and stoichiometric mixtures at 0.1% concentrations in burned gases. (τ_{50} is the time to convert 50% of hydrocarbons to complete products of oxidation). Open symbols are for the original values of A_0 and E_a given by Wu and closed symbols are for A_0 and E_a fit to the 0.1% data.

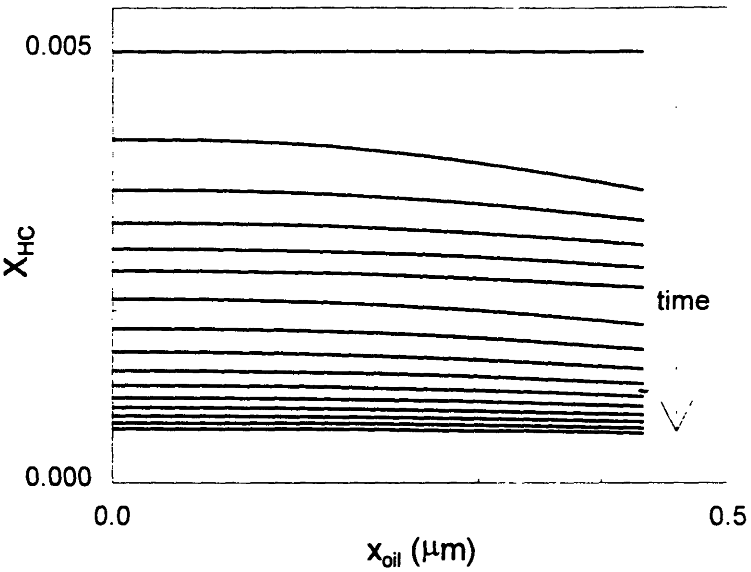

Fig. 6.8 Evolution of the toluene dopant mass fraction in oil near the mid-stroke stroke position under baseline conditions. Lines are 2 CAD apart, starting at 60 CAD after top-center, when first uncovered by the top compression ring.

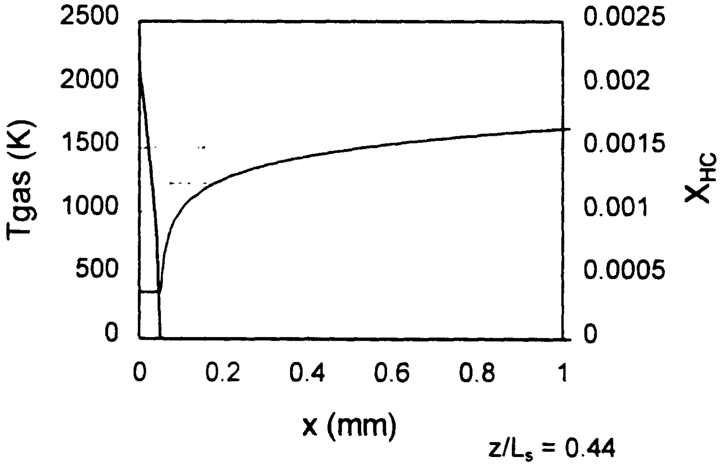

Fig. 6.9 Temperature and dopant mass fraction, when first exposed to cylinder gases after being uncovered by top of piston crown at axial location 0.44 •L_s for baseline case with toluene dopant.

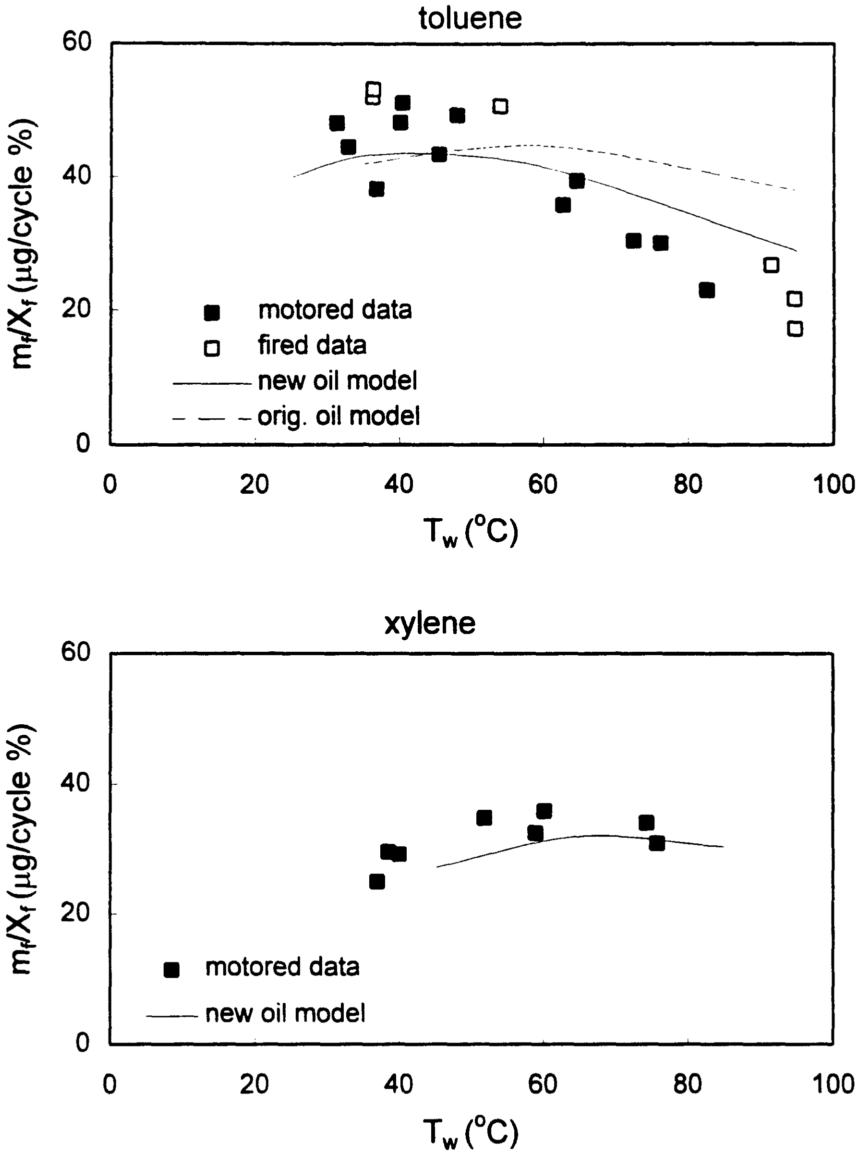

Fig. 6.10 Comparing model prediction of dopant desorbed vs. data for toluene and m-xylene dopants at 1500 rpm, motored at WOT or fired at IMEP - 3.6 bar. Data normalized by fuel concentration in bulk oil.

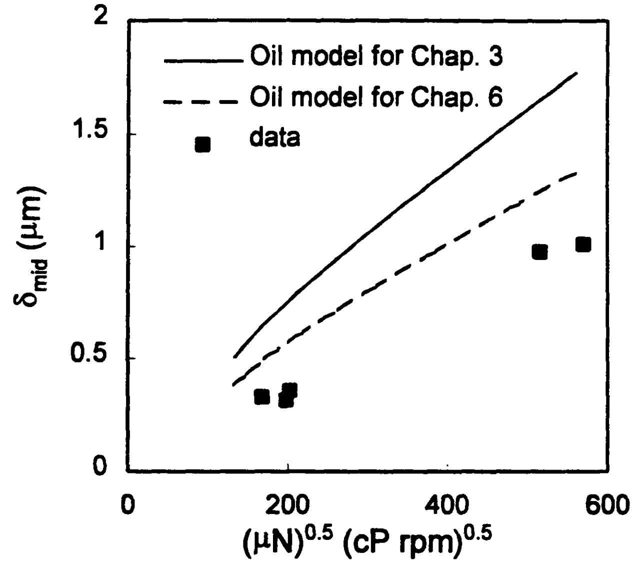

Fig. 6.11 Oil layer thickness at mid-stroke position versus square root of engine speed times viscosity for oil layer model used in the analytical model of Chapter 3, the one-dimensional model of Chapter 6 and measurements made in a Kholer CH14 engine with 10w-50 oil by Tamai [46].

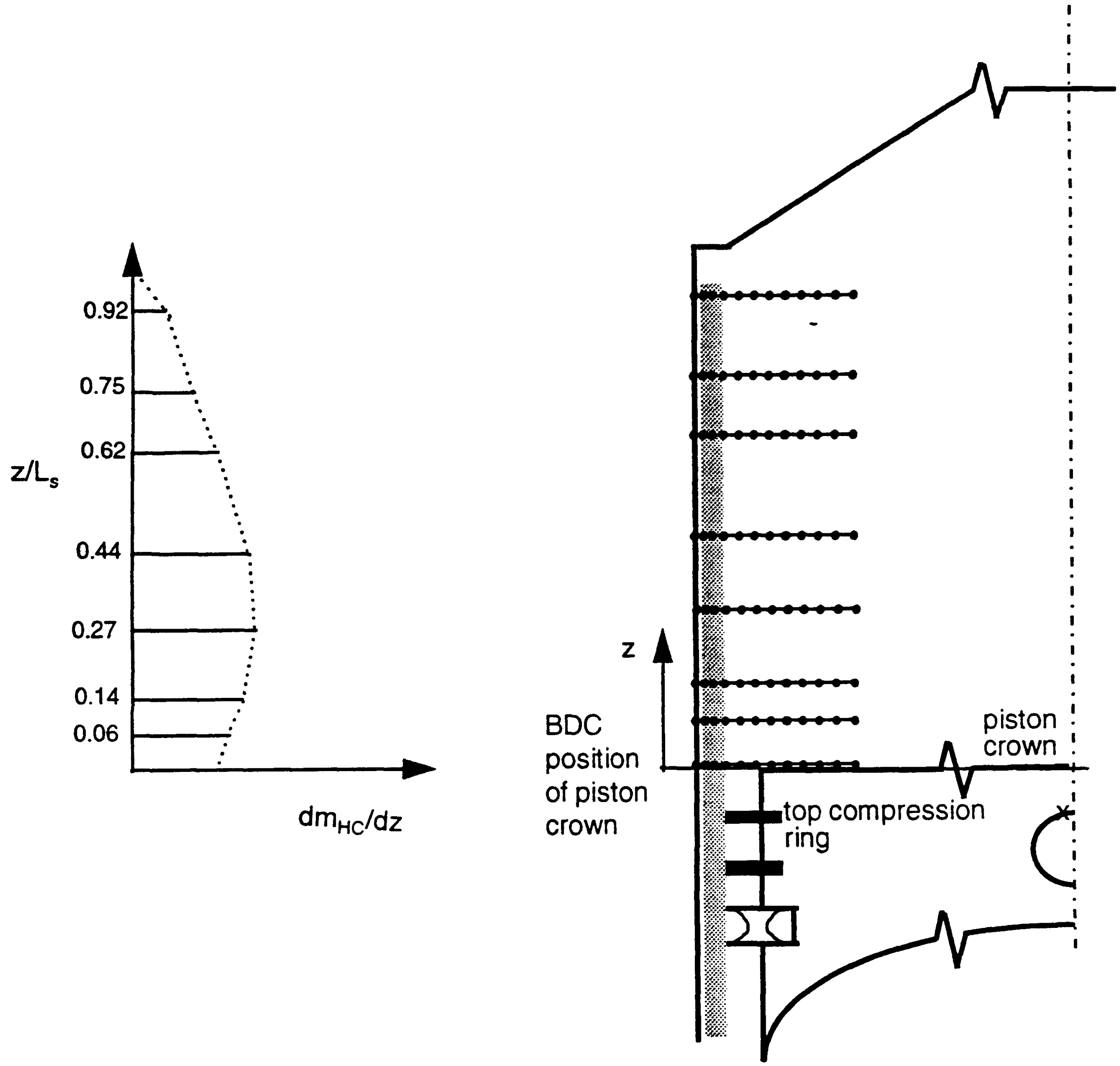

Fig. 6.12 Schematic of the one-dimensional model. Equations 6.1 through 6.10 are solved at axial positions corresponding to the piston crown position every 20 CAD. The resulting dm_{HC}/dz values are integrated along the axial length using the trapezoidal rule to get the total hydrocarbon mass surviving as shown in the graph on the left.

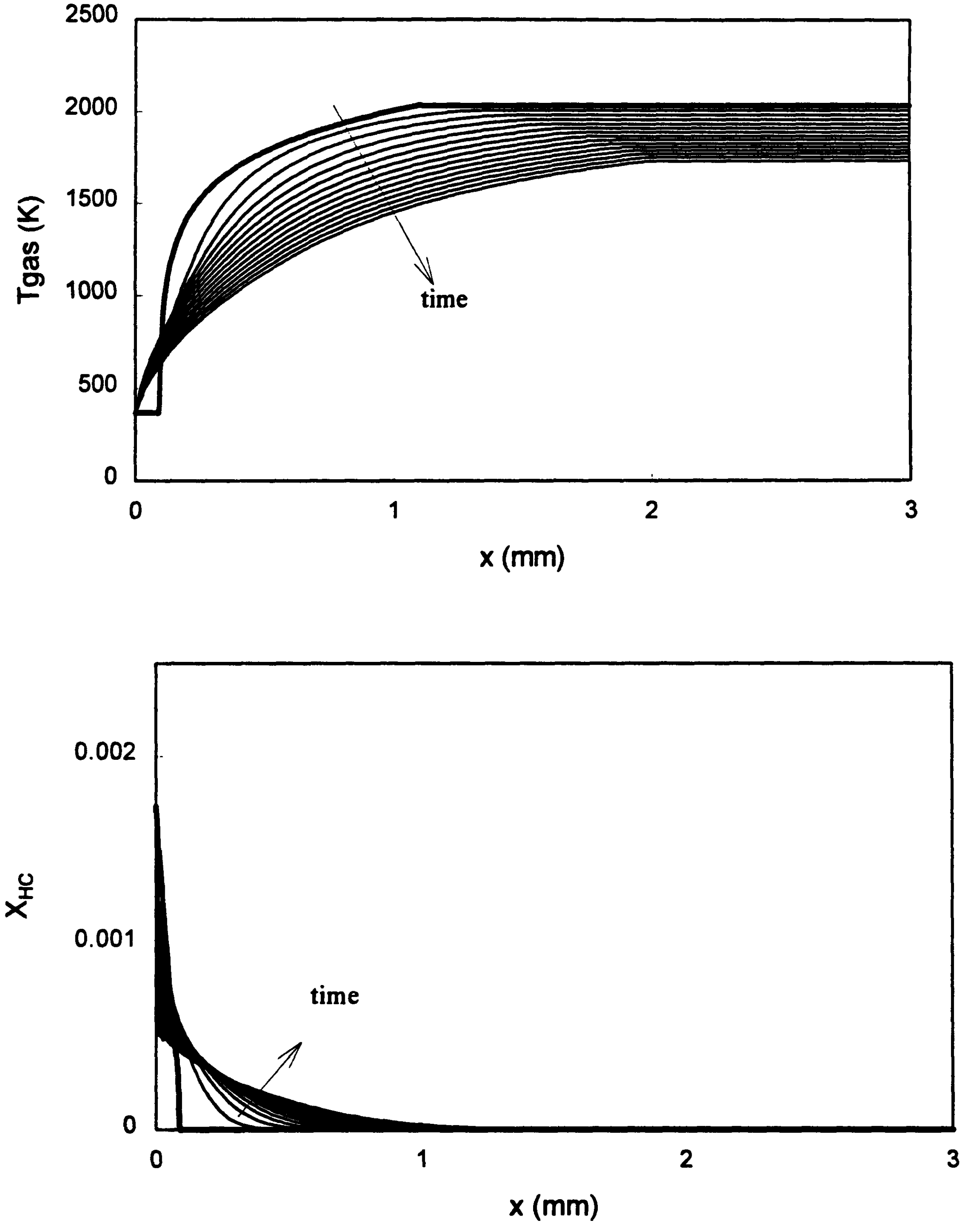

Fig. 6.13 Temperature and hydrocarbon mass fraction evolution versus radial distance from oil layer for axial location 0.75 •L_s above bottom center at baseline conditions with toluene dopant. The lines are 2 CAD apart, and the first line (thick) corresponds to 48 CAD after top-center.

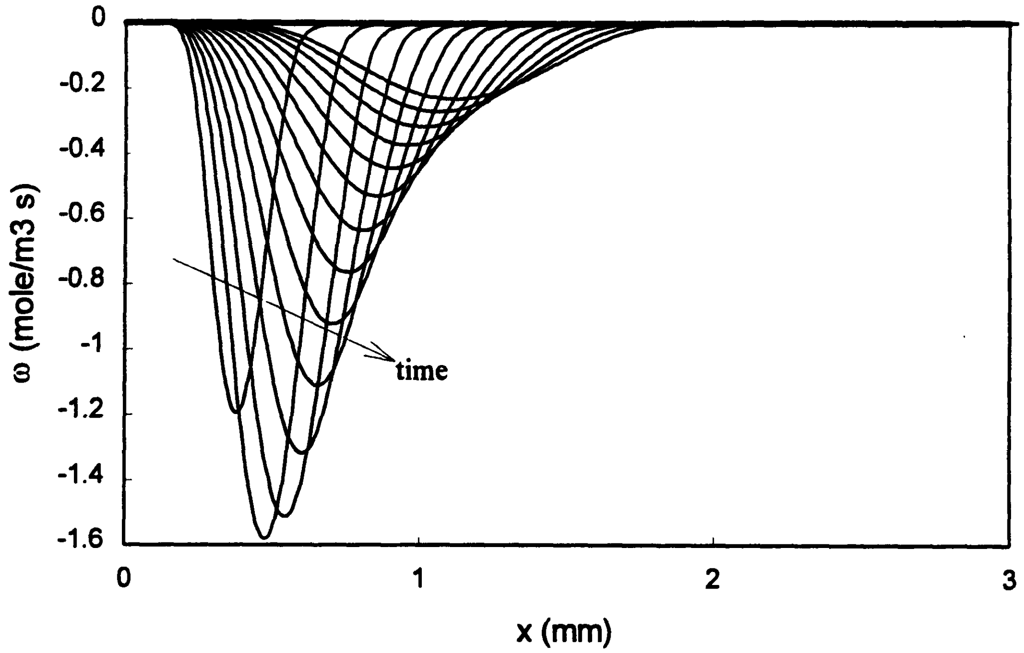

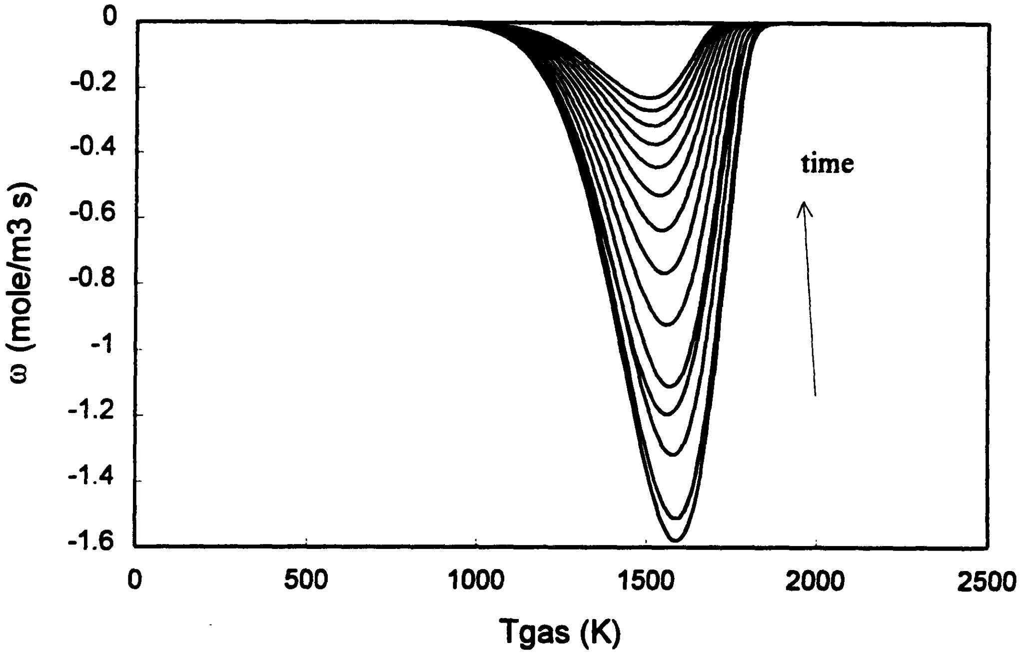

Fig. 6.14 Oxidation rate evolution versus radial distance from the oil layer and gas temperature for axial location 0.75 •L_s above bottom center at baseline conditions with toluene dopant. The lines are 2 CAD apart, and the first line corresponds to 48 CAD after top-center. Note the oxidation rate is zero at 48 CAD.

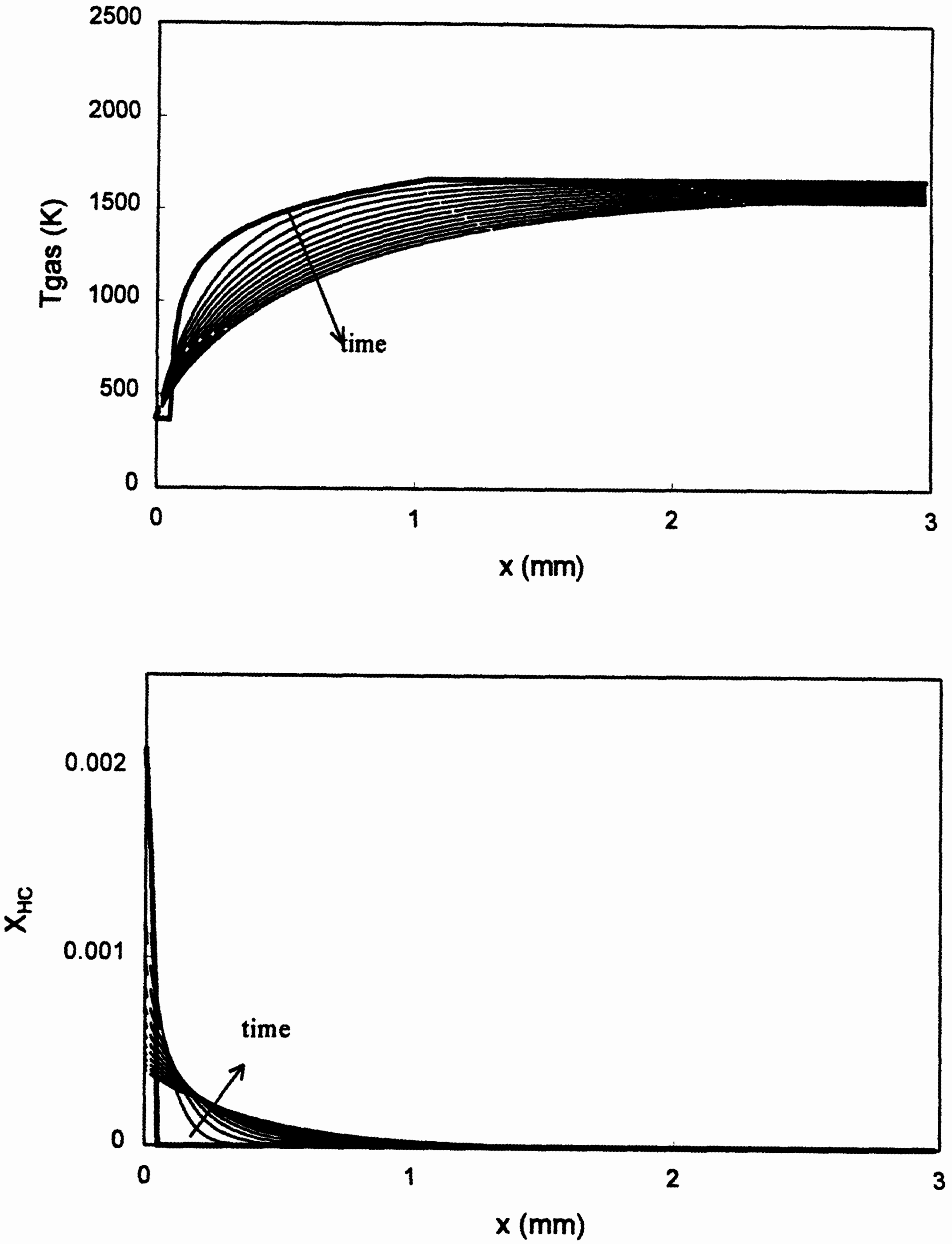

Fig. 6.15 Temperature and hydrocarbon mass fraction evolution vs. radial distance from oil layer for axial location 0.44•L_s above bottom center at baseline conditions with toluene dopant. The lines are 2 CAD apart, and the first line (thick) corresponds to 88 CAD after top-center.

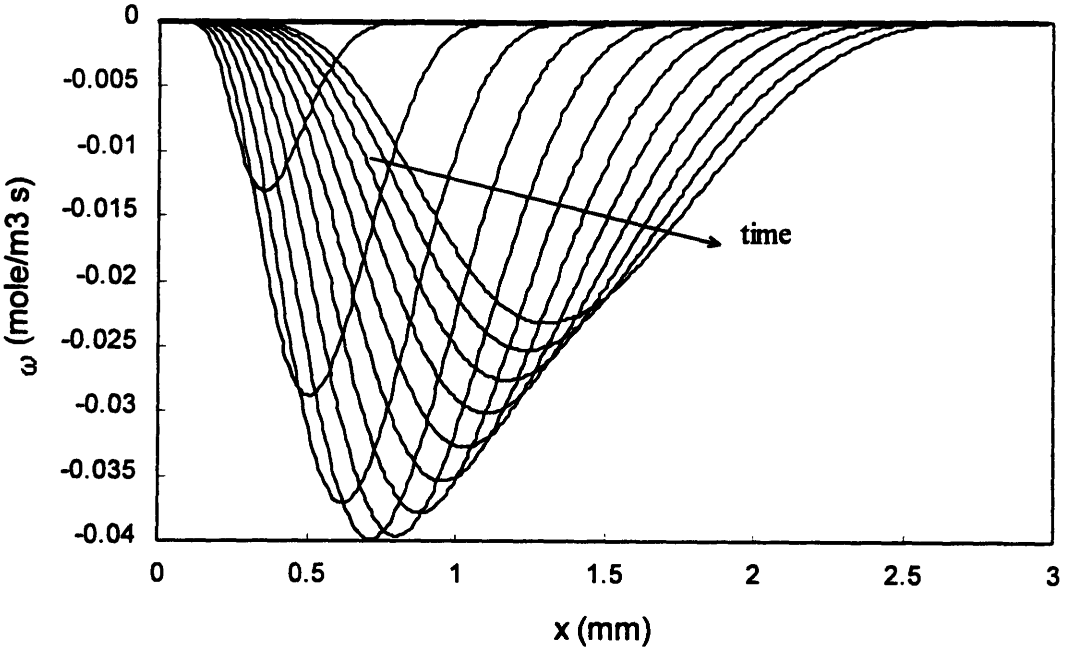

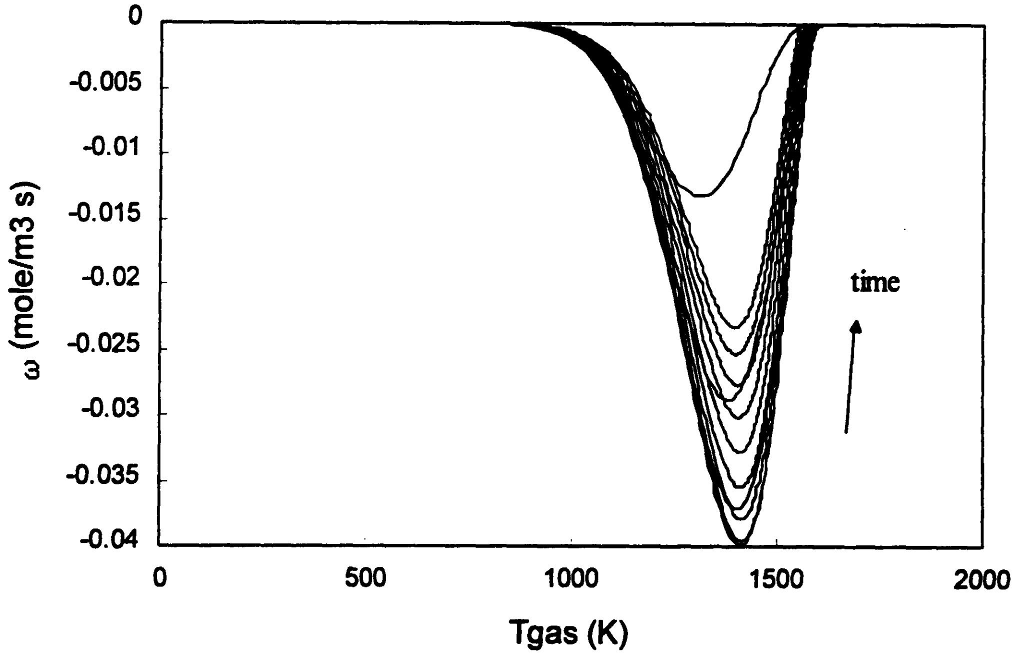

Fig. 6.16 Oxidation rate evolution versus radial distance from the oil layer and gas temperature for axial locations 0.44•L_S above BDC at baseline conditions with toluene dopant. The lines are 2 CAD apart, with the first line corresponds to 88 CAD after top-center. Note the oxidation rate is zero at 88 CAD.

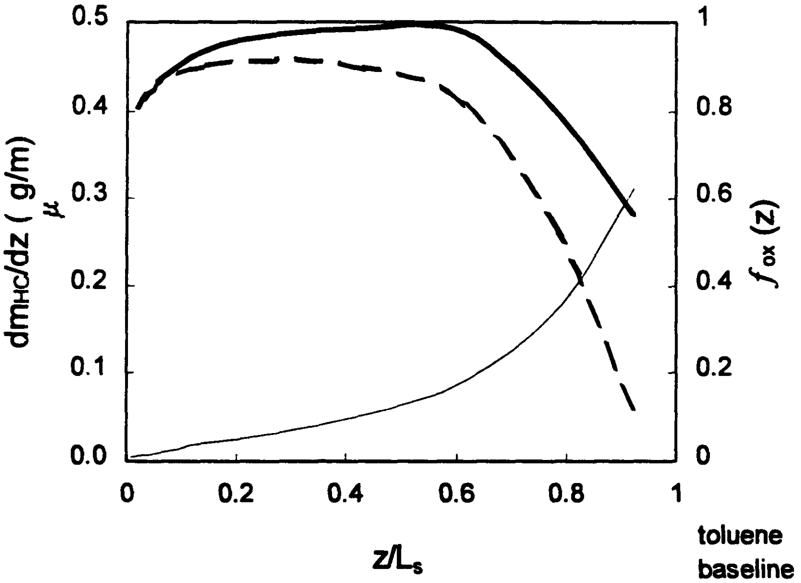

Fig. 6.17 Axial distribution of desorbed (thick solid line) and surviving (thick dashed) toluene dopant for baseline conditions and the fraction oxidized in-cylinder as a function of axial location (thin line).

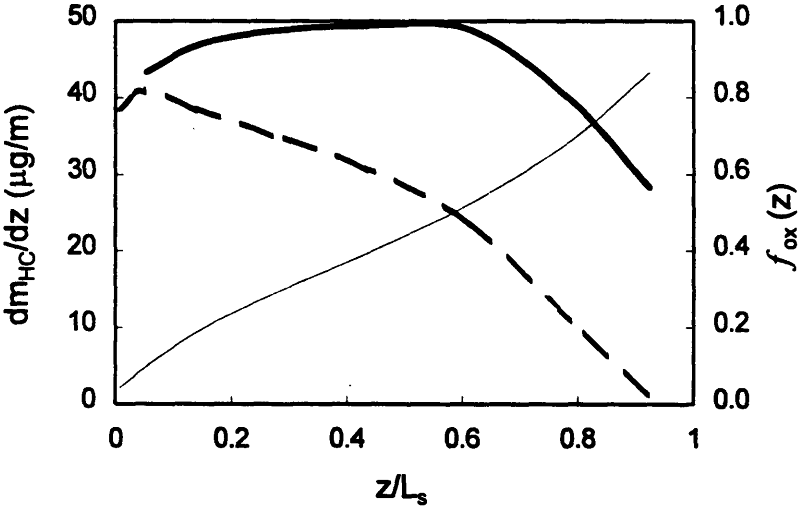

Fig. 6.18 Predicted result for chemical activation energy reduced by 15% from nominal values in Table 6.1. Axial distribution of desorbed (thick solid line) and surviving (thick dashed) toluene dopant for baseline conditions and the fraction oxidized in-cylinder as a function of axial location (thin line).

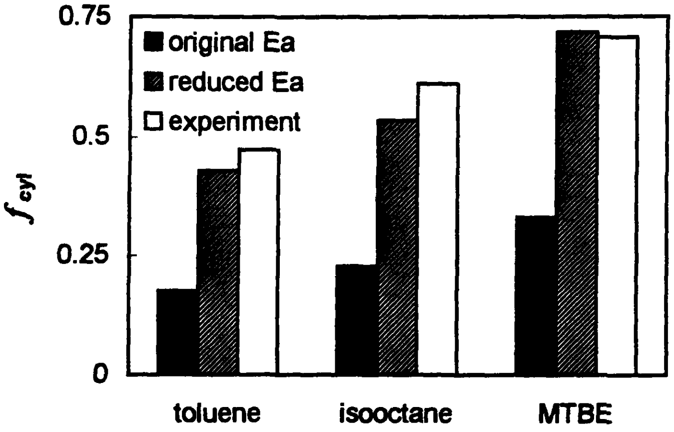

Fig 6.19 Fraction of post-flame desorbed dopant oxidized in-cylinder (f_{cyl}): model vs. values estimated from data at baseline operating condition. Predicted values calculated with nominal chemical activation energy (E_a) and activation energy reduced by 15%. Nominal values are listed Table 6.1.

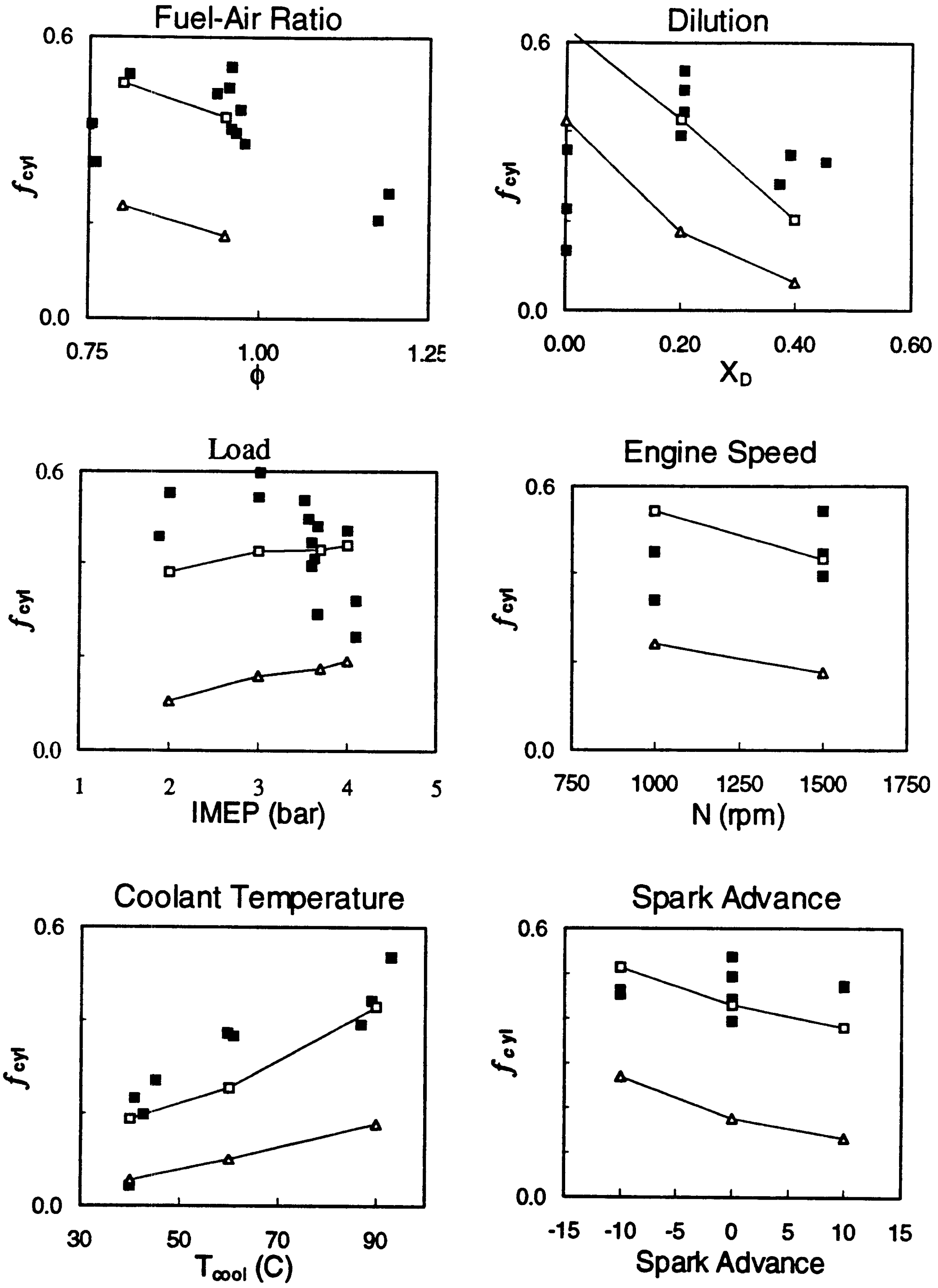

Fig. 6.20 Predicted (open) vs. estimated (closed) fraction of post-flame desorbed dopant oxidized in-cylinder for toluene dopant. Predicted values calculated with nominal chemical activation energy (triangles) and activation energy reduced by 15% (squares). Nominal values in Table 6.1.

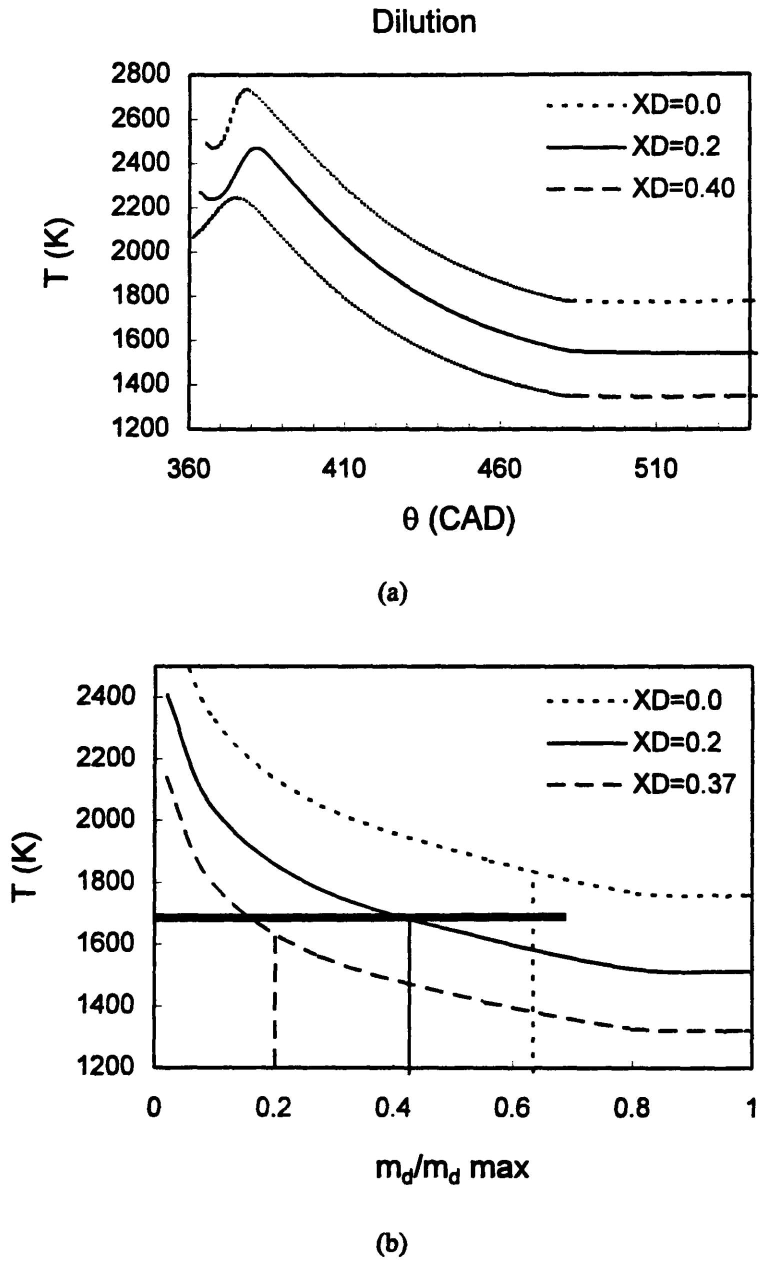

Fig. 6.21 Cylinder temperatures versus crank angle (a) and fraction of dopant desorbed (b) for variation in levels of dilution. Verticle lines in (b) are the levels of in-cylinder oxidation prediced by the one-dimensional cycle simulation. The correspondance of the intersction of the curves with the horizontal bar iat 1700 °K with the verticle lines indicates the level of correlation between the mass fraction desorbed at 1700 °K and the fraction oxidized.

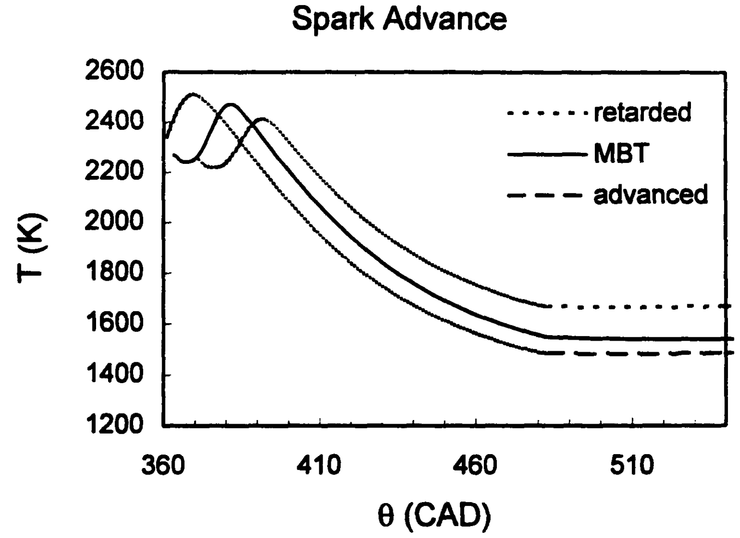

(a)

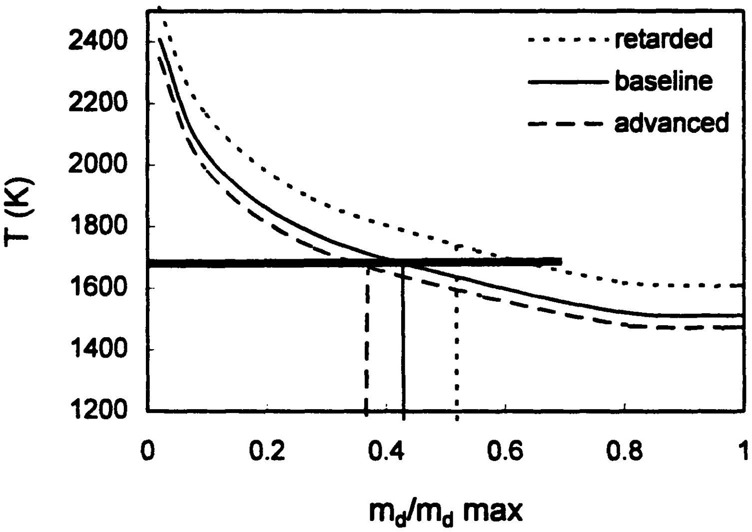

(b)

Fig. 6.22 Cylinder temperatures versus crank angle (a) and fraction of dopant desorbed (b) for variation in spark timing. Verticle lines in (b) are the levels of in-cylinder oxidation prediced by the one-dimensional cycle simulation. The correspondance of the intersction of the curves with the horizontal bar iat 1700 °K with the verticle lines indicates the level of correlation between the mass fraction desorbed at 1700 °K and the fraction oxidized.

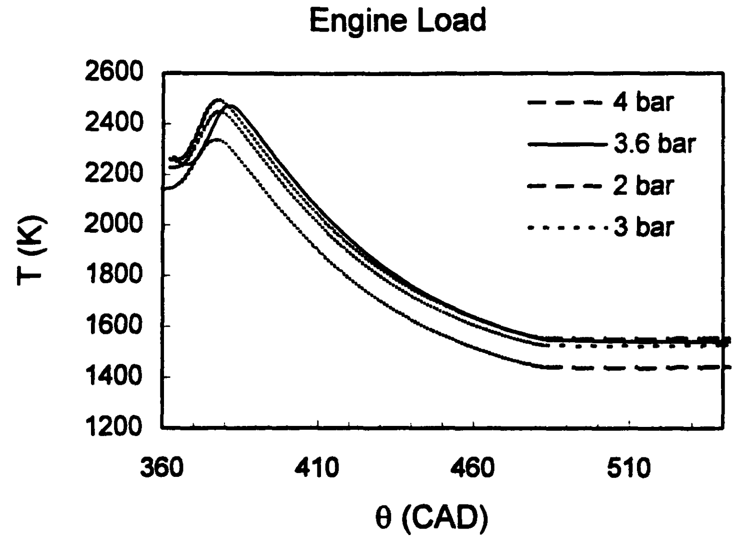

(a)

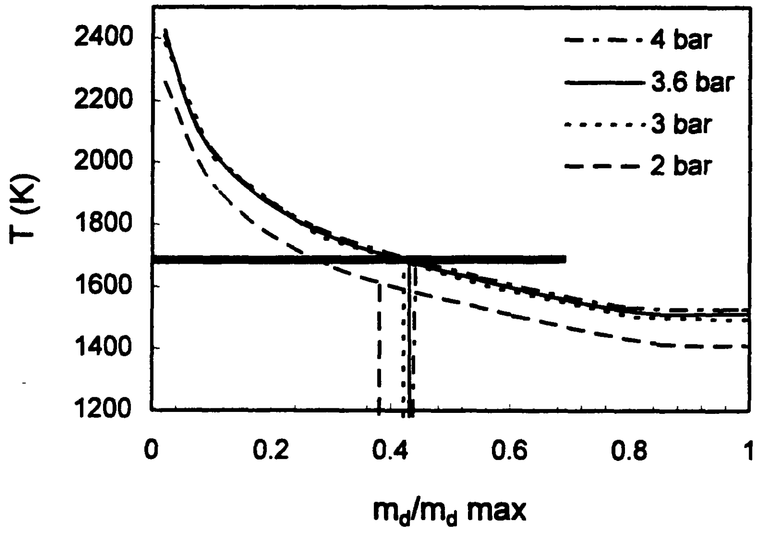

(b)

Fig. 6.23 Cylinder temperatures versus crank angle (a) and fraction of dopant desorbed (b) for variation in engine load. Verticle lines in (b) are the levels of in-cylinder oxidation prediced by the one-dimensional cycle simulation. The correspondance of the intersction of the curves with the horizontal bar iat 1700 °K with the verticle lines indicates the level of correlation between the mass fraction desorbed at 1700 °K and the fraction oxidized.

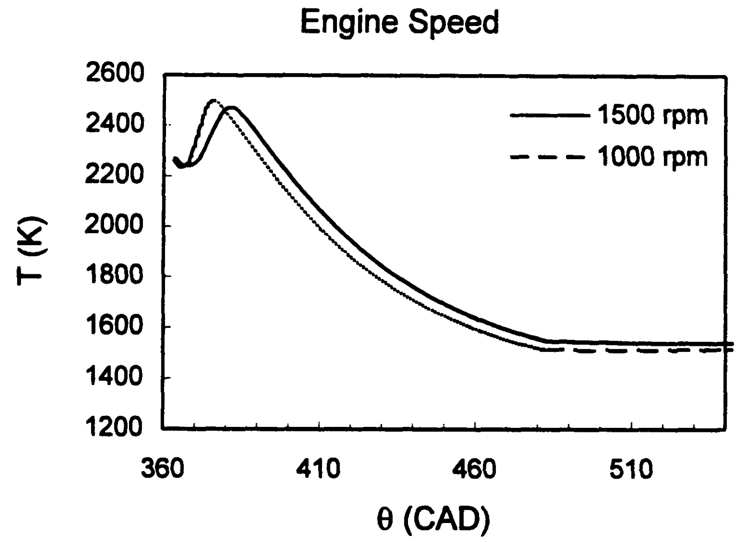

(a)

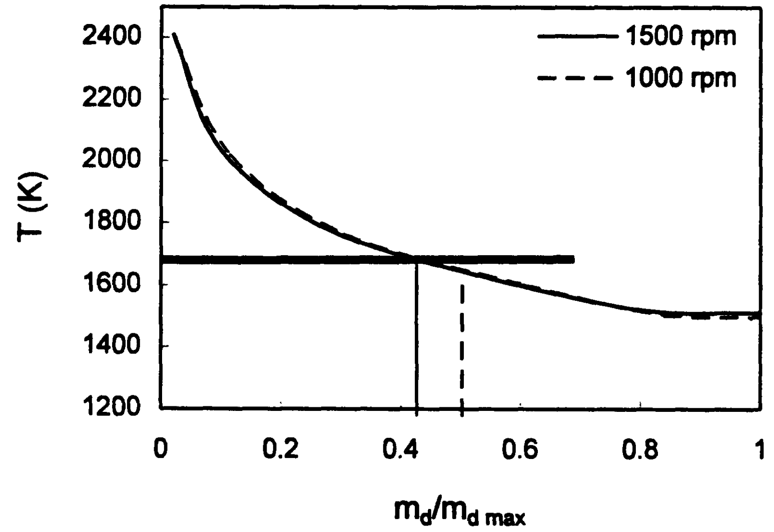

(b)

Fig. 6.24 Cylinder temperatures versus crank angle (a) and fraction of dopant desorbed (b) for variation in engine speed. Verticle lines in (b) are the levels of in-cylinder oxidation prediced by the one-dimensional cycle simulation. The correspondance of the intersction of the curves with the horizontal bar iat 1700 °K with the verticle lines indicates the level of correlation between the mass fraction desorbed at 1700 °K and the fraction oxidized.

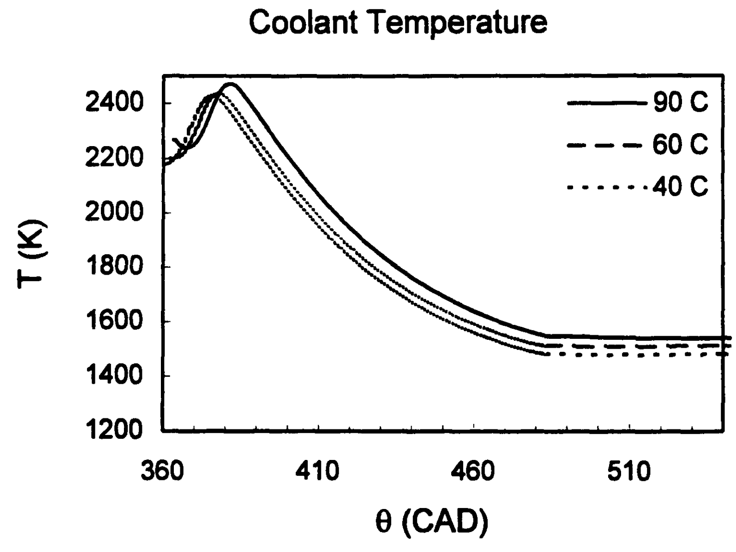

(a)

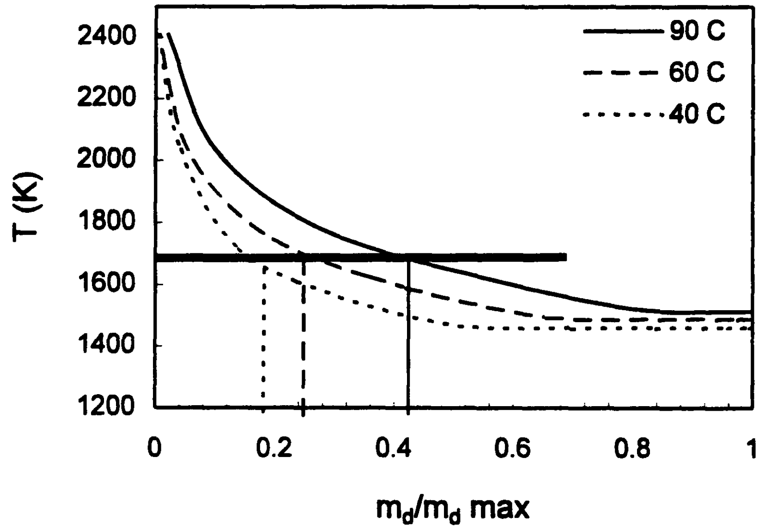

(b)

Fig. 6.25 Cylinder temperatures versus crank angle (a) and fraction of dopant desorbed (b) for variation in coolant temperature. Verticle lines in (b) are the levels of in-cylinder oxidation prediced by the one-dimensional cycle simulation. The correspondance of the intersction of the curves with the horizontal bar iat 1700 °K with the verticle lines indicates the level of correlation between the mass fraction desorbed at 1700 °K and the fraction oxidized.

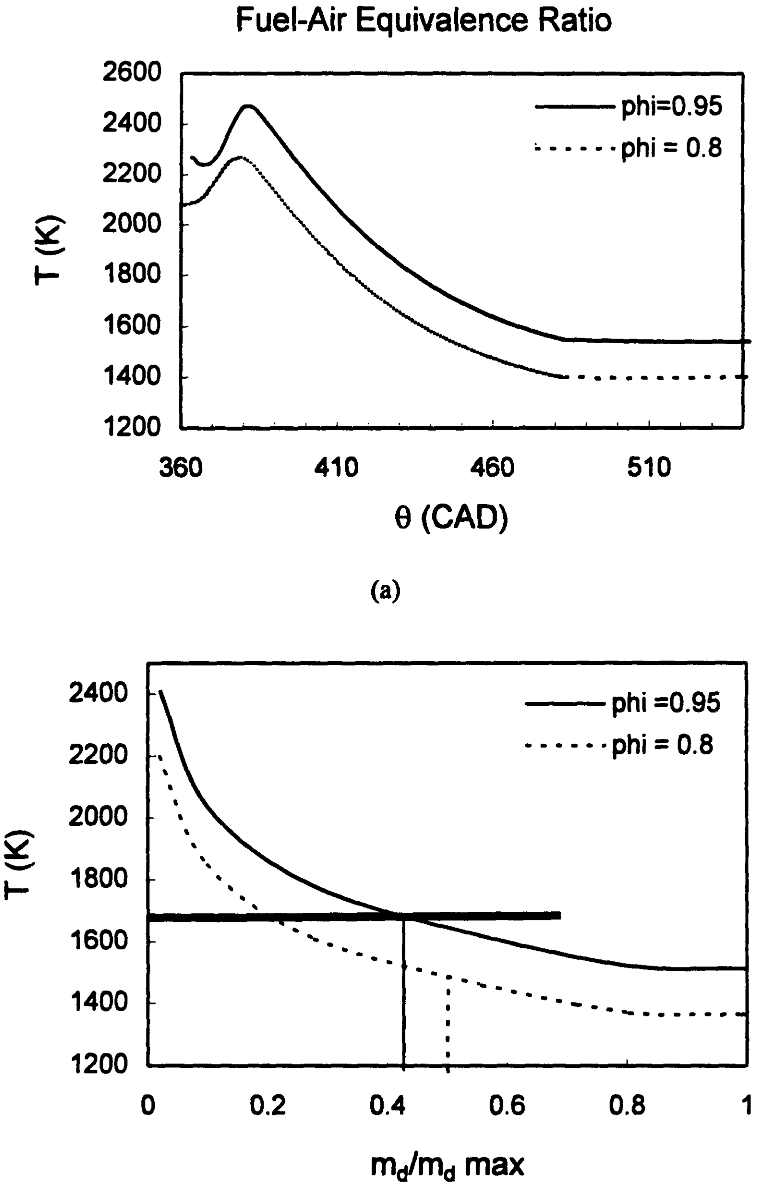

(a)

(b)

Fig. 6.26 Cylinder temperatures versus crank angle (a) and fraction of dopant desorbed (b) for variation in fuel-air equivalence ratio. Verticle lines in (b) are the levels of in-cylinder oxidation prediced by the one-dimensional cycle simulation. The correspondance of the intersction of the curves with the horizontal bar iat 1700 °K with the verticle lines indicates the level of correlation between the mass fraction desorbed at 1700 °K and the fraction oxidized.

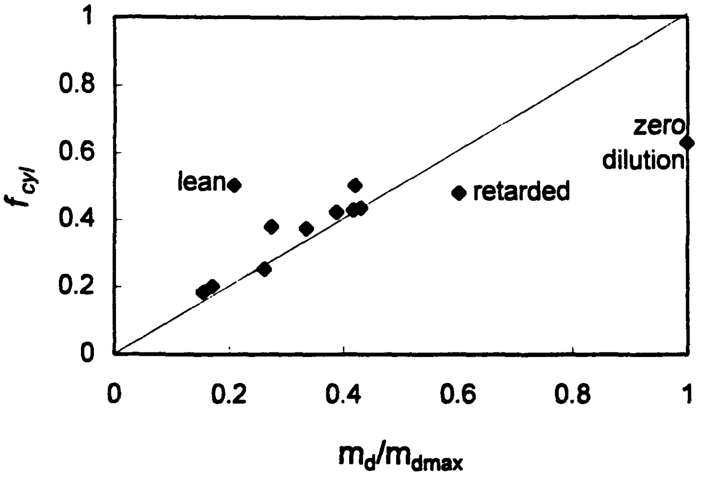

Fig. 6.27 Correlation of in-cylinder oxidation levels predicted by the one-dimension model and the fraction of mass desorbed, when the cylinder core temeprature reaches 1700 K.

CHAPTER 7

SUMMARY AND CONCLUSIONS

An experimental setup was developed to directly measure the oxidation of hydrocarbons desorbing from the lubricant oil layer on the cylinder walls. The engine was fired with a hydrogen-air-nitrogen mixture to produce a representative burned gas environment. Liquid hydrocarbons such as toluene were added to the oil which desorb from the cylinder walls into the combustion chamber similar to the desorption of fuel absorbed by the oil layer in gasoline fired engines. The desorbed hydrocarbons were the only source of carbon compounds in the exhaust thereby allowing the hydrocarbon source (sum of carbon compounds) to be measured simultaneously with the hydrocarbon in the exhaust. The level of oxidation was then directly determined from the measure of the hydrocarbon source strength and hydrocarbon concentrations.

Initial tests to characterize the nature of the hydrocarbon source in this experiment revealed the desorption of gasoline hydrocarbons is not rate limited, but rather limited by the amount of fuel in the oil layer. Thus in the analysis of the absorption-desorption of gasoline in the lubricant oil, the absorption is the limiting process. Analysis of the data showed that the oil layer is in this Nissan 2-liter engine was less than a micrometer thick. Analysis also showed the dopant concentration on the cylinder liner to be approximately 10% of the bulk concentration. Finally no difference was seen between motored experiments at WOT and fired experiments at an IMEP of 3.6 bar.

Oxidation experiments found the fraction of dopant surviving to exit the engine (f_{HC}) fell between those values expected for hydrocarbons desorbing from the oil layer and for hydrocarbons stored in the crevices. At mid-speed, mid-load, warmed up conditions (baseline) the fraction of post-flame desorbed dopant exiting the engine as hydrocarbons (f_{HC}) varied from 15% for MTBE to 23% for toluene. Dilution levels, equivalence ratio and engine load had the largest effect on the fraction of hydrocarbons surviving, while spark timing, engine speed and coolant temperature had little effect. At the operating conditions tested, the fraction of dopant surviving varied from a low of 0.11 for MTBE at zero dilution to a high of 0.52 at 50% dilution. The in-cylinder oxidation levels were estimated to range between 45% for toluene to 70% for MTBE at the baseline condition. The in-cylinder oxidation level was obtained from the measured engine-out oxidation levels and models of the fraction oxidized in the port and retained in the residual.

A one-dimensional model of the cylinder wall boundary layer based on Min (1993) showed good agreement with the sensitivity of in-cylinder oxidation levels to operating conditions and dopant types.

Although the model under-predicted the in-cylinder oxidation level by a factor of two to three, it was shown that reasonable changes in the predicted cylinder temperatures, initial boundary layer or chemical reactivity could produce oxidation rates comparable to those estimated for the experiment. Analysis of the modeling results showed that the levels of in-cylinder oxidation is controlled by the a) chemical reactivity of the dopant, b) the temperature history the dopant is exposed to and c) the oxygen content of the burned gases.

References

1. W.K. Cheng, D. Hamrin, J.B. Heywood, S. Hochgreb, K.D. Min, and M.G. Norris, "An Overview of Hydrocarbon Emissions Mechanisms in Spark-Ignition Engines," *SAE Paper 932708* (1993).

2. G.A. Lavoie and P.N. Blumberg,"A Fundamental Model for Predicting Fuel Consumption, NO_x and HC Emissions of the Conventional Spark-Ignited Engine," *Combustion Science and Technology*, Vol. 21, pp. 225-258 (1980).

3. M. Namazian and J.B. Heywood, "Flow in the Piston-Cylinder-Ring Crevices of a Spark-Ignition Engine: Effect on Hydrocarbon Emissions, Efficiency and Power," *SAE Paper 820088* (1988).

4. J.C. Dent and P.A. Lakshminarayanan, "A Model for Absorption and Desorption of Fuel Vapour by Cylinder Lubricating Oil Films and Its Contribution to Hydrocarbon Emissions," *SAE Paper 830652* (1983).

5. W.A. Daniel and J.T. Wentworth, "Exhaust Gas Hydrocarbons - Genesis and Exodus." SAE Technical Progress Series, Vol. 6, "*Vehicle Emissions*," New York: Society of Automotive Engineers, Inc. (1964).

6. C.K. Westbrok, A.A. Adamczyk, and G.A. Lavoie, "A Numerical Study of Laminar Wall Quenching'" *Combustion and Flame*, vol. 40, pp. 81-99 (1981).

7. P. Bergner, H. Eberius, and H. Pokorny, "Flame Quenching and Exhaust Hydrocarbons in a Combustion Bomb as a Function of Pressure, Temperature and Equivalence Ratio for Methanol and Other Alcohols," paper presented at the Third Alcohols Symposium, May 1979.

8. A.A. Adamczyk, E.W. Kaiser, J.A. Cavolowsky, and G.A. Lavoie, "An Experimental Study of Hydrocarbon Emissions from Closed Vessel Explosions," *Eighteenth Symposium (International) on Combustion*, The Combustion Institute (1981).

9. B. Gatellier et al., "Hydrocarbon Emissions of SI Engines as Influenced by Fuel Absorption-Desorption in Oil Films," *SAE Paper 920095* (1992).

10. S. Ishizawa and Y. Takagi, "A Study of HC Emission from a Spark Ignition Engine (The Influence of Fuel Absorbed into Cylinder Lubricating Oil Film)," *JSME International Journal*, Vol. 30, no. 260, 1987.

11. E.W. Kaiser, W.O. Siegl, and S.G. Russ, "Fuel composition Effects on Hydrocarbon Emissions from a Spark-Ignited Engine - Is Fuel Absorption in Oil Significant," *SAE Paper 952542* (1995).

12. T.H. Valtadoros, V.W. Wong and J.B. Heywood, "Fuel Additive Effects on Deposit Build-Up and Engine Operation Characteristics," *ACS Preprints*, vol. 36, no. 1 (1991).

13. H.E. Leikkanen and E.W. Beckman, "The Effects of Leaded and Unleaded Gasolines on Exhaust Emissions as Influenced by Combustion Chamber Deposits," *SAE Paper 710843* (1971).

14. O.L. Nelson, Jr., J.E. Larson, R.S. Fein, D.D. Fuller, G.K. Rightmire, R.W. Krumm, and G.E. Ducker, "A Broad-Spectrum, non-metallic additive for gasoline and diesel fuels-Performance in Gasoline Engines," *SAE Paper 890214* (1989).

15. R.J. Boyle, D.J. Boam and I.C. Finlay, "Cold Start Performance of an Automotive Engine using Prevaporized Gasoline," *SAE Paper 93710* (1993).

16. K.D. Min, "The Effects of Crevices on the Engine-out Hydrocarbon Emissions in Spark Ignition Engines," PhD Thesis, MIT, 1994.

17. R.D. Reitz and T.W. Kuo, "Modeling of HC Emissions Due to Crevice Flows in Premixed-Charge Engines," *SAE Paper892085* (1989).

18. J.D. Mendillo and J.B. Heywood, "Hydrocarbon Oxidation in the Exhaust Port of a Spark Ignition Engine," *SAE Paper 810019* (1981).

19. K. Drobot, W.K. Cheng, F. Trinker, E.W. Kaiser, W.O. Siegl, D.F. Cotton and J. Underwood, "Hydrocarbon Oxidation in the Exhaust Port and Runner of a Spark Ignition Engine," Combustion and Flame, Vol. 99, No. 2, November 1994.

20. Y. Murakami, and H. Aihara, "Analysis of Mechanism Intermixing Combustion Products in Engine Oil (Quantity and Composition of Unburned Gasoline in Engine Oil and Crankcase Gas)," *JSME Int. J.*, Series II, Vol. 34. No. R (1991).

21. J.B. Heywood, *Internal Combustion Engine Fundamentals*, McGraw-Hill, New York, 1988

22. K.K. Kuo, *Principles of Combustion,* John Wiley and Sons, New York, 1986.

23. B.E. Milton and J.C. Keck, "Laminar Burning Velocities in Stoichiometric Hydrogen and Hydrogen-Hydrocarbon Gas Mixtures," *Combustion and Flame*, no. 58, pp. 13-22 (1994).

24. J. Sterlepper, U. Spicher and H. Ruhland, "Lame Propagation into Top Land Crevice and Hydrocarbon Emissions from a SI Engine during Engine Warm-Up," *SAE paper 932648* (1993).

25. G.A. Lavoie, "Correlations of Combustion Data for S.I. Engine Calculations-Laminar Flame Speed, Quench Distance and Global Reaction Rates," *SAE Paper780229* (1978).

26. ASTM, *The Relationship Between High-Temperature Oil Rheology and Engine Operation: A Status Report*, ASTM Data Series DS62, ASTM, Philadelphia, PA (1984).

27. R.C. Reid, J.M. Prausnitz, and B.E. Poling, *The Properties of Gases and Liquid,* 4th Ed., McGraw-Hill, New York, 1988.

28. J. Schramm, and S.C. Sorenson, "Solubility of Gasoline Components in Different Lubricants for Combustion Engines Determined by Gas-Liquid Partition Chromatography," *J. Chromatography, 538*: pp. 241-248 (1991).

29. F.P. Incropera, and D.P. DeWitt, *Fundamentals of Heat and Mass Transfer*, 3rd Ed., John Wiley and Sons, New York, 1990.

30. K.C. Wu, "Chemical Kinetic Modeling of Oxidation of Hydrocarbon Emissions in Spark Ignition Engines," S.M. Thesis, MIT, 1994.

31. R.J. Tabaczynski, D.P. Hoult, and J.C. Keck, "High Reynolds Number Flow in a Moving Corner," *J. Fluid Mech.* vol. 42, pp. 249-255 (1970).

32. I.C. Finlay, D.J. Boam, J.F. Bingham and T.A. Clark, "Fast Response FID Measurement of Unburned Hydrocarbons in the Exhaust Port of a Firing Gasoline Engine," *SAE Paper 902165* (1990).

33. P. Weiss and J.C. Keck, "Fast Sampling Valve Measurements in the cylinder of a CFR Engine," *SAE Paper 810149* (1981).

34. D.A. Hamrin and J.B. Heywood, "Modeling of Egnine-Out Hydrocarbon Emissions for Prototype Production Engines," *SAE Paper 950984* (1995).

35. J.W. Fox, W.K. Cheng and J.B. Heywood, "A Model for Predicting Residual Gas Fraction in Spark-Ignition Engines," et al. *SAE Paper 931025* (1993).

36. W.A. Daniel, "Why Engine Variables Affect Exhaust Hydrocarbon Emission," *SAE Paper 700108* (1970).

37. S.G. Poulos, "The effect of Combustion Chamber Geometry on S.I. Engine Combustion Rates - A Modeling Study," SM Thesis, MIT, 1982.

38. E.J. Lyford-Pike and J.B. Heywood, "Thermal Boundary Layer Thickness in the Cylinder of a Spark-Ignition Engine," *International Journal of Heat and Mass Transfer*, vol. 27, pp. 1873-1878, (1984)

39. R.P. Lucht, D. Dunn-Rankin, T. Walter, T. Dreier, and S.C. Bopp, "Heat Transfer in Engines: Comparison of Cars Thermal Boundary Layer Measurements and Heat Flow Measurements", *SAE Paper 910722* (1992).

40. M.J. Hall, F.V. Bracco and D.A. Santavicca, "Cycle-Resolved Velocity and Trubulence Measurements in an IC Engine with Combustion ", *SAE Paper 860320* (1986).

41. D.E. Foster and P.O. Witze, "Velocity Measurements in the Wall Boundary Layer of a Spark-Ignited Research Engine", *SAE Paper 872105* (1987).

42 B.E. Launder and D.B. Spalding, *Mathematical Models of Turbulence*, Academic Press, New York, 1972.

43 O. Hadded and I. Denbratt, "Turbulence Characteristics of Tubling Air Motion in Four-Valve S.I. Engines and their Correlation with Combustion Parameters," *SAE Paper 910478* (1991).

44 A.A. Sonin, 2.273 Lecture, MIT, 1993.

45 *Journal of Fluid Mechanics*, vol. 25, p. 651, 1966.

46 J.H. Feziger, *Numerical Mehtods for Engineering Applications*, A Wiley-Interscience Publication, 1981.

C1. T. Tian , Sloan Automotive Laboratory, MIT, 1995.

Appendix A

Experimental Results

The following tables list all the experimental results for the oxidation and the desorption experiments. The tables for the oxidation experiments list the following data:

date	date of experiment
CO2 amb	ambient level of CO2
case	run label
N	engine speed
IMEP	gross indicated mean effective pressure
θ_{Pmax}	timing of maximum pressure
P_{in}	intake manifold pressure
m'_{air}	air flow rate
O2/l	oxygen concentration or air-fuel ratio in exhaust
O2(N2)	oxygen concentration in intake mixture w/o fuel
T_{cool}	coolant temperature
T_{exh}	exhaust coolant temperature
CO	carbon monoxide concentration
CO2	carbon dioxide concentration
HC	hydrocarbon concentration
variable	value of independent variable
f_{ox}	resulting fraction oxidized $(1-f_{HC})$

The desorption data tables presents the following data

date	date of experiment
run	run label
T_{wall}	cylinder wall temperature
rpm	engine speed
X_{hex} or X_{tol} or X_{xyl}	mass fraction of dopant in bulk oil
HCm	mass desorbed per cycle

OXIDATION TEST RESULTS

Toluene Dopant

date	CO2 amb	case	N	IMEP	Θ_{max}	Pin	Pivo	m'air	O2 / λ	O2 (N2)	Tcool	Texh	CO	CO2	HC	variable	" = fox
	(ppm)		(rpm)	bar	A BDC	bar	bar	g/s	%	%	(C)	(C)	ppm	ppm	ppmC	Tcool (C)	
	Fuel-Air Ratio															φ	
3/13/95	450	H2TMI	1500	3.52	198	0.66	1.16	2.03	3.5	16.5	89.5	464	0	1020	94	0.76	0.66
2/17/95	428	H2tgb	1500	3.5	197	0.71	1.18	2.26	3.6	16.6	93	468	40	1230	120	0.76	0.69
3/12/95	404	H2TLI	1500	3.6	197	0.635	1.21	1.95	2.8	16.6	90	478	0	1720	127	0.81	0.77
1/5/95	380	CS	1500	3.67	197.4	0.62	1.19	1.8	0.9	16.6	89	407	10	1150	70	0.94	0.78
1/4/95	390	CD2	1500	3.63	197	0.61	1.19	1.75	0.6	16.6	85.3	408	40	1200	86	0.96	0.75
3/13/95	450	H2TMc	1500	3.5	198	0.6	1.17	1.73	0.6	16.5	93	515	50	2130	131	0.96	0.81
2/17/95	428	H2tga	1500	3.56	196.5	0.61	1.18	1.76	0.65	16.5	91.5	513	170	1530	110	0.95	0.78
3/9/95	390	H2tjc	1500	3.6	197	0.595	1.09	1.74	0.4	16.5	89	516	0	1643	122	0.97	0.76
3/12/95	404	H2TLc	1500	3.6	197	0.59	1.18	1.73	0.5	16.6	87	514	0	1740	134	0.96	0.75
1/5/95	380	CP	1500	3.57	197	0.61	1.18	1.73	0.31	16.5	90	405	20	915	60	0.98	0.74
2/17/95	428	H2tgc	1500	3.55	197	0.64	1.19	1.73	**0.84**	16.6	87.4	501	850	1250	243	1.19	0.66
1/5/95	380	CN	1500	3.67	195	0.61	1.25	1.63	**0.85**	16.6	89	386	440	800	131	1.18	0.66
		Dilution														Xd	
1/5/95	380	H2TCI	1500	3.34	197	0.56	1.29	1.83	0.76	20.9	87.4	426	105	1950	155	0.00	0.73
2/17/95	428	H2tgd	1500	3.55	197	0.57	1.19	1.9	0.7	20.9	88.8	565	130	2850	185	0.00	0.79
3/13/95	450	H2TMK	1500	3.68	198	0.55	1.15	1.88	0.6	20.9	73.6	548	70	2910	220	0.00	0.75
2/17/95	428	H2tga	1500	3.56	196.5	0.61	1.18	1.76	0.65	16.5	91.5	513	170	1530	110	0.20	0.78
3/9/95 -	390	H2tjc	1500	3.6	197	0.595	1.09	1.74	0.4	16.5	89	516	0	1643	122	0.20	0.76
3/13/95	450	H2TMc	1500	3.52	198	0.6	1.17	1.73	0.6	16.5	93	515	50	2130	131	0.20	0.81
3/12/95	404	H2TLc	1500	3.6	197	0.59	1.18	1.73	0.5	16.6	87	516	0	1740	134	0.20	0.75
3/12/95	404	H2TLL	1500	3.46	194	0.7	1.18	1.7	0.8	12.9	93.4	447	0	1343	200	0.37	0.60
2/17/95	428	H2tge	1500	3.55	194	0.82	1.19	1.83	0.5	11.2	94.8	440	60	1140	188	0.45	0.59
3/13/95	450	H2TML	1500	3.55	196	0.7	1.14	1.7	0.7	12.5	82.2	445	0	1620	220	0.39	0.64
	Engine Speed															N (rpm)	
3/9/95	390	H2tjc	1500	3.6	197	0.595	1.09	1.74	0.4	16.5	89	516	0	1643	122	1500	0.76
3/12/95	404	H2TLG	1000	3.54	196	0.66	1.26	1.2	0.4	16.4	90.6	439	0	1380	78	1000	0.80
3/12/95	404	H2TLG2	1000	3.53	196	0.652	1.21	1.2	0.7	16.6	90.7	442	0	1940	105	1000	0.82
3/12/95	404	H2TLc	1500	3.6	197	0.59	1.18	1.73	0.5	16.6	87	514	0	1740	134	1500	0.75
3/13/95	450	H2TMc	1500	3.6	197	0.6	1.17	1.73	0.6	16.5	93	515	50	2130	131	1500	0.81

O2\λ is measured in the exhaust and O2(N2) is measured in the intake.
bold entries in O2\λ column are λ measurements and the rest are O2.

Toluene Dopant

date	CO2 amb	case	N	IMEP	Θ_{pmax}	Pin	Pivo	m'air	O2 / λ	O2 (N2)	Tcool	Texh	CO	CO2	HC	variable	" = fox
	(ppm)		(rpm)	bar	A BDC	bar	bar	g/s	%	%	(C)	(C)	ppm	ppm	ppmC		
		IMEP														Ld (bar)	
3/8/95	380	H2tid2	1500	1.85	198	0.32	1	1	0.6	16.6	91.1	480	200	2870	140	1.85	0.86
3/9/95	390	H2tjd	1500	2	196	0.329	1.03	1	0.7	16.6	90.3	468	70	2600	149	2.00	0.83
3/12/95	404	H2TLd	1500	1.89	197	0.32	1.03	0.98	1	16.6	91.2	447	170	2750	205	1.89	0.79
3/9/95	390	H2tjc	1500	3.6	197	0.595	1.09	1.74	0.4	16.5	89	516	0	1643	122	3.60	0.76
3/9/95	390	H2tje	1500	3	197	0.505	1.14	1.52	0.7	16.6	92.2	498	0	1855	105	3.00	0.82
3/9/95	390	H2tjf	1500	4	197	0.65	1.16	1.92	0.5	16.6	90	527	0	1620	112	4.00	0.77
3/12/95	404	H2TLE	1500	3.01	197	0.5	1.13	1.49	0.7	16.7	92.6	497	50	2050	105	3.01	0.84
3/13/95	450	H2TMF	1500	4.1	197	0.68	1.19	1.97	0.6	16.5	87.9	523	30	1185	96	4.10	0.70
3/13/95	450	H2TMFa	1500	4.1	197	0.68	1.19	1.97	0.6	16.5	87.9	523	30	1440	144	4.10	0.67
1/4/95	390	CD	1500	3.66	197	0.614	1.19	1.80	0.6	16.6	87.8	414	65	1030	88	3.66	0.70
1/4/95	390	CD2	1500	3.63	197	0.61	1.18	1.75	0.6	16.6	85.3	408	40	1200	86	3.63	0.75
1/5/95	380	CS	1500	3.67	197.4	0.62	1.19	1.8	0.9	16.6	89	407	10	1150	70	3.67	0.78
2/17/95	428	H2tga	1500	3.56	196.5	0.61	1.18	1.76	0.65	16.5	91.5	513	170	1530	110	3.56	0.78
3/12/95	404	H2TLc	1500	3.6	197	0.59	1.18	1.73	0.5	16.6	87	514	0	1740	134	3.60	0.75
3/13/95	450	H2TMc	1500	3.52	198	0.6	1.17	1.73	0.6	16.5	93	515	50	2130	131	3.52	0.81
		Twall														Tcool (C)	
3/9/95	390	H2tja	1500	3.56	197	0.52	1.21	1.61	0.5	16.6	40.8	468	0	1880	175	40.8	0.712036
3/9/95	390	H2tja2	1500	3.5	196	0.514	1.18	1.61	0.8	16.6	42.8	464	0	2240	245	42.8	0.68349
3/9/95	390	H2tjb	1500	3.49	198	0.536	1.12	1.66	0.6	16.5	61	493	0	1639	130	61	0.741911
3/9/95	390	H2tjb2	1500	3.5	198	0.54	1.11	1.67	0.8	16.6	59.8	489	0	2115	181	59.8	0.739228
3/9/95	390	H2tjc	1500	3.6	197	0.595	1.09	1.74	0.4	16.5	89	516	0	1643	122	89	0.756399
3/12/95	404	H2TLa	1500	3.51	197	0.52	1.22	1.62	0.3	16.6	45	477	0	1755	146	45	0.73128
3/12/95	404	H2TLc	1500	3.6	197	0.59	1.18	1.73	0.5	16.6	87	514	0	1740	134	87	0.749533
3/13/95	450	H2TMc	1500	3.52	198	0.6	1.17	1.73	0.6	16.5	93	515	50	2130	131	93	0.805137
3/10/95	406	H2Tka	1500	3.53	197	0.51	1.21	1.61	0.6	16.7	40	462	150	2976	408	40	0.643766
		Spark														θ_{ss}	
3/13/95	450	H2TLN	1500	3.58	208	0.656	1.14	1.94	0.7	16.5	90.4	557	0	1800	109	-10	0.784634
3/13/95	450	H2TLN2	1500	3.61	209	0.656	1.15	1.94	0.7	16.6	89.7	554	0	1930	117	-10	0.78633
2/17/95	428	H2tga	1500	3.56	196.5	0.61	1.18	1.76	0.65	16.5	91.5	513	170	1530	110	0	0.782867
3/12/95	404	H2TLc	1500	3.6	197	0.59	1.18	1.73	0.5	16.6	87	514	0	1740	134	0	0.749533
3/9/95	390	H2tjc	1500	3.6	197	0.595	1.09	1.74	0.4	16.5	89	516	0	1643	122	0	0.756399
3/13/95	450	H2TMc	1500	3.52	198	0.6	1.17	1.73	0.6	16.5	93	515	50	2130	131	0	0.805137
3/13/95	450	H2TLM	1500	3.48	188	0.57	1.23	1.67	0.9	16.5	93.3	491	50	1990	159	10	0.760165
3/13/95	450	H2TLM2	1500	3.51	188	0.57	1.25	1.67	0.6	16.5	88.6	496	80	2260	178	10	0.77033

Isooctane Dopant

date	CO2 amb	case	N	IMEP	Qpmax	Pm	Pivo	m'air	O2 / λ	O2 (N2)	Tcool	Texh	CO	CO2	HC	variable	
	(ppm)		(rpm)	bar	A BDC	bar		g/s	%	%	(C)	(C)	ppm	ppm	ppmC		fox
		IMEP														Ld (bar)	
3/16/95	470	h2icd	1500	2	198	0.345	1.1	1.02	0.5	16.7	92		150	3005	170	2.00	0.83
3/16/95	470	h2idd	1500	1.8	194	0.308	1.1	0.9	0.2	16.6	91	456	250	2880	145	1.80	0.86
3/16/95	470	h2ice	1500	3.15	197	0.515	1.15	1.52	0.7	16.6	87	495	70	2050	117	3.15	0.82
3/16/95	470	h2ide	1500	3.12	196	0.5	1.15	1.47	0.6	16.8	91	499	0	1410	73	3.12	0.80
3/14/95	426	h2iac	1500	3.57	197	0.595	1.15	1.78	0.7	16.7	89.5	518	50	1805	105	3.57	0.81
3/14/95	426	h2ibc	1500	3.5	196	0.577	1.15	1.71	0.65	16.5	88.9	509	50	1780	93	3.50	0.83
3/16/95	470	h2icc	1500	3.5	196	0.595	1.15	1.69	0.7	16.6	89.4	507	0	1710	125	3.50	0.76
3/16/95	470	h2icf	1500	4.26	196	0.695	1.15	1.99	0.8	16.7	88.2	530	0	1350	92	4.26	0.75
3/16/95	470	h2idf	1500	4.26	196	0.7	1.15	2.04	0.9	16.7	92	523	0	1205	78	4.26	0.75
		Dilution														Xd	
3/14/95	426	h2iak	1500	3.58	197	0.54	1.14	1.82	0.4	20.9	90.9	550	50	1990	90	0.00	0.83
3/14/95	426	h2ibk	1500	3.53	196	0.54	1.14	1.81	0.2	20.9	91	545	0	1455	61	0.00	0.81
3/14/95	426	h2iac	1500	3.57	197	0.595	1.14	1.78	0.7	16.7	89.5	518	50	1805	105	0.20	0.81
3/14/95	426	h2ibc	1500	3.5	196	0.595	1.14	1.71	0.65	16.5	88.9	509	50	1780	93	0.20	0.83
3/14/95	426	h2iaL	1500	3.53	196	0.67	1.12	1.69	0.7	12.9	93	461	0	1350	138	0.37	0.71
3/14/95	426	h2iBL	1500	3.58	198	0.7	1.12	1.74	0.5	12.9	93.9	468	0	1000	78	0.37	0.74
		Fuel-Air Ratio														ϕ	
3/14/95	426	h2iai	1500	3.53	197	0.63	1.14	1.9	2.9	16.6	92	477	0	1280	74	0.80	0.80
3/14/95	426	h2ibi	1500	3.5	197	0.65	1.14	2	3.5	16.5	95	460	0	1610	120	0.76	0.77
3/14/95	426	h2iac	1500	3.57	197	0.595	1.14	1.78	0.7	16.7	89.5	518	50	1805	105	0.95	0.81
3/14/95	426	h2ibc	1500	3.5	196	0.577	1.14	1.71	0.65	16.5	88.9	509	50	1780	93	0.95	0.83
3/14/95	426	H2IAJ	1500	3.49	196	0.585	1.14	1.6	0.91	16.4	89.6	495	300	1250	135	1.10	0.72
3/14/95	426	H2IBJ	1500	3.42	196	0.56	1.14	1.58	0.9	16.4	89	489	250	1089	123	1.11	0.69
		Spark Advance														θ_{RS}	
3/14/95	426	h2iam	1500	3.55	188	0.57	1.28	1.68	0.78	16.6	87.5	489	50'	2260	175	10.00	0.78
3/14/95	426	h2ibm	1500	3.5	187	0.565	1.19	1.64	0.5	16.4	91	489	0	1310	84	10.00	0.77
3/14/95	426	h2iac	1500	3.57	197	0.595	1.14	1.78	0.7	16.7	89.5	518	50	1805	105	0.00	0.81
3/14/95	426	h2ibc	1500	3.5	196	0.577	1.14	1.71	0.65	16.5	88.9	509	50	1780	93	0.00	0.83
3/14/95	426	h2ian2	1500	3.5	208	0.63	1.1	1.83	0.6	16.3	91	553	0	1410	56	-10.00	0.85
3/14/95	426	h2ibn	1500	3.4	209	0.636	1.1	1.87	0.9	16.6	91	550	0	1370	67	-10.00	0.81

p-Xylene Dopant

date	CO2 amb	case	N	IMEP	Qpmax	Pm	Pivo	m'air	O2 / λ	O2 (N2)	Tcool	Texh	CO	CO2	HC	variable	" = fox
	(ppm)		(rpm)	bar	A BDC	bar	bar	g/s	%	%	(C)	(C)	ppm	ppm	ppmC		
		Dilution														Xd	
16-Mar	430	H2XAK	1500	3.49	196	0.525	1.17	1.68	0.4	20.9	86.4	542	150	2710	157	0.00	0.81
16-Mar	430	H2XBK	1500	3.5	197	0.534	1.17	1.72	0.9	20.9	90.3	538	80	2250	129	0.00	0.80
16-Mar	430	H2XAC	1500	3.56	197	0.59	1.18	1.68	0.5	16.6	93	516	100	1960	140	0.20	0.79
16-Mar	430	H2XBC	1500	3.5	197	0.585	1.14	1.67	0.7	16.65	93	507	100	1970	141	0.20	0.79
16-Mar	460	H2XCC	1500	3.6	197	0.59	1.16	1.67	0.4	16.5	88	512	110	1760	130	0.20	0.77
16-Mar	430	H2XAL	1500	3.55	197	0.7	1.15	1.69	0.8	12.8	92.2	460	60	1394	159	0.38	0.70
16-Mar	460	H2XCL	1500	3.6	195	0.695	1.15	1.68	0.4	12.9	92	457	50	1040	110	0.37	0.68
		Fuel-Air Ratio														ϕ	
16-Mar	430	H2XAI	1500	3.56	197	0.665	1.18	2	3.7	16.6	91.5	460	50	1960	215	0.75	0.70
16-Mar	430	H2XBI	1500	3.6	197	0.66	1.18	2.04	3.6	16.8	89	464	20	1600	154	0.76	0.71
16-Mar	430	H2XAC	1500	3.56	197	0.59	1.18	1.68	0.5	16.6	93	516	100	1960	140	0.96	0.79
16-Mar	430	H2XBC	1500	3.5	197	0.585	1.14	1.67	0.7	16.65	93	507	100	1970	141	0.95	0.79
16-Mar	460	H2XCC	1500	3.6	197	0.59	1.16	1.67	0.4	16.5	88	512	110	1760	130	0.97	0.77
16-Mar	430	H2XAJ	1500	3.53	197	0.58	1.16	1.65	0.92	16.4	93.5	507	400	1630	215	1.09	0.69
16-Mar	430	H2XBJ	1500	3.51	197	0.585	1.17	1.58	0.9	16.3	91.2	502	420	1410	174	1.11	0.71

Hexane Dopant

date	CO2 amb	case	N	IMEP	Qpmax	Pm	Pivo	m'air	O2 / λ	O2 (N2)	Tcool	Texh	CO	CO2	HC	variable	" = fox
	(ppm)		(rpm)	bar	A BDC	bar	bar	g/s	%	%	(C)	(C)	ppm	ppm	ppmC		
		Dilution														Xd	
3/18/95	400	H2HAK	1500	3.47	196	0.52	1.19	1.68	0.9	20.9	90	544	70	1890	72	0.00	0.86
3/18/95	400	H2HBK	1500	3.47	196	0.515	1.19	1.68	0.9	20.9	88	541	0	1544	60	0.00	0.84
3/18/95	400	H2HAC	1500	3.54	198	0.59	1.17	1.71	0.8	16.6	91	515	20	1120	50	0.20	0.83
3/18/95	400	H2HBC	1500	3.55	197	0.58	1.17	1.67	0.85	16.6	89.4	515	0	1400	65	0.20	0.84
3/18/95	400	H2HAL	1500	3.54	198	0.69	1.16	1.68	0.5	12.9	89	475	50	1020	87	0.37	0.75
3/18/95	400	H2HBL	1500	3.51	196	0.685	1.16	1.67	0.6	12.8	92.1	465	0	882.5	60	0.38	0.77
		Fuel-Air Ratio														ϕ	
3/18/95	400	H2HAI	1500	3.55	197	0.65	1.21	1.95	3.65	16.7	92	471	50	960	66	0.75	0.76
3/18/95	400	H2HBI	1500	3.57	199	0.656	1.21	1.9	3.5	16.5	89	475	0	812	44.5	0.76	0.77
3/18/95	400	H2HAC	1500	3.54	198	0.59	1.17	1.71	0.8	16.6	91	515	20	1120	50	0.94	0.83
3/18/95	400	H2HBC	1500	3.55	197	0.58	1.17	1.67	0.85	16.6	89.4	515	0	1400	65	0.94	0.84
3/18/95	400	H2HAJ	1500	3.55	198	0.59	1.17	1.6	0.9	16.6	89	509	320	1410	100	1.11	0.81
3/18/95	400	H2HAJ2	1500	3.6	196	0.595	1.17	1.58	0.84	16.6	90	498	400	712	75	1.19	0.75

MTBE Dopant

date	CO2 amb	case	N	IMEP	Qpmax	Pm	Pivo	m'air	O2 / λ	O2 (N2)	Tcool	Texh	CO	CO2	HC	variable	" = fox
	(ppm)		(rpm)	bar	A BDC	bar	bar	g/s	%	%	(C)	(C)	ppm	ppm	ppmC		
		Dilution														Xd	
18-Mar	412	h2mAK	1500	3.4	196	0.51	1.18	1.68	89.5	544	0.9	20.9	0	1482.5	55	0.00	0.84
18-Mar	412	h2mBK	1500	3.49	196	0.512	1.18	1.7	90	537	1	20.9	0	1320	32	0.00	0.89
18-Mar	412	h2mAC	1500	3.48	198	0.586	1.18	1.68	91.5	521	0.7	16.8	0	1230	43	0.19	0.86
18-Mar	412	h2mBC	1500	3.56	196	0.595	1.18	1.67	94	519	0.7	16.7	0	1081	34	0.20	0.87
18-Mar	412	h2mAL	1500	3.56	197	0.7	1.17	1.68	93	464	0.5	12.6	0	770	52	0.39	0.76
18-Mar	412	h2mBL	1500	3.65	196	0.7	1.17	1.7	88	465	0.6	12.9	0	710	38	0.37	0.79
		Fuel-Air Ratio														ϕ	
18-Mar	412	h2mAI	1500	3.56	198	0.657	1.2	2.02	93	467	3.7	16.8	0	880	47	0.75	0.78
18-Mar	412	h2mBI	1500	3.58	197	0.65	1.2	1.96	88	470	3.5	16.6	0	1130	57	0.76	0.82
18-Mar	412	h2mAC	1500	3.48	198	0.586	1.18	1.68	91.5	521	0.7	16.8	0	1230	43	0.95	0.86
18-Mar	412	h2mBC	1500	3.56	196	0.595	1.18	1.67	94	519	0.7	16.7	0	1081	34	0.95	0.87
18-Mar	412	h2mAJ	1500	3.54	197	0.588	1.17	1.58	87	493	0.85	16.4	280	565	55	1.18	0.72

Desorption Data

Toluene Motored Desorption Data					
Correcting HCmotor for air+CH4 by decreasing march and april HCm values by 10%					
Data taken in July and August were calibrated with CH4+air std at 1500					
1500 rpm, Tw=32C		Twall	Rpm	Xtol (%)	**HC ug/cycle**
3/22/94	A	31.3	1492	3.06	**163.6**
3/22/94	C	32.9	1462	5.14	**254.4**
4/5/94	j	48	1500	**3.40**	**186.3**
4/26/94	msc1e	62.7	1500	**5.89**	**234.2**
3/22/94	D	72.5	1531	**6.20**	**209.3**
4/26/94	msc1b	82.6	1500	**6.55**	**166.5**
8/8/94	mtc2c	45.5	1505	**3.66**	**158.8**
8/8/94	mtc2d	64.3	1505	**3.21**	**126.6**
8/8/94	mtc2e	76.2	1505	**2.97**	**89.2**
4/5/94	i	72.5	1000	**4.07**	**125.4**
4/26/94	msc1d	70.9	1036	**6.68**	**165.1**
4/5/94	g	72.5	2500	**2.43**	**154.3**
4/16/94	b	71.8	2487	**2.28**	**99.9**
4/26/94	msc1c	75.8	2497	**7.32**	**318.7**
8/8/94	mtc2f	75.2	2503	**2.76**	**131.1**
7/8/94	mtcb	36.8	1517	**3.82**	**146**
	mtcd	40.4	1500	**3.04**	**155.6**
	mtce	40.1	1500	**4.69**	**226**
1000 rpm					
3/22/94	mch4B	32.9	1028	5.17	**270.7**
4/5/94	i	72.5	1000	4.07	**125.4**
4/26/94	msc1d	70.9	1036	**6.68**	**165.1**
7/8/94	mtca	36	1050	**3.45**	**129**
7/8/94	mtcf	40.3	1021	**4.45**	**198.2**
7/8/94	mtcc	39.3	1002	**3.69**	**136**
4/5/94	g	72.5	2500	**2.43**	**154.3**
4/16/94	b	71.8	2487	**2.28**	**99.9**
4/26/94	msc1c	75.8	2497	**7.32**	**318.7**
8/8/94	mtc2b	45	2504	**3.46**	**187.1**
8/8/94	mtc2f	75.2	2503	**2.76**	**131.1**

	Hexane Data				
	Using CH4 + Air std to calibrate Rosemount Analyzer, which				
	gives values ~10% lower than those measured with a C3H8 + N2 std				
	Oil had about 0.8% xylene left from previous experiment despite two oil changes				
	Data all taken 7-13-94				
Note	run	Twall	rpm	Xhex(%)	HCm (ug/cycle)
	7/13/94				
1500 rpm	mhc4e	64.3	1506	2.78	95.7
	Mhc3e	66	1503	4.23	93.8
	Mhc3f	74.7	1500	4.26	62.7
	Mhc2e	65.5	1496	4.42	86
	Mhc2f	76.4	1495	4.15	52.2
	Mhc2b	37	1506	4.94	234
	Mhc2d	42.8	1495	4.5	192.9
	Mhc3b	38.3	1505	3.9	184.3
	Mhc3d	44	1503	3.16	123.3
	mhc4b	42	1503	3.93	177.4
	mhc4d	48.6	1506	2.77	111.2
1000 rpm	Mhc2a	37	1005	4.71	175.1
	Mhc3a	35.5	992	4.85	179.7
	mhc4a	39.1	1043	4.17	162
2500 rpm	Mhc2c	42.3	2500	4.71	246.4
	Mhc3c2	45	2504	2.94	127.2
	Mhc3c	44	2503	3.51	167.7
	mhc4c	48	2496	3.42	158.4

	Xylene Data						
	Using CH4 + Air std to calibrate Rosemount Analyzer, which						
	gives values ~10% lower than those measured with a C3H8 + N2 std						
	oil had ~ 0.8% contanmination of Toluene ~10% of Xylene concentration						
	Data all taken 7-9-94						
	run	Twall	rpm	Xtol%	Xxyl%	Xfuel(%)	HCm (ug/cycle)
7/9/94	mxc2b	37	1503	0.7	8.55	9.25	231.4
7/9/94	mxc2d	40	1506	0.5	6.99	7.49	218.9
7/9/94	mxc2c	39	2495	0.71	8	8.71	234.4
7/16/94	mxc3b	38.5	1505	0	6.16	6.16	182
7/9/94	mxc2a	36	999	0.67	6.67	7.34	213.7
7/16/94	mxc3d	51.9	1505	0	5.65	5.65	196.4
7/16/94	mxc3g	75.8	2498	0	4.7	4.7	200.4
7/9/94	mxc2e	59	1503	0.57	6.8	7.37	239.5
7/9/94	mxc2f	75.8	1503	0.61	6.1	6.71	207.7
7/16/94	mxc3e	60.2	1506	0	5.49	5.49	197.2
7/16/94	mxc3f	74.4	1506	0	5.26	5.26	179.6
7/16/94	mxc3h	74.4	992	0	4.27	4.27	117

Appendix B

Experimental Calculations

The total amount of dopant desorbed and the fraction oxidized in the post-flame environment were calculated from the measurements in Table B1.

Table B.1 Instrumentation

Measurement	Symbol	Units	Instrument
Hydrocarbon mole fraction in exhaust	Y_e	ppmC1	Rosemount Total HC Analyzer (FID)
Carbon monoxide mole fraction in exhaust	Y_{CO}	ppm	Beckman 864 (NDIR)
Carbon dioxide mole fraction in exhaust	Y_{CO2}	ppm	Rosemount 880A (NDIR)
Oxygen mole fraction in intake mixture	Y_{O2I}	%	NTK MO-1000
Oxygen mole fraction in exhaust mixture	Y_{O2E} or λ^a	% or -	Horiba Mexa-110λ
Air mass flow rate	m_a	g/s	Kurz 505-9A-02
Engine speed	N	rpm	
Cylinder pressure	P	bar	Kistler 6051A
Intake manifold pressure	P_i	bar	
Coolant temperature	T_c	^oC	type K thermocouple
Cylinder wall temperature	T_w	^oC	type K thermocouple
Exhaust temperature	T_e	^oC	type K thermocouple

a. If mixture is lean, used Y_{O2E} and if rich used λ.

The equations to calculate the total amount of dopant desorbed, the amount desorbed after flame passage and the fraction of the post-flame desorbed dopant oxidized are presented in chapter 2 and repeated here as eqns. B.1 through B.4. Then equations are presented to calculate all the terms in equations B.1 through B.4 from the species measurements in the engine intake and exhaust manifolds (Table B.1).

The mass of dopant desorbed after the end of combustion (m_d) is defined as

$$m_d = \frac{m_c}{2}\frac{L_{EOC}}{L_S} \qquad (B.1)$$

where m_c is the total mass of hydrocarbon desorbed, L_s is the stroke length and L_{EOC} is the amount of cylinder covered at the end of combustion (EOC). The timing of EOC is determined from an averaged trace of 100 cycles of pressure data, by noting where the pressure-volume plot becomes a flat line on a log-log plot. The fraction surviving then is simply the mass of hydrocarbons in the exhaust over the mass of dopant desorbed after EOC or post-flame

$$f_{HC} = \frac{m_{HC}}{(m_c/2)(L_{EOC}/L_S)} \qquad (B.2)$$

The total amount of dopant desorbed is calculated by summing the total carbon contained in hydrocarbons, carbon dioxide and carbon monoxide and converting to the equivalent amount of dopant mass,

$$m_c = \frac{M_{HC}}{c_n}\left[Y_e \frac{m_e}{M_e} + \frac{m_d}{M_d}\left(Y_{CO} + Y_{CO2} - Y_{CO2A}\right)\right] \qquad \text{(B.3)}$$

where Y_{HC}, Y_{CO} and Y_{CO2} are the molar concentrations of hydrocarbons, carbon monoxide and carbon dioxide, m_e and m_d are the mass flow rates of wet and dry exhaust gases, M_{HC}, M_e and M_d are the molecular masses and c_n is the carbon number of the hydrocarbon dopant. The ambient CO_2 concentration (Y_{CO2A}), which is determined by motoring the engine, is corrected for the water removed from the burned gas during fired experiments. In the motored experiments, the mass fuel desorbed (m_c) is determined from the air mass flow rate (m_{air}) and the hydrocarbon concentration in the exhaust (HC)

$$m_c = \frac{m_{air}}{M_{air}} \frac{M_{HC}}{c_n} Y_{HC} \qquad \text{(B.4)}$$

The equations relating the various terms in eqns B.1 through B.4 to the physical measurements are based on the following stoichiometric equation,

$$2\phi \cdot H_2 + (O_2 + 3.773 \cdot N_2) + \eta N_2 \rightarrow \begin{array}{ll} 2\phi H_2O + (1-\phi)O_2 + (3.773+\eta)N_2 & \text{if } \phi \le 1.0 \\ 2H_2O + 2(\phi - 1)H_2 + (3.773+\eta)N_2 & \text{if } \phi > 1.0 \end{array},$$

where η is the number of moles of diluent nitrogen added to the intake air. The first set of equations obtain the wet and dry exhaust flow rates and average molecular weight from the air mass flow rate (m_{air}) and the oxygen concentration measurements. The exhaust mass flow rate (m_e) is

$$m_e = m_a(1 + F/A_S)(1 + X_D), \qquad \text{(B.5)}$$

where F/A_s is the stoichiometric fuel to air ratio. The molecular weight of the exhaust (M_e) is

$$M_e = \begin{array}{ll} \dfrac{2\phi M_{H_2O} + (1-\phi)M_{O_2} + \psi M_{N_2}}{\phi + 1 + \psi} & \text{if } \phi \le 1.0 \\ \dfrac{2\phi M_{H_2O} + (\phi - 1)M_{H_2} + \psi M_{N_2}}{21 + \psi} & \text{if } \phi > 1.0 \end{array} . \qquad \text{(B.6)}$$

The carbon monoxide and carbon dioxide measurements are made on a dry air basis as the NDIR sensors require dry air samples. The gas flow rate (m_{ed}) and molecular weight (M_{ed}) for dry exhaust are

$$m_{ed} = \begin{cases} m_e\left[1-\left(\dfrac{M_{H_2O}}{M_e}\right)\left(\dfrac{2}{\phi+1+\psi}\right)\right] & \text{if } \phi \le 1.0 \\ m_e\left[1-\left(\dfrac{M_{H_2O}}{M_e}\right)\left(\dfrac{2}{2\phi+\psi}\right)\right] & \text{if } \phi > 1.0 \end{cases} \tag{B.7}$$

and

$$M_{ed} = \begin{cases} \dfrac{(1-\phi)M_{O_2}+\psi M_{N_2}}{1-\phi+\psi} & \text{if } \phi \le 1.0 \\ \dfrac{(\phi-1)M_{H_2}+\psi M_{N_2}}{\phi-1+\psi} & \text{if } \phi > 1.0 \end{cases} \quad . \tag{B.8}$$

The CO_2 measurements are of the order 2000 ppm and thus require correction for the level ambient CO_2 present in the dry exhaust gas (Y_{CO2Ad}). The Y_{CO2A} is calculated based on the constant ratio of ambient carbon dioxide (Y_{CO2A}) to ambient nitrogen (Y_{N2A}). The concentration of ambient CO_2 in the dry exhaust is

$$Y_{CO2Ad} = \begin{cases} \dfrac{Y_{CO2A}}{0.79}\,\dfrac{3.773}{1-\phi+\psi} & \text{if } \phi \le 1.0 \\ \dfrac{Y_{CO2A}}{0.79}\,\dfrac{3.773}{2\phi+\psi-2} & \text{if } \phi > 1.0 \end{cases} \quad . \tag{B.9}$$

The diluent mass fraction (X_D) and the nitrogen-oxygen ratio ($\psi = 3.773+\eta$) are obtained from the intake oxygen concentration (Y_{O2I}), which is measured after the addition of the nitrogen dilution, but before the addition of hydrogen fuel. The diluent mass fraction (X_D) is calculated as

$$X_D = \frac{28 \cdot Y_\eta}{2 \cdot 2\phi\, F/A_s + 32 + 28 \cdot 3.773 + 28 \cdot Y_\eta} \tag{B.10}$$

where

$$Y_\eta = 100/Y_{O2I} - 4.773$$

and F/A_S is the stoichiometric fuel to air mass ratio for hydrogen (0.0292).

As the oxygen-lambda meter calculates the air-fuel ratio based on among other things the hydrogen to carbon ratio, the actual fuel-air equivalence ratio (ϕ) is calculated from the measured oxygen concentration (Y_{O2E}) for lean cases. Under rich conditions, the oxygen concentration is zero, so the relative air-fuel ratio (λ) was measured directly after setting the hydrogen to carbon ratio to 9.99. The fuel-air equivalence ratio (ϕ) is calculated as

$$\phi = \frac{1-(1+\psi)Y_{O2E}}{1+Y_{O2E}} \quad . \qquad \text{(B.11)}$$

APPENDIX C

DOPANT-OIL PROPERTIES AND OIL THICKNESS MODEL

Oil viscosity

Viscosity (μ) was calculated as a function of temperature using the Walther equation [27]

$$\log_{10}\log_{10}(\mu / \rho_o + 0.7) = C - D \cdot \log_{10}(T) \tag{C.1}$$

with μ in cP (10^{-3} kg/m·s), T in kelvin, oil density (ρ_o) in g/cm^3 (10^3 kg/m^3) and the constants C and D are fit to viscosity measurements of the 10W-30 oil (C=2.86, D=7.41).

Dopant diffusivity in oil

The diffusivity of dopant in the oil is calculated from an empirical equation fitted to a wide range of hydrocarbon data [27],

$$D_o = \frac{1.33 \cdot 10^{-13} T^{1.47} \mu^{(10.2/v_{hc} - 0.791)}}{v_{hc}^{0.71}} \tag{C.2}$$

where T is the wall temperature in kelvin, μ is the viscosity in centipoise and v_{hc} is the dopant molecular volume in cubic centimeter. The dopant molecular volume is related to the critical volume as

$$v_{hc} = 0.285\, v_{crt}^{\,1.048}$$

where v_{crt} is 316 cm^3 for xylene, 370 cm^3 for toluene, 331 cm^3 for isooctane, 468 cm^3 for hexane and 329 cm^3 for MTBE [27].

Dopant solubility in oil

An expression for a modified Henry's constant, which is the ratio of the dopant partial pressure to the mass fraction of the dopant in the oil, was obtained from solubility data [29]:

$$H^* = 10^{[E \cdot \log_{10}(T) + F]} \tag{C.3}$$

where H^* is the modified henry's constant in kPa, T in kelvin and E and F are constants for each dopant-oil combination. Table C1 lists the constants from fits to data by Schramm and Sorenson for several dopants in 10w-30 oil [29].

Table C1. Constants for equation C3 for Henry's Constant

Dopant	E	F
m-xylene, p-xylene	9.81	-23.3
toluene	7.86	-17.9
isooctane	7.47	-16.8
hexane	5.45	-11.2
MTBE	4.13	-7.66

Oil thickness model

An approximate expression for the free standing oil thickness ($\delta(z)$) as a function of the wall temperature and engines speed was obtained from the results of a fluid dynamics model of the oil layer under the piston rings developed by Tian [C1],

$$\delta = A_0 + B_0\sqrt{\mu N} \qquad \text{(C.4)}$$

where

$$A_0 = 0.425 - 0.0025\cdot(T - 273.15)$$

and

$$B_0 = 1.03\cdot\sqrt{2L_S\left[1+\left(1+\frac{\cos\theta}{\sqrt{r^2-\sin^2\theta}}\right)\frac{\pi}{2}\sin\theta\right]}\cdot\sqrt{\frac{z}{0.35L_s}} \qquad \text{for } z \le 0.35\cdot L_s$$

$$B_0 = 1.03\cdot\sqrt{2L_S\left[1+\left(1+\frac{\cos\theta}{\sqrt{r^2-\sin^2\theta}}\right)\frac{\pi}{2}\sin\theta\right]} \qquad \text{for } z > 0.35\cdot L_s$$

where $\delta(z)$ is in μm, μ is the oil viscosity in kg/m s and N is the engine speed in rps, T is in kelvin, z, the axial location relative to TDC, L_S the stroke length and r is the ratio of the connecting rod length to half the stroke length. The average oil thickness is obtained by averaging B_O over the stroke: $B_{O\,avg} = 0.063\ L_S^{0.5}$. Typical results for a 10w-30 oil at 1500 rpm are shown in Figs. C.1 and C.2.

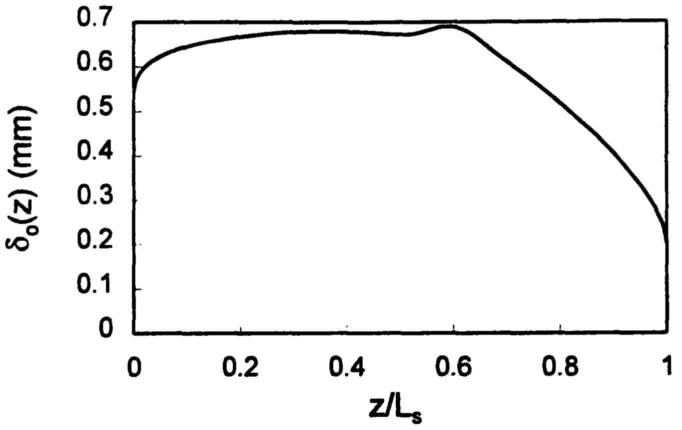

Fig. C.1 Oil thickness along cylinder liner at 1500 rpm and $T_W = 90$ °C.

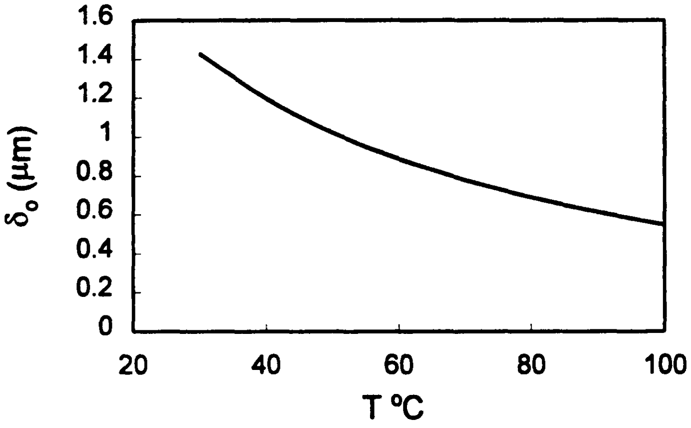

Fig. C.2 Oil thickness at mid-cylinder versus wall temperature for 1500 rpm.

Appendix D

Cycle Simulation Results

Each of the operating conditions listed in Table 2.1 were simulated using a thermodynamic or zero-dimensional cycle simulation code. The code was most recently described by Poulos [D1]. Two changes were made to simulate these hydrogen-fired experiments. The code would not accept a carbonless fuel such as H_2 because the stoichiometry is based on ratios to carbon atoms. Therefore, a pseudo-fuel was used, CH_{100}, which minimized the carbon added to the system. It was also necessary to deactivate the non-equilibrium chemistry module which was based on a hydrocarbon-fuel and therefore not appropriate for hydrogen.

The inputs to the model are listed in Table D1. The spark timing (θ_{spark}), burn duration ($\theta_{\Delta t}$), engine speed (N), nitrogen dilution (X_D) and fuel-air equivalence ratio (ϕ) were taken directly from the experiments. The intake pressure (P_{in}) was the measured intake pressure corrected for the denser pseudo-fuel. The temperatures for the piston (T_p), cylinder wall (T_{cw}), cylinder head (T_{hd}), intake mixture temperature (T_{fresh}) were estimated from the measured coolant temperature (T_c) and the measured temperature at the top of cylinder wall (T_h) as follows:

$$T_{hd} = T_c$$

$$T_{cw} = (T_c + T_h)/2$$

$$T_p = T_{cw} + 50$$

$$T_{fresh} = T_c - 10$$

Table D.1 Inputs to cycle simulation for all operating conditions.

case		N (rpm)	P_m (bar)	P_{in} (bar)	ϕ	X_D	θ_{spark} (ATC)	$\theta_{\Delta t}$
A	T_w=40 °C	1500	3.54	0.397	0..95	0.2	357	26
B	T_w=60 °C	1500	3.36	0.412	0.95	0.2	359	25
C	baseline	1500	3.48	0.458	0.95	0.2	360	24
D	IMEP:2 bar	1500	1.62	0.244	0.95	0.2	356	28.5
E	IMEP:3 bar	1500	2.92	0.397	0.95	0.2	359	25.5
F	IMEP:4 bar	1500	4.03	0.519	0.95	0.2	360	23.5
G	1000 rpm	1000	3.67	0.496	0.95	0.2	363	16.5
H	2000 rpm	2000	3.50	0.458	0.95	0.2	354	33
I	$\phi = 0.8$	1500	3.49	0.523	0.80	0.2	356	31
J	$\phi = 1.2$	1500	3.64	0.410	1.20	0.2	363	20.5
K	$X_D = 0$	1500	3.27	0.396	0.95	0.0	365	17
L	$X_D = 0.4$	1500	3.41	0.559	0.95	0.4	351	33
M	Spark Advanced	1500	3.53	0.435	0.95	0.2	350	25
N	Spark Retarded	1500	3.50	0.488	0.95	0.2	370	29.5

case		T_c	T_h	T_p	T_{fresh}
A	T_w=40 °C	313	323	373	303
B	T_w=60 °C	333	343	393	323
C	baseline	363	373	423	353
D	IMEP:2 bar	363	373	423	353
E	IMEP:3 bar	363	373	423	353
F	IMEP:4 bar	363	373	423	353
G	1000 rpm	363	373	423	353
H	2000 rpm	363	373	423	353
I	$\phi = 0.8$	363	373	423	353
J	$\phi = 1.2$	363	373	423	353
K	$X_D = 0$	363	373	423	353
L	$X_D = 0.4$	363	373	423	353
M	Spark Advanced	363	373	423	353
N	Spark Retarded	363	373	423	353

The resulting pressure and temperature traces for each case are plotted in the following figures and compared to the measure pressure traces.

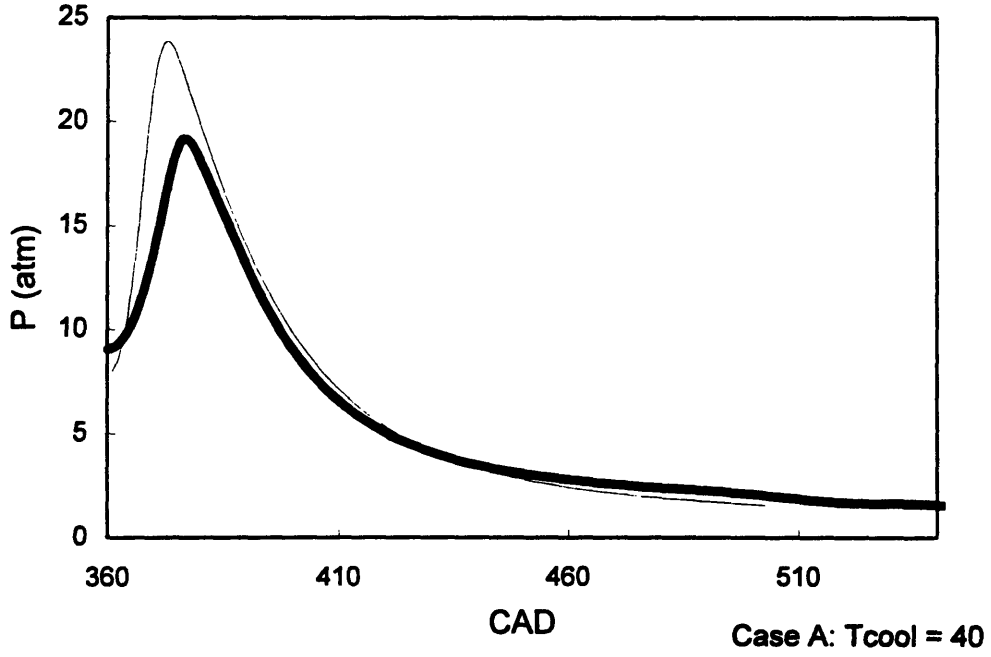

Fig. D.1 Measured and predicted pressure trace for case A along with the bulk temperature history during expansion and part of the exhaust stroke.

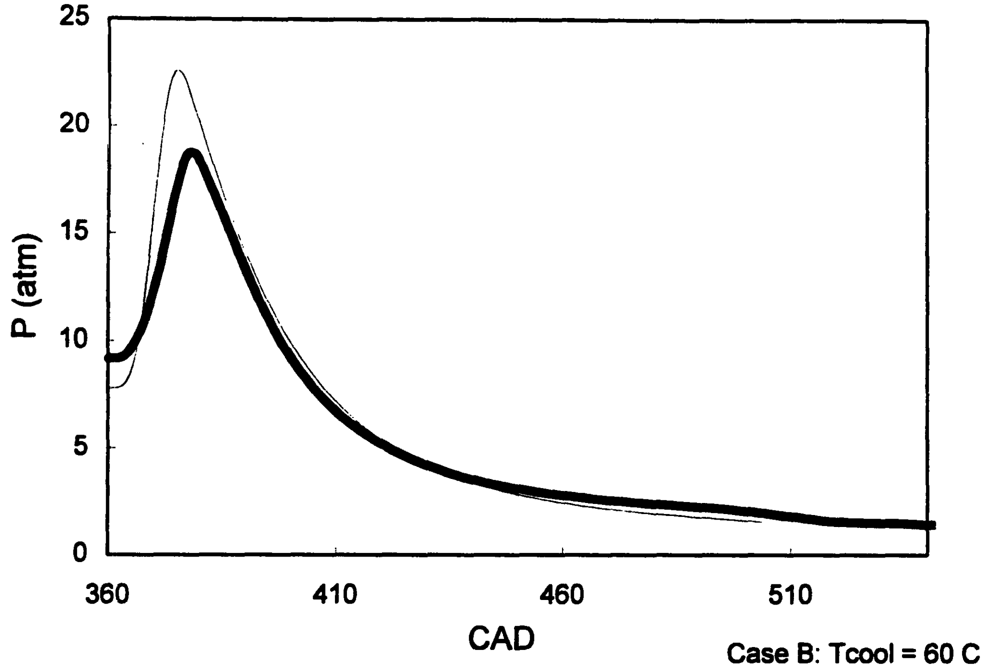

Fig. D.2 Measured and predicted pressure trace for case B along with the bulk temperature history during expansion and part of the exhaust stroke.

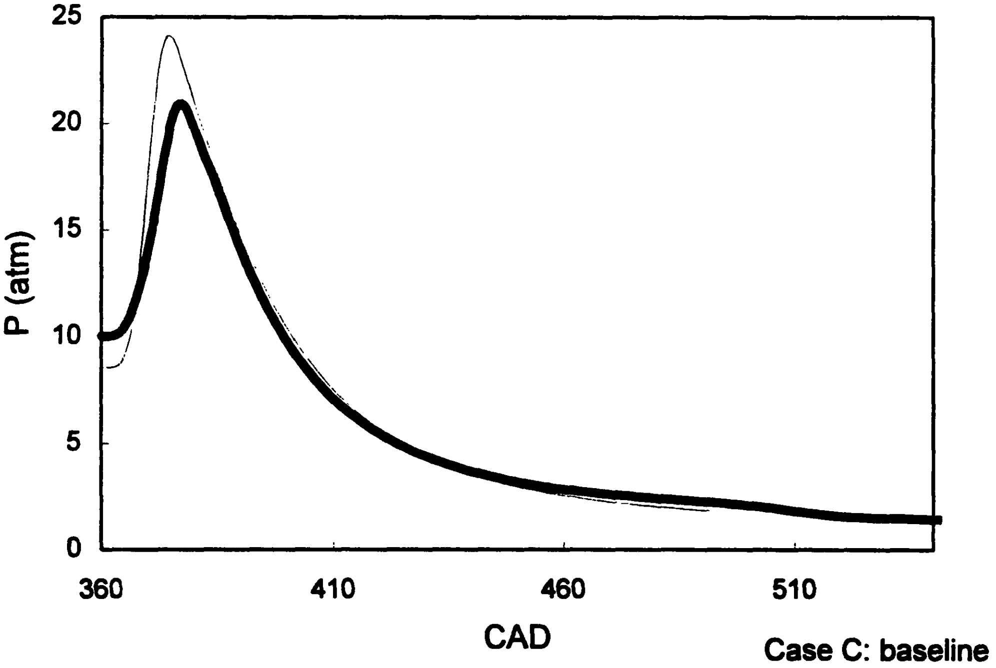

Fig. D.3 Measured and predicted pressure trace for case C along with the bulk temperature history during expansion and part of the exhaust stroke.

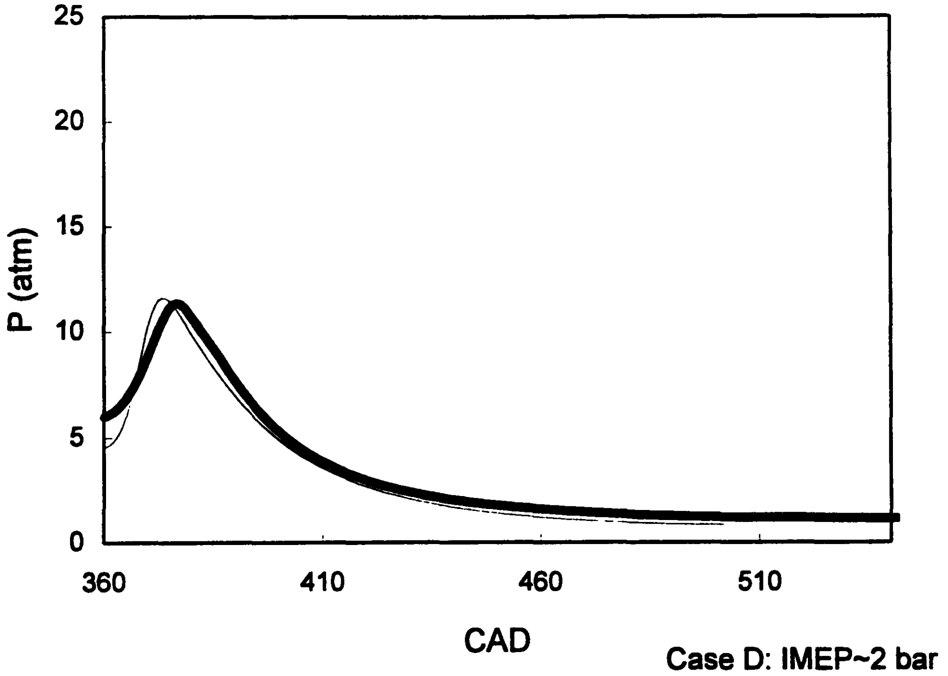

Fig. D.4 Measured and predicted pressure trace for case D along with the bulk temperature history during expansion and part of the exhaust stroke.

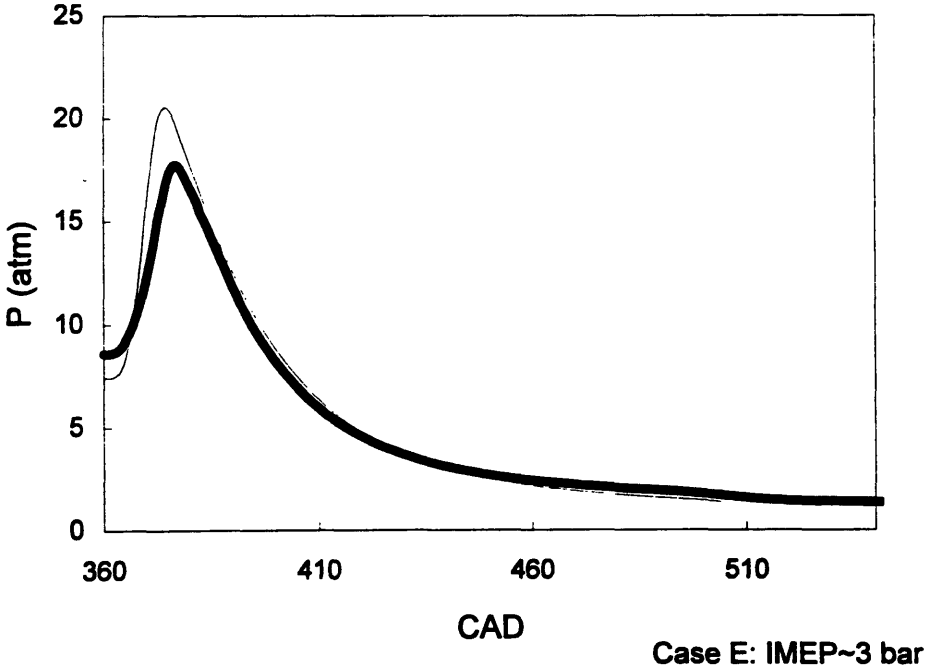

Fig. D.5 Measured and predicted pressure trace for case E along with the bulk temperature history during expansion and part of the exhaust stroke.

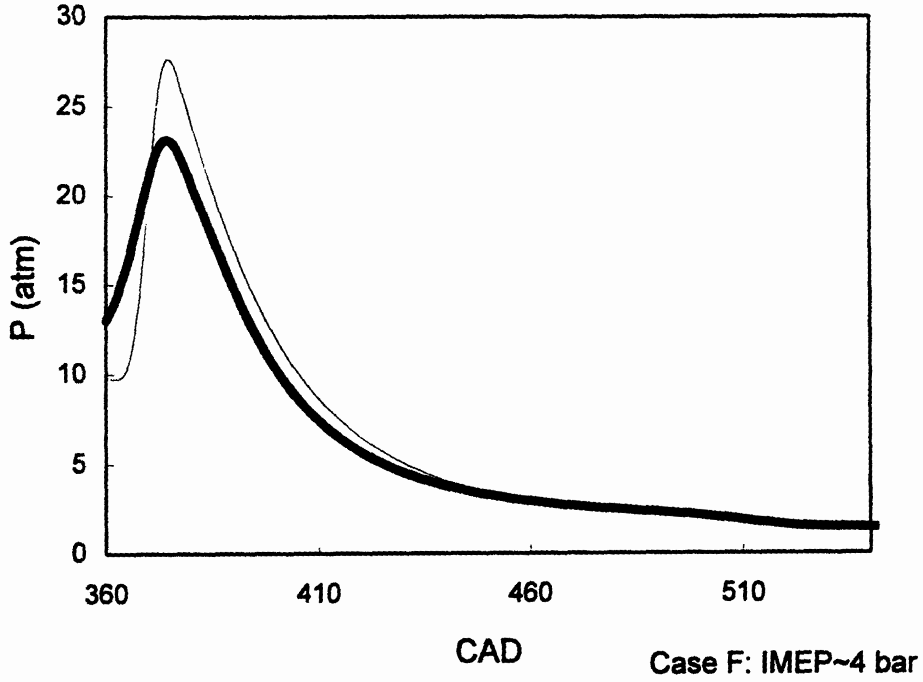

Fig. D.6 Measured and predicted pressure trace for case F along with the bulk temperature history during expansion and part of the exhaust stroke.

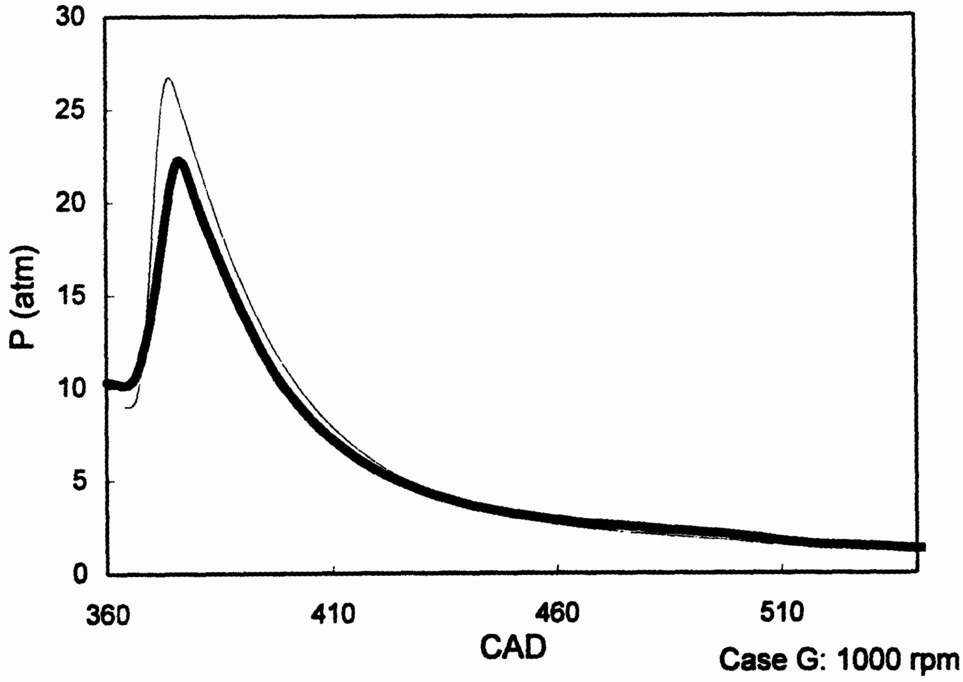

Fig. D.7 Measured and predicted pressure trace for case G along with the bulk temperature history during expansion and part of the exhaust stroke.

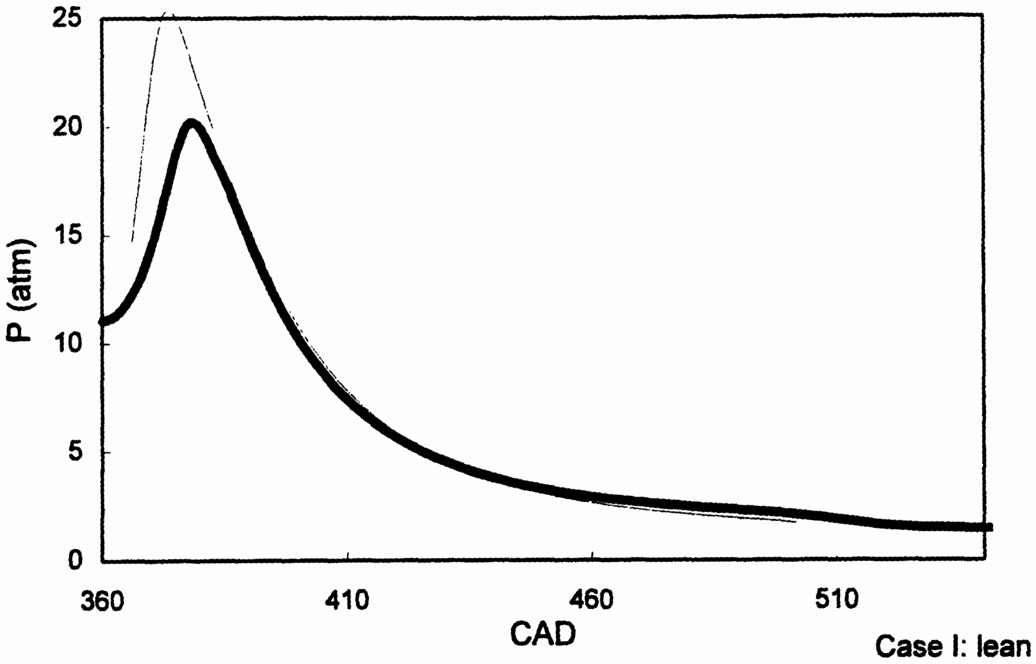

Fig. D.8 Measured and predicted pressure trace for case I along with the bulk temperature history during expansion and part of the exhaust stroke.

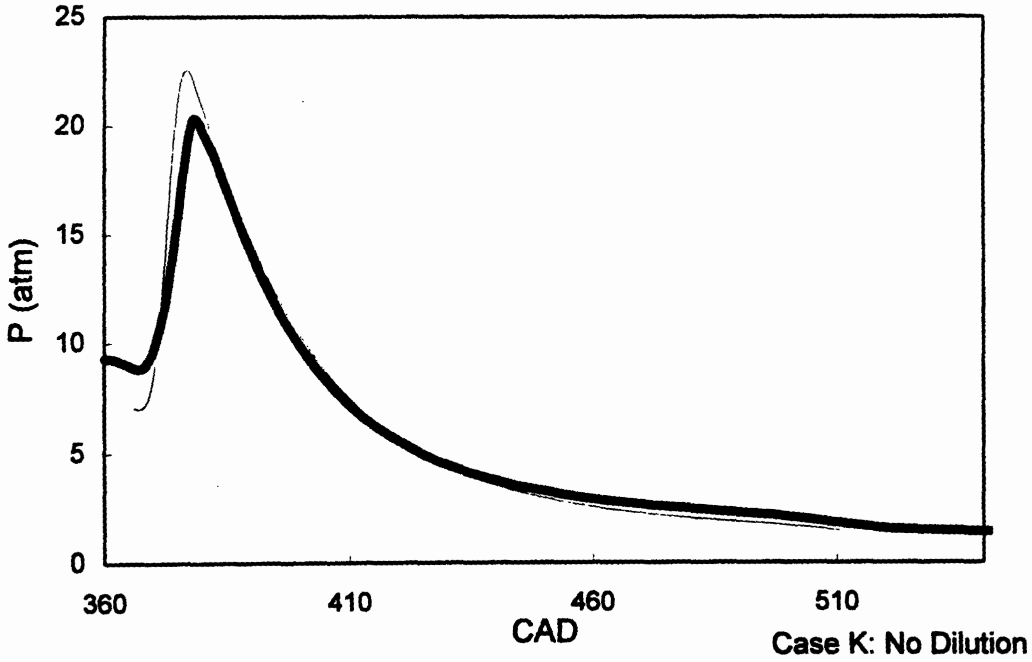

Fig. D.9 Measured and predicted pressure trace for case K along with the bulk temperature history during expansion and part of the exhaust stroke.

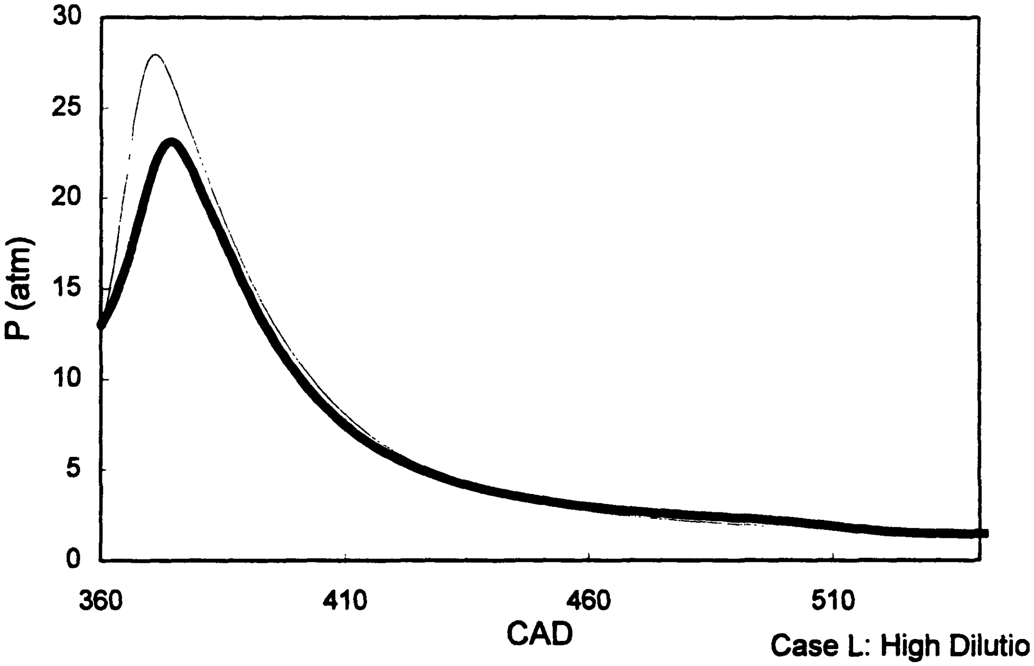

Fig. D.10 Measured and predicted pressure trace for case L along with the bulk temperature history during expansion and part of the exhaust stroke.

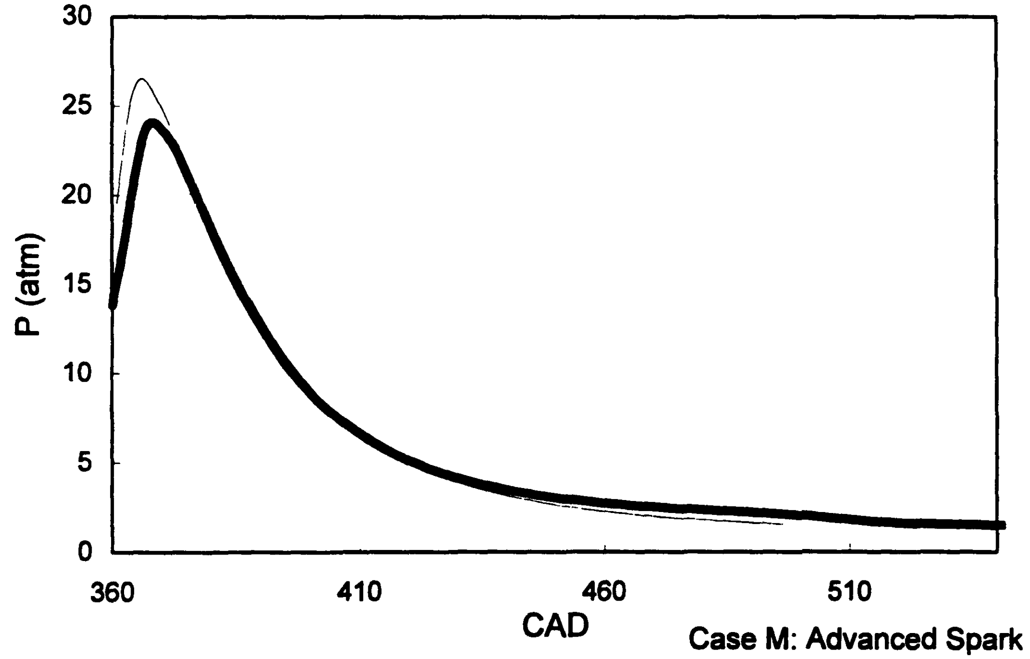

Fig. D.11 Measured and predicted pressure trace for case M along with the bulk temperature history during expansion and part of the exhaust stroke.

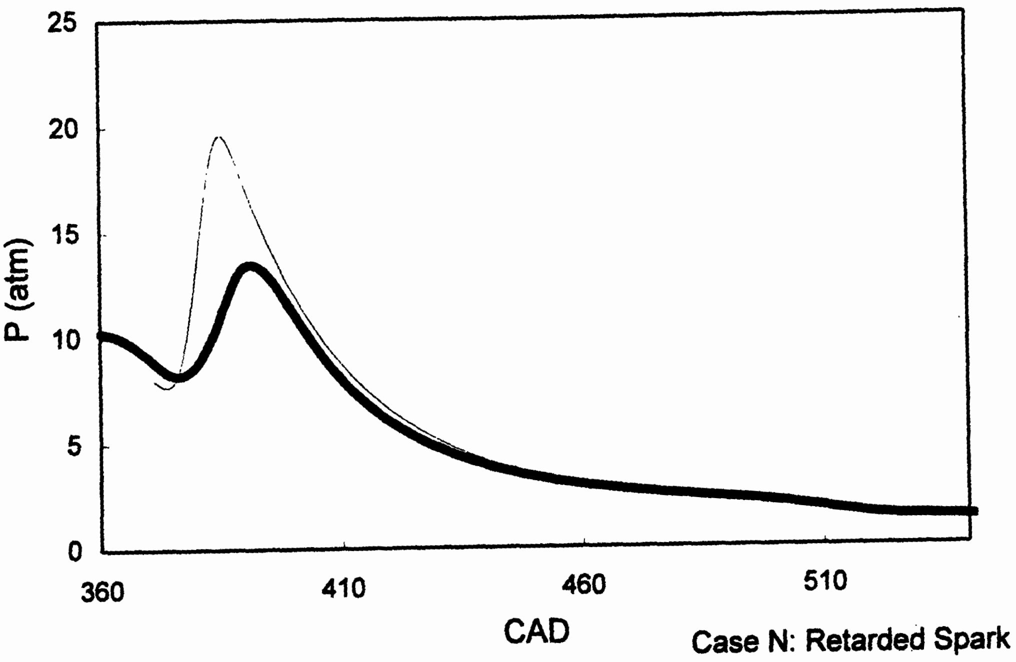

Fig. D.12 Measured and predicted pressure trace for case N along with the bulk temperature history during expansion and part of the exhaust stroke.

Apppendix E

One-Dimensional Code

```
C THIS PROGRAM IS TO CALCULATE THE BOUNDARY LAYER TEMP.
PROFILE AND
C HC PROFILE BY SOLVING UNSTEADY DIFFUSION EQUATIONS
      parameter (minax=0,maxax=90) ! 1st and last index of axial location
      parameter (loilmax = 50,loilmin=2) ! no. to dim. vectors in oil,
                              ! second is arbitrary min no. of cells in oil
      parameter (safty=2.) ! 1 = stability margin for euler in oil layer
      parameter (pi=3.141592654)
      COMMON /VAR1/ TB(360),PRESS(360),jmin,jmax,ncad
      COMMON /VAR2/ TGAS(minax:maxax,0:300)
      COMMON /VAR3/ CONC(2,minax:maxax,0:300)
      COMMON /VAR4/ dmdx(100),DIS(100),SP(100)
      COMMON /VAR5/ STROKE,CONROD,RPM,Vcr
      dimension coil0(0:loilmax),coil1(0:loilmax)
      dimension doil(minax:maxax), toil(minax:maxax),
     &         henrystar(minax:maxax), twallm(minax:maxax)
      DIMENSION CP(0:300),RKAPA(0:300),RHO(0:300),RHO1(0:300)
     * ,VEL(0:300),A(0:300),B(0:300),C(0:300),BB(0:300),R(0:300)
      DIMENSION CONV(0:300),A1(0:300),C1(0:300),DAB(2,0:300)
     * ,DHDT(0:300),CONC1(0:300),DELTA(360),TEMP(300),TGAS1(0:300)
      DIMENSION TMASS(minax:maxax,minax:maxax),
     *          Tdesrb(minax:maxax,minax:maxax)
c    DOUBLE PRECISION XXX,TM0,TM1,TM2
      real o2fls, lcr, gapcr, mfoil, mfgas

      OPEN(2,FILE='f16.fb',STATUS='OLD')
      OPEN(10,FILE='ftn40.ca',STATUS='new')
      OPEN(14,FILE='ftn14.df',STATUS='new')
      OPEN(15,FILE='ftn15.df',STATUS='new')
      OPEN(16,FILE='ftn16.df',STATUS='new')

C  SURROUTINE START : CALCULATING PISTON SPEED AND PISTON
DISTANCE

C INPUT DATA -----------------
      rpm = 1500.            ! ENGINE SPEED
      ncad = 2               ! number of CADs per j step
      jmax = int(180/ncad)  ! last CAD/2 of simulation
      phi = 0.95             ! fuel/air ratio
      Xd = 0.2               ! N2 dilution
      Vcr = 0.511e-6         ! crevice volume of nissan warmed m3
```

```
        write (14,450) dis(1),(float(l*ncad),l=0,84,12)
        write (15,450) dis(1),(float(l*ncad),l=0,84,12)

Cmgn READ THE pressure and burned gas temperature
c         for every other crank angle

         pmax = 0.
        DO K=1,jmax
               do nr = 1,ncad-1
                 READ(2,*) CC1,cc2,cc3,cc4
               enddo
        if (itac.eq.1.) then
                 READ(2,*) cad,press(K),cc3,Tb(K) !adiabatic core T
        else
                 READ(2,*) cad,press(K),Tb(K)                !bulk Temp
        endif
                 if (pmax.le.press(k))then
                       pmax = press(k)
                       jmin = k
                 endif
        ENDDO

        CALL START(RPM,bore,stroke,conrod,cr)

        CALL oilprop(Twallm,toil,doil,henrystar,minax,maxax,rhol,iwu,
    &              A0,EOR,eta,beta,HCM,vhc,o2fls,ifuel,Twl,Tcl)

c... determine friction velocity from input data

        spmean = 2. * stroke * rpm / 60.
        sqrtk = sqrt (1.5*(turbratio*spmean)**2)
        ustar = turbftr*0.09 * sqrtk / 0.4  ! cmu * ustar = kappa * sqrtk

c+10++++++++++++this is the loop over all axial elements++++++++++++++++++++++

cmgn

        DO 10 J =jmin,jmax

         WRITE(*,*) 'axial element created at CRANK ANGLE = ',(j*ncad)

         CALL BOUND(J,RPM,STROKE,totalm,DELTAO,DELTA,Vcr,Twallm(j))

        do ij = j,jmax
```

```
           if (delta(ij).le.0.) then
                  delta(ij) = delta(ij-1)
           endif
      enddo

       if (deltao.le.0.) deltao = 0.

     KK2=INT(DELTAO/DELTAX)   !DELTAO : CREVICE GAS INIT. THICKNESS
       DELTA1=DELTAO

       XDIS=DELTAO
       TGAS(J,0)=Twallm(j)         !TGAS : GAS TEMP. IN THE BOUNDARY LAYER
       TGAS(J,N)=TB(J)          ! TB : BURNED GAS TEMP.
       KK=INT(DELTAO/DELTAX)
       KKK=KK
       kcr = kk2

       CONC(1,J,0)=CONHC         ! CONC(1 ) : PROPANE MASS FRACTION
       CONC(2,J,0)=CONO21        ! CONC(2 ) : OXYGEN MASS FRACTION
       CONC1(0)=CONHC
       IF((KK+1).GE.(N-1)) KK=N-2

       HCoilinit = coilinit*rhol*Toil(j)*(dis(j)-dis(j+1)) !dopant in oil

        DO 20 I=1,KK+1
             TGAS(J,I)=Twallm(j)     ! TGAS : TEMP. OF BOUNDARY AT LOCATION
X
             CONC(1,J,I)=CONHC
             CONC1(I)=CONHC
             CONC(2,J,I)=CONO21
20     CONTINUE

c
c...   determine grid in oillayer, redone for every axial segment
c
c...   characteristic gas diffusivity
       dgas = 0.04357*twallm(J)**(3./2.)/(100000.*PRESS(j))
    *           *((Vair)**(1./3.)+(vhc)**(1./3.))**(-2.)*
    *           SQRT(1./airm+1./hcm)

c 1st deltaxoil from ratio matching to gas side
       deltaxoil = sqrt(doil(j)/dgas)*deltax
       loil1 = toil(j)/deltaxoil+1

c 2nd from stability criterion for euler integration
```

```
        deltaxoil = sqrt(2.*doil(j)*deltat*safty)
        loil2 = toil(j)/deltaxoil

c...more stable w/ less cells. Hence:
        lmax = loil2    !  min(loil1,loil2)
        deltaxoil = toil(j)/float(lmax)
        write(*,*)
     &  'no. of elements in oillayer: gasside match, stab, actual'
        write(*,*)loil1,loil2,lmax
        if (lmax.lt.loilmin) then
                write(*,*)'decreasing timestep by factor:',
     &          float(loilmin)/float(lmax)
                tftr = float(loilmin)/float(lmax)
                deltat = delta0/tftr
        endif
        if (lmax.gt.loilmax)then
                write(*,*)'dimension vectors in oillayer longer'
                write(*,*)'loilmax larger than=',lmax
                stop
        endif

        do iwolf=0, lmax
                coil0(iwolf) = coilinit
        enddo

        DO 24 I=KK+2,N
                TGAS(J,I)=TB(J)
                CONC(1,J,I)=0.0
                CONC1(I)=0.0
                CONC(2,J,I)=CONO22
24      CONTINUE
                DO I=1,100
                        TEMP(I)=TB(J)+(TB(J)-Twallm(j))*LOG10((I)/
     *          (100.))/2.6     ! SET THE INIT. BOUNDARY TEMP.
                ENDDO

                DO I= 1,100
                        TGAS(J,I+KK+1)=TEMP(I)
                ENDDO

31          DO 30 I=0,N
                CP(I)=947.8+0.24937*TGAS(J,I)   ! CP :SPECIFIC HEAT (J/kg/K)
                RHO(I)=100000.*PRESS(J)/(8.314/totalm*TGAS(J,I)) !:DENSITY (kg/m3)
                RKAPA(I)=ALPHA(TGAS(J,I),PRESS(J),totalm)*RHO(I)*CP(I)  !: THEairmL
COND.
```

```
30      CONTINUE

            L2=0
            MM2=1
            iwout = 1
            j2 = j

33    if (abs(dis(j2)-dis(j)).lt.lcr) then
            j2 = j2-1
            goto 33
      endif
      if (j2.lt.0) j2=1


      DO 40 I=J2,jmax    ! start w/ CA of element creation till CA end

            write(*,*) 'axial element, crank angle= ',j*ncad,i*ncad

c     flux check
      if (i.gt.j2+1) then
      mfoil = doil(j)/deltaxoil*rhol*(coil0(lmax-1)-coil0(lmax))
      mfgas = Dab(1,0)/deltax*rho(0)*(conc(1,j,0)-conc(1,j,1))
      endif
cmgn
c     next part of code allows the HCs to desorb into the top land crevice
c     before being exposed to the cylinder gases, calculations indicate
c     that the diffusion penetration depth is the same size as the gap
c     so this effect is important

      if (i.lt.j) then
            write (*,*) ' in crevice',dis(j)-dis(i)
            do ik = 0,kcr
             Tgas(j,ik) = Twallm(j)
            enddo

      elseif (i.eq.j) then        !resets I, Tgas(j,i) at top of land
            KK=INT(DELTAO/DELTAX)
            do ik=0,kk+1
                  Tgas(j,ik) = Twallm(j)
            enddo
            do ik=kk+2,kk+2+100
                  Tgas(j,ik) = TB(J)+(TB(J)-Twallm(j))
     *            *LOG10((ik-kk-1)/(100.))/2.6  ! SET INIT.thermal BL
            ENDDO
            do ik=kk+2+100,n
```

```
                  Tgas(j,ik) = Tb(j)
            enddo
      endif

            iwout = iwout + 1
c     if (iwout .ge. 1) then ! disable print out for full axial case
            if (i.lt.j) then
                  nprime = kcr
            else
                  nprime = n-2
            endif

            if ((float(i)/2.-int(i)/2.).eq.0.) then
                  write(10,*) 'axial: ',j*ncad,' cad= ',i*ncad
                  do iw = 0, nprime   ! stuff from the gas side
                    write (10,*) real(iw)*deltax, tgas(j,iw),
   &              conc(1,j,iw),conc(2,j,iw),dhdt(iw),dab(j,iw)
                  enddo
            endif

       L2=L2+1
       L1=INT((I-J)/10.)

C------- NUMBER OF STEP ------- : NN

            NN=ncad/(rpm*6*deltat)
            if (tftr.ne.1.0) write (*,*) 'nn, tftr ',nn,tftr

            DELPRESS=(PRESS(I+1)-PRESS(I-1))*100000./2.
            XMULT=(TB(I+1)-TB(I))/TB(I)/NN

c+45++++++++++++++This is the subcycling in time per CA++++++++++++++++++++++++

            DO 45 L=1,NN

c            write (*,*) '1 delta(i,+1)',i,delta(i),delta(i+1)

             KK4=INT((DELTAO+DELTA(I)/2.+(DELTA(I+1)-DELTA(I))
   *        /NN*L/2.)/DELTAX)

51       IF(DELTA(I+1).LE.DELTA(I)) DELTA(I+1)=DELTA(I)
             IF(DELTA(I+1).GE.0.0035)DELTA(I+1)=0.0035

               KK=INT((0.001+DELTA(I)+(DELTA(I+1)-DELTA(I))
   *        /NN*L)/DELTAX)
```

```
cmgn   settin BL to crevice width, when in crevice
c      and limting diffusion past piston surface in top land
               if (i.lt.j) then
                      kk = kcr
                      kk4 = kcr
               endif
cmgn

                PRESS1=PRESS(I)+(PRESS(I+1)-PRESS(I))/NN*(L)

               IF(KK.GE.299) THEN
                KK=299
               ENDIF
               IF(KK4.GE.299) THEN
                KK4=299
               ENDIF
               GAS=TGAS(J,N)

               DO K= KK+1,N
                TGAS(J,K)=TB(I)+(TB(I+1)-TB(I))/NN*(L)
                RHO(K)=100000.*PRESS1/(8.314/totalm*TGAS(J,K))

               ENDDO
               VEL(0)=0.
               CONC(1,J,N)=0.0
               CONC1(N)=0.0
               CONC(2,J,N)=CONO22

c       WRITE (*,*) 'PATH 0'


        DO 46 K=0,N

                RHO1(K)=RHO(K)

                RHO(K)=100000.*PRESS1/(8.314/totalm*TGAS(J,K))

                CP(K)=947.8+0.24937*TGAS(J,K)
                XHC=CONC(1,J,K)/HCM*0.001*RHO(K)  !HC MOLE CONCENTRATION
(MOL/cM3)
                                          !looks like this is [cc]
                XO2=CONC(2,J,K)/O2M*0.001*RHO(K)  !O2 MOLE CONCENTRATION
(MOL/cM3)
```

```
               XHC1=CONC(1,J,K)*TOTALM*1000./HCM      ! PROPANE MOLE
FRACTION
               XO21=CONC(2,J,K)*TOTALM*1000./O2M      ! O2 MOLE FRACTION


               DAB(1,K)=0.04357*TGAS(J,K)**(3./2.)/(100000.*PRESS1)
     *         *((Vair)**(1./3.)+(vhc)**(1./3.))**(-2.)*
     *         SQRT(1./airm+1./hcm)

               DAB(2,K)=0.04357*TGAS(J,K)**(3./2.)/(100000.*PRESS1)
     *         *((Vair)**(1./3.)+(vo2)**(1./3.))**(-2.)*
     *         SQRT(1./airm+1./o2m)

c...  add turbulent diffusivity, use reichhard's empircal expression,
c     which accounts for mixing length reduction in the buffer layer
c     (see mit 2.273 turbulence lecture)

               alphaw = alpha(tgas(j,k),press1,totalm)
               yw = k * deltax
c              Prandtl = 0.69
               GAM=1.3655-6.105*0.00001*tgas(j,k)
               Prandtl=0.05+4.2*(GAM-1.)-6.7*(GAM-1.)**2
               y0w = 11. * alphaw * Prandtl / ustar
               scaleL = yw-y0w*tanh(yw/y0w)
               alphaturb = 0.4 * ustar * (yw-y0w*tanh(yw/y0w))

      if (i.lt.j) goto 46        !disabling turb and kinetics in crevice

c             do iw = 1, 2
               iw = 1
               dabm1 = dab(1,k)
               dab(iw,k) = dab(iw,k) + alphaturb
               iw = 2
               dabm2 = dab(2,k)
               dab(iw,k) = dab(iw,k) + alphaturb
c             enddo

               RKAPA(K)=(ALPHAw+alphaturb)*RHO(K)*CP(K)

            DHDT(K)= -1.*10**6. * A0 * A0ftr * (XHC**(ETA+1)) *
     &         (XO2**BETA) * EXP(-EOR*EORFTR/TGAS(J,K)) !cmgn [imoles/m3/sec]

46    CONTINUE

C   CALCULATE THE VELOCITY IN THE BOUNDARY LAYER
```

```
          DO 16 K=1,KK4+1
               VEL(K)=(RHO(K-1)+RHO1(K-1))/(RHO(K)+RHO1(K))*VEL(K-1)
   *      -DELTAX/DELTAT*2.*(RHO(K)-RHO1(K))/(RHO(K)+RHO1(K))

16        CONTINUE

47         DO K=KK4+2,N
               VEL(K)=0.
             ENDDO

cmgn  skiping Temperature solution in crevice as it is isothermal
c      and no reaction take place
       if (i.lt.j) goto 96

C
C----- SOLVE THE TEMPERATURE PROFILE -------------

C------ THE CRANK-NICHOLSON METHOD-----

       NM1=N-1
       NM2=N-2
       DO 50 K=1,NM1
        CONV(K)=VEL(K)*DELTAT/2./DELTAX
        RKAPA1=2.*RKAPA(K-1)*RKAPA(K)/(RKAPA(K)+RKAPA(K-1))
        RKAPA2=2.*RKAPA(K+1)*RKAPA(K)/(RKAPA(K)+RKAPA(K+1))

        A1(K)= -DELTAT/DELTAX**2*RKAPA1/RHO(K)/CP(K)
        C1(K)= -DELTAT/DELTAX**2*RKAPA2/RHO(K)/CP(K)
        A(K)=A1(K)-CONV(K)
        C(K)=C1(K)+CONV(K)
        B(K)= 2.-A(K)-C(K)
50   CONTINUE

       DO 60 K=1,NM2

        IF(CONC(1,J,K).LE.RLIMIT) THEN
          RATIO1=-2*CONC(1,J,K)
          SOURCE = 0.
         GOTO 55
        ENDIF
        SOURCE=2*DHDT(K)*DELTAT*HCM/1000./RHO(K)  ! cw probably [-]

        RATIO=CONC(2,J,K)/CONC(1,J,K)
        IF(RATIO.LE.O2FLS) THEN
         RATIO1=2*CONC(2,J,K)/O2FLS
```

```
      ELSE
       RATIO1=2*CONC(1,J,NM1)
      ENDIF

      IF(ABS(SOURCE).GE.RATIO1) SOURCE=-RATIO1

57    SOURCE1=-SOURCE*HLV/CP(NM1)     ! cw looks like [K]

      R(NM1)=(-C1(NM1)-CONV(NM1))*(TGAS(J,N)+GAS)+(2+C1(NM1)+A1(NM1))
     *      *TGAS(J,NM1)+(-A1(NM1)+CONV(NM1))*TGAS(J,NM2)+
     *      2*DELPRESS/RHO(NM1)/CP(NM1)/NN +SOURCE1

C -------SOLVES TRIDIAGONAL EQUATION---------------------------------

      DO 70  K=1,NM1
       BB(K)=B(K)
70    CONTINUE

      DO 80 K=2,NM1
       T=A(K)/BB(K-1)
       BB(K)=BB(K)-C(K-1)*T
       R(K)=R(K)-R(K-1)*T
80    CONTINUE

      TGAS1(N-1)=R(N-1)/BB(N-1)

      DO 90 K=1,NM1-2
       K1=NM1-1-K
       TGAS(J,K1)=(R(K1)-C(K1)*TGAS(J,K1+1))/BB(K1)
90    CONTINUE

      KK1=KK

      DO K1=1,KK1+1
           IF(TGAS(J,K1).GT.TGAS(J,N)) THEN
             KKK=K1
             GO TO 96
           ELSE
                 KKK=KK+2
            ENDIF
      ENDDO

96    CONTINUE

c------solve for concentration in oil layer
```

```
C       no reaction at interface, problem doesn't pop up in T
c       equation because T(0)=Twallm(j) anyway
        dhdt(0)=0.

c       propgate euler
        ceuler = doil(j)*deltat/deltaxoil**2
        do lw = 1, lmax-1
        coil1(lw)=coil0(lw)+ceuler*(coil0(lw+1)-2.*coil0(lw)+coil0(lw-1))
        enddo
c       slope at wall = 0.
        coil1(0)=coil1(1)
c       coil1(lmax) will result from crank nicholson w/ domain matching
c      (henry's law etc.)


C------ SOLVE THE CONCENTRATION PROFILE  , HC AND O2 ----------------

C------ THE CRANK-NICHOLSON METHOD-----


        NM1=N-1
        NM2=N-2

        if (i.lt.j) then   ! test for crevice
                nm1=kcr
                nm2=kcr-1
        endif

        DO 100 II=1,2           ! 1:HC,  2: O2
                if (i.lt.j.and.ii.eq.2) goto 100

        DO 150 K=0,NM1
         KK=K
         IF(K.EQ.0) KK=1
         CONV(K)=VEL(K)*DELTAT/2./DELTAX
         DAB1=2.*DAB(II,KK-1)*DAB(II,K)*RHO(KK-1)*RHO(K)/
     *      (RHO(KK-1)*DAB(II,KK-1)+RHO(K)*DAB(II,K))
         DAB2=2.*DAB(II,K+1)*DAB(II,K)*RHO(K+1)*RHO(K)/
     *      (RHO(K+1)*DAB(II,K+1)+RHO(K)*DAB(II,K))

         A1(K)= -DELTAT/DELTAX**2*DAB1/RHO(K)
         C1(K)= -DELTAT/DELTAX**2*DAB2/RHO(K)
         A(K)=A1(K)-CONV(K)
```

```
         C(K)=C1(K)+CONV(K)
         B(K)= 2.-A(K)-C(K)
 150   CONTINUE

              C(0)=C(0)+A(0)          ! DUE TO NO PENERTATION
              if(i.lt.j) C(kcr) = C(kcr)+A(kcr)

 156  DO 160 K=1,NM2

         IF(CONC1(K).LE.RLIMIT) THEN
          SOURCE=-2*CONC1(K)
          GOTO 157
         ENDIF
         SOURCE=2*DHDT(K)*DELTAT*HCM/1000./RHO(K)
        RATIO=CONC(2,J,K)/CONC1(K)
         IF(RATIO.LE.O2FLS) THEN
          RATIO1=2*CONC(2,J,K)/O2FLS
         ELSE
          RATIO1=2*CONC1(K)
         ENDIF
         IF(ABS(SOURCE).GE.RATIO1) SOURCE=-RATIO1

 157    IF(II.EQ.2)SOURCE=SOURCE*O2FLS

         R(K)=(-C1(K)-CONV(K))*CONC(II,J,K+1)+(2+C1(K)+A1(K))*
    *     CONC(II,J,K)+(-A1(K)+CONV(K))*CONC(II,J,K-1)
    *    + SOURCE


 160  CONTINUE

         IF(CONC1(0).LE.RLIMIT) THEN
          SOURCE=-2*CONC1(0)
          GOTO 161
         ENDIF
         SOURCE=2*DHDT(0)*DELTAT*hcm/1000./RHO(0)
         RATIO=CONC(2,J,0)/CONC1(0)

         IF(RATIO.LE.O2FLS) THEN
          RATIO1=2*CONC(2,J,0)/O2FLS
         ELSE
          RATIO1=2*CONC1(0)
         ENDIF

         IF(ABS(SOURCE).GE.RATIO1) SOURCE=-RATIO1
```

```
161    IF(II.EQ.2) SOURCE=SOURCE*O2FLS

         if (ii.eq.1)then
         henryprime = henrystar(j)*HCM/(1.e2*press1*29.5)
         r(0)=-doil(j)*rhol/deltaxoil*coil1(lmax-1)
         b(0)=-(dab(1,0)*rho(0)/deltax +
   *            1/henryprime*doil(j)*rhol/deltaxoil) ! 2x fishy dab
         c(0)=  dab(1,0)*rho(0)/deltax
         else
         R(0)=(-C1(0)-A1(0))*CONC(II,J,1)+(2+C1(0)+A1(0))*CONC(II,J,0)
   *      +SOURCE
         endif


         IF(CONC1(NM1).LE.RLIMIT) THEN
          SOURCE=-2*CONC1(NM1)
          GOTO 162
         ENDIF

         SOURCE=2*DHDT(NM1)*DELTAT*hcm/1000./RHO(NM1)
         RATIO=CONC(2,J,NM1)/CONC1(NM1)

         IF(RATIO.LE.O2FLS) THEN
           RATIO1=2*CONC(2,J,NM1)/O2FLS
         ELSE
           RATIO1=2*CONC1(NM1)
         ENDIF

         IF(ABS(SOURCE).GE.RATIO1) SOURCE=-RATIO1
162    IF(II.EQ.2) SOURCE=SOURCE*O2FLS

cmgn
        if (i.lt.j) then
         R(kcr)=(-C1(kcr)-A1(kcr))*CONC(II,J,kcr-1) +
   *            (2+C1(kcr)+A1(kcr))*CONC(II,J,kcr) + SOURCE
        else
         R(NM1)=2*(-C1(NM1)-CONV(NM1))*CONC(II,J,N)+(2+C1(NM1)+A1(NM1))
   *      *CONC(II,J,NM1)+(-A1(NM1)+CONV(NM1))
   *      *CONC(II,J,NM2)+SOURCE
        endif


C -------SOLVES TRIDIAGONAL EQUATION---------------------------------
        DO 170  K=0,NM1
         BB(K)=B(K)
```

```
170    CONTINUE

        DO 180 K=1,NM1
          T=A(K)/BB(K-1)
          BB(K)=BB(K)-C(K-1)*T
          R(K)=R(K)-R(K-1)*T
180    CONTINUE

        XXX=R(N-1)/BB(N-1)
        IF(XXX.LE.RLIMIT) THEN
          CONC(II,J,N-1)=0.0
          GO TO 185
        ENDIF

        CONC(II,J,N-1)=R(N-1)/BB(N-1)
        IF(CONC(II,J,N-1).LE.0) CONC(II,J,N-1)=0.0
cw here is a try to fix the dip in air concentration in the cell next
cw to the outmost cell

 185    continue
        if (ii .eq. 1) then
        CONC(II,J,N-1)=CONC1(N-1)
    else
        CONC(II,J,N-1)=cono22
    endif

        if (i.lt.j) then
                nprime = kcr
        else
                nprime = n-2
        endif

        DO 190 K=0,nprime
          K1=nprime-K

          IF (II.EQ.1) GO TO 186
          CONC1(K1)=CONC(1,J,K1)
186    XXX=(R(K1)-C(K1)*CONC(II,J,K1+1))/BB(K1)
          IF(XXX.LE.RLIMIT) THEN
          CONC(II,J,K1)=0.0
          GO TO 187
        ENDIF

          CONC(II,J,K1)=(R(K1)-C(K1)*CONC(II,J,K1+1))/BB(K1)
```

```
187     IF(CONC(II,J,K1).LE.0) CONC(II,J,K1)=0.0

190  CONTINUE

100  CONTINUE

c       re-shuffle array of concentration in oil for next time step euler
        coil1(lmax)=1./henryprime*conc(1,j,0)
                ! 3x fishy   1. I assume henryprime still stored
                !                2. I guessed that conc... is what I want
                !                3. I didn't really check whether here is the
                !             right place for this statement
        do lw = 0, lmax
          coil0(lw)=coil1(lw)
        enddo

        TMASS(J,I)=0.0
cmgnb keeping track of dopant mass in elements, by
c    keeping track of the dopant desorbed and dopant
c    oxidized, which leads to the equivalent length of the gas
c    segment as the pressure drops


        HCoil = 0.

        do ii = 1,lmax            !loop to sum dopant in oil
        HCoil = HCoil + rhol*toil(j)/lmax*(dis(j)-dis(j+1))*coil1(ii)
        enddo
        HCdesrb = HCoilinit-HCoil   ! dopant in gas

        concsum = 0.
        dhdtsum = 0.
        concchk = 0.

        do ii = 1,kcr
        concchk = concchk + deltax * rho(ii) * conc(1,j,ii)
        enddo

        do ii = 1,n
        concsum = concsum + deltax * rho(ii) * conc(1,j,ii)
        dhdtsum = dhdtsum - deltax * dhdt(ii) * deltat * HCM/1000.
        enddo

        if (abs(concsum-concchk).gt.consum/100.and.i.lt.j) then
        write (*,*)
```

```
  *     'conchk',j,i,l,concsum,concchk,(concsum-concchk)/concsum
        endif

        deltaL = (HCdesrb-HCburnd)/(concsum+dhdtsum)   !equivalent seg length

        HCgas = deltaL*concsum
        HCburnd = HCburnd + deltal*dhdtsum         !burned mass for next time step

        hcgaschk = (HCgas-(HCdesrb-HCburnd))/HCdesrb  ! check

45  CONTINUE
c++++++++++++++++This is the end of subcycling in time per CA++++++++++++++++++++


c     WRITE (*,*) 'PATH 3'
c next section adds up mass if mass came from crevice, not
c compatable with oil desorbed mass, if both occur together
c will need new logic. MGN (7-4-95)

        Tdesrb(j,i) = HCdesrb*bore*pi          ! (kg) logic for oil desorbed HC
        Tmass(j,i) = HCgas*bore*pi  ! (kg) logic for oil desorbed HC

40    CONTINUE

              HCburnd = 0.0                     ! resetting burned mass to zero

              write (14,450) dis(j),(tdesrb(j,l),l=0,84,12)
              write (15,450) dis(j),(tmass(j,l),l=0,84,12)
              write (*,450) dis(j),(tdesrb(j,l),l=0,84,12)
              write (*,450) dis(j),(tmass(j,l),l=0,84,12)

10  CONTINUE
c+10+++++++++++++this is the end of the loop over all axial elements++++++++++++++


        do ii = jmin,jmax
              totald = 0.0
              totalg = 0.0
              do ij = jmin,ii
                    totald = totald + tdesrb(ij,ii)
                    totalg = totalg + tmass(ij,ii)
              enddo
        write (16,*) ii*ncad,totald,totalg,(totald-totalg)/totald
        enddo
```

```
      write (*,*) 'I guess I am ready'

410   FORMAT(I10,F10.5,2F18.13)
450   FORMAT(f8.4,8F18.13)
460   FORMAT(I10,2F18.13)
420   FORMAT(I6,F18.10)
430   FORMAT(2F15.10)
      STOP
      END

C ----------------------------------------------
      FUNCTION ALPHA(TEMP,P,totalm)
C    TEMP :TEMPERATURE , P: PRESSURE(BAR)
      RH=100000.*P/(8.314/totalm*TEMP) ! cw probably [kg/m^3]
      RMU=0.00000033*TEMP**(0.7)/1.02537 ! cw looks like it is in SI
      GAM=1.3655-6.105*0.00001*TEMP
      PR=0.05+4.2*(GAM-1.)-6.7*(GAM-1.)**2
      ALPHA=RMU/RH/PR              ! UNIT : M2/S
      END

C  CALCULATING BOUNDARY LAYER THICKNESS

      SUBROUTINE BOUND (J,RPM,STROKE,totalm,DELTAO,DELTA,Vcr,Twallj)

      COMMON /VAR1/ TB(360),PRESS(360),jmin,jmax,ncad
      COMMON /VAR4/dmdx(100),DIS(100),SP(100)

      DIMENSION DELTA(360)
      TIME=0.0

     TEMP=(TB(J)+twallj)/2.
      RHO1=100.*PRESS(J)/(8.314/totalm*twallj)*1000.
cmgn new calc of dmdx from pressure data, consistent with KD Mins resutls
      dmdx(j) = 1000/(dis(j)-dis(j+1))*
   &  (press(j)-press(j+1))*(10**5)*Vcr/(8.314/totalm*twallj)  !(g/m)
      DELTAO=DMDX(J)/(1000.*3.141592*STROKE*RHO1)                     !(m)

11    DO 20 I=J,jmax-1
           TEMP=(TB(I)+twallj)/2.
           RHO=100.*PRESS(I)/(8.314/totalm*TEMP)*1000.
           VIS=3.3*0.0000001*TEMP**(0.7)/1.002835
           GAMMA=1.345-4.78*0.00001*TEMP
           PRANTL=0.05+4.2*(GAMMA-1)-6.7*(GAMMA-1)**2
           ALPHA=VIS/RHO/PRANTL
           REYNOLD=RHO/VIS/(stroke-DIS(I))*
```

```
  &                     (stroke-DIS(J))**2*(SP(I))
              TIME=(I-J)/(RPM*6.)*ncad
              DELTA(I)=SQRT(ALPHA*TIME)*.6*(REYNOLD)**0.2
              RHO1=101.325*PRESS(I)/(8.314/totalm*twallj)*1000.
20   CONTINUE
       GO TO 30
10   CONTINUE
30   continue
       RETURN
       END

c *********************************************************************
c       subroutine: start

c       purpose: returns piston position (dis) and speed (sp)

c *********************************************************************

        SUBROUTINE START(RPM,bore,stroke,conrod,cr)

        COMMON /VAR1/ TB(360),PRESS(360),jmin,jmax,ncad
        COMMON /VAR4/ DMDX(100),DIS(100),SP(100)

        DO 10  ITHETA =1,jmax
        PHI=3.141592
        THETA=FLOAT(ITHETA*ncad)*PhI/180.
        CS=COS(THETA)
        SC=SIN(THETA)
        R1=2.*CONROD/STROKE
        KK=1
        LL=1
        SQ=SQRT(R1*R1-SC*SC)
cmgn    SP(ITHETA)=-3.141592*STROKE/2.*SC*(1.+CS/SQ)*2.*RPM/60.
        SP(ITHETA)=3.141592*STROKE/2.*SC*(1.+CS/SQ)*2.*RPM/60.
        IF(ITHETA*ncad .Ge.180) THEN
          KK=2
          LL=2
          IF (ITHETA*ncad.GE.360) THEN
                KK=3
                LL=1
                IF(ITHETA*ncad.GE.540) THEN
                 LL=2
                 KK=4
                ENDIF
          ENDIF
```

```
        ENDIF
       XX1=STROKE/2.*(CS+SQ)
       DIS(ITHETA)=(XX1-CONROD+STROKE/2.)
10   CONTINUE
20   CONTINUE
      RETURN
      END


C*******************************************************************
C     subroutine: oilprop
C
C     PURPOSE:      Produces oil properties and fuel-oil properties
C                   at each 2 crank angles from 20 ATC to 120 ATC
c
C     WRITTEN BY:   MICHAEL NORRIS, SLOAN LABS, MIT, 1993
C*******************************************************************
C     LIST OF VARIABLES
C
C COMP  VARIABLE NAME   TYPE    DESCRIPTION
C ----  -------------   ----    -----------
C Physical Parmeters:
C     Twl     in    top of cylinder wall temperature (K)
C     Tcl     in    coolant temperature (K)
C       Tl(j)  out    wall temperature at fcn(temperature) (K)
C       rhol   in     density of liquid (kg/m^3)
C       rgas   in     gas constant (j/Kg K ~292)
C Coeffiecents of Diffusivity and Henry's Constant
C       Doil   in     Liquid diffusion (m2/s)
C     Al      in      coeff in fit to oil viscosity data
c       Bl     in     temperature coeff in fit to oil visocity data (1/C)
C     vcrt   in       critical volume of fuel (cm^3/mol)
C     AH      in      coeff in fit to Henrys Constant data
c       BH     in     temperature coeff in fit to Henrys Constant data (1/C)
c       R      in     conrod/crank length ratio
C CONSTANTS:
C     PI              PI (CIRCUMFERENCE/DIAMETER OF CIRCLE)
C
C ******************************************************************
C
      SUBROUTINE oilprop(Tl,toil,doil,henrystar,minax,maxax,rhol,iwu,
   &                  A0,EOR,ETA,BETA,hcm,vhc,o2fls,ifuel,Twl,Tcl)

      COMMON /VAR1/ TB(360),PRESS(360),jmin,jmax,ncad
      common /var5/ stroke,conrod,RPM,Vcr
```

```
      real Tl(minax:maxax), Doil(minax:maxax),
     &    Henrystar(minax:maxax), Toil(minax:maxax)
      real vcrt(5), ahc(5),bhc(5),cnc(5),hnc(5),ONC(5)
      real A0wu(5), EORwu(5), ETAwu(5), BETAwu(5)
      real A0wd(5), EORwd(5), ETAwd(5), BETAwd(5)
      real stroke, mul, sp, spl, ctoil1, ctoil2, root, r, theta, Z
      integer ifuel
      real o2fls, hn,ON


      PARAMETER (PI=3.141592654,e=2.7182818)

c Input

c ifuel = 1: hexane, 2: toluene, 3: xylene, 4: iso-octane, 5: MTBE
      data vcrt / 370., 316., 331., 468., 329./
      data AHc / 5.45, 7.86, 9.81, 7.468, 4.13/
      data BHc / -11.2, -17.9, -23.3, -16.76, -7.657/
      data CNc / 6, 7, 8, 8, 5/
      data HNc / 14, 8, 10, 18, 12/
      data ONc / 0, 0, 0, 0, 1/
c KC Wu data from Chemical Kinetics for PFR
c taking hexane = iso-octane and xylene=toluene
      data A0wu / 6.36e16, 4.35e14, 4.35e14, 6.36e16, 2.62e13 /
      data EORwu / 47615., 40239., 40239., 47615., 54906. /
      data ETAwu / -0.164, -0.417, -0.417, -0.164, -0.157/
      data BETAwu / 1.08, 1.515, 1.515, 1.08, 0.489/
c Westbrook and Dryer data from Chemical Kinetics for flames
c taking xylene = toluene, and MTBE as propane
      data A0wd / 5.7e11, 1.6e11, 1.6e11, 7.2e12, 8.6e11 /
      data EORwd / 30000., 30000., 30000., 40000., 30000./
      data ETAwd / 0.25, -0.1, -0.1, 0.25, 0.1/
      data BETAwd / 1.5, 1.85, 1.85, 1.5, 1.65/


c gas side constants
      Mg = 28.9      !molecular mass of air
      Vg = 17.9      !critical volume of air

      Al = 7.41      !oil side diffusivity constant
      Bl = 2.86      !oil side diffusivity constant


c Setting values for fuel molecular mass, Henry's Constant
```

```
      HCM = cnc(ifuel)*12.011 + hnc(ifuel)*1.008 + oNC(IFUEL)*15.9994
      ah = ahc(ifuel)
      bh = bhc(ifuel)
      cn = cnc(ifuel)
      hn = hnc(ifuel)
      on = onc(ifuel)

      o2fls = (cn+hn/4-on/2)*32./HCM

      if (iwu.eq.1) then               ! KC Wu PFR results
            A0 = A0wu(ifuel)
            EOR = EORwu(ifuel)/1.986
            ETA = ETAwu(ifuel)
            BETA = BETAwu(ifuel)
      else                             !Westbrook and Dryer flame results
            A0 = A0wd(ifuel)
            EOR = EORwd(ifuel)/1.986
            ETA = ETAwd(ifuel)
            BETA = BETAwd(ifuel)
      endif

c calc ratio of conrod/half stroke

      R = 2*conrod/stroke

c loop over 90 2 CAD elements

      Do 10 j = jmin,jmax

c calculating the oil thickness and temperature of each element
c based on KD Mins model
c theta: 0 at TDC, Tcl:coolant termp, Twl: top of cylinder wall temp

        SPL = 2*stroke*RPM/60.
        THETA = (j*ncad)/180.*PI
        ROOT =SQRT(R*R-SIN(THETA)*SIN(THETA))
        SP = SPL*(PI/2.*SIN(THETA)*(1.+COS(THETA)/ROOT)+1.)
        Z  = R*stroke/2+stroke/2.-stroke/2.*(COS(THETA)+ROOT)

        Tl(j)=Twl-Z/stroke*(Twl-Tcl)  ! TEMPERATURE OF EACH ELEMENT


C  Calculating diffusivity in Oil and Henry's constant
```

```
      RHOL =(890-0.63*(Tl(j)-(273.16+15)))   ! kg/m3
      mul = 1.e-6* rhol*(0.7+10**(10**(Al-Bl*log10(Tl(j))) )) ! (kg/m s)
      Vhc  = 0.285 * vcrt(ifuel)**1.048      ! molar vol of sat liquid (cm^3/mol)
      eps = 10.2/vhc - 0.791

c Liq Diff (m^2/s)
      Doil(j) = 13.3e-12*Tl(j)**1.47 * (mul*1000.)**eps / vhc**0.71

      Henrystar(j) = 10**(AH*log10(Tl(j))+BH)   !  Henry's Constant (kPa)

c oil thickness model (toil)

      ctoil1=-0.0025*(Tl(j)-273)+0.425
      IF(Z.LE.0.35*stroke) THEN
            ctoil2=0.0325*sqrt(1000.)*SQRT(Z/(0.35*stroke))
      ELSE
            ctoil2=0.0325*sqrt(1000.)
      ENDIF

    toil(j)=1.e-6*(ctoil1+ctoil2*sqrt(MUL*sp))

10    continue
```

6130-7